

Chapter 26

Comfort Performance



The definition of comfort in a motor vehicle is at once complex and subjective, changing not only with time (cars considered comfortable just twenty years ago are nowadays considered unsatisfactory) but also from user to user. The same user may change his appraisal depending on circumstances and his psycho-physical state. But comfort remains an increasingly important parameter in customer choice and a strongly competitive factor among manufacturers.

This chapter will deal primarily with vibrational comfort, although it is difficult to separate it from acoustic comfort without entering into details linked more with the driveability and handling of the vehicle. Not just driving comfort, but vibrational and acoustic comfort as well (the latter deeply affects the conditions in which the driver operates), all have a strong impact on vehicle safety.

It is possible to distinguish between *vibrational and acoustic comfort*—linked with the vibration and noise produced inside vehicles by mechanical devices or on its surface by the air—and *ride comfort*, which is linked primarily with the ability of the tires and the suspensions to filter out vibration caused by motion on a road that is not perfectly smooth.

With this distinction in mind, SAE defines:

- *ride*, low frequency (up to 5 Hz) vibration of the vehicle body
- *shake*, vibration at intermediate frequency (between 5 and 25 Hz), at which some natural frequencies of subsystems of the vehicle occur
- *harshness*, high frequency vibration (between 25 and 100 Hz) of the structure and its components, felt primarily as noise
- *noise*, acoustic phenomena occurring between 100 Hz and 22 kHz, i.e. up to the threshold of human hearing.

26.1 Internal Excitation

The sources of vibration on board a vehicle are essentially three: The wheels, the driveline and the engine. All contain rotating parts and, as a consequence, a first cause of dynamic excitation is imbalance. A rotor is perfectly balanced when its rotation axis coincides with one of its principal axes of inertia; however, this condition can only be met approximately and balancing tolerances must be stated for any rotating object.¹ As a consequence of the residual imbalance a rotating object exerts on its supports, a force whose frequency is equal to the rotational speed Ω and its amplitude is proportional to its square Ω^2 . Because the engine, the driveline and the wheels rotate at different speeds, the excitations they cause are characterized by different frequencies.

Apart from the excitation due to imbalance, there are other effects that are peculiar to each element. Wheels may show geometrical and structural irregularities. The outer shape of the tires cannot be exactly circular and is characterized by a runout (eccentricity) having the same effect as mass imbalance, exciting vibrations with a frequency equal to the rotational speed, plus other harmonic components which excite higher harmonics. An ovalization of the shape excites a vibration with frequency equal to 2Ω , a triangular shape with frequency 3Ω , etc. The very presence of the tread excites higher frequencies, which are usually found in the acoustic range; to avoid a strong excitation with a period equal to the time of passage of the single tread element, the pattern of the tread is usually made irregular, with randomly spaced elements.

The same effect occurs for variations of stiffness; these induce dynamic forces with frequencies equal to the rotational speed and its multiples. As various harmonics are present in differing degrees in different tires, the spectrum of the dynamic force exerted by the tire on the unsprung mass depends upon each tire. As is common in the dynamics of machinery, such a typical spectrum is referred to as the mechanical signature of the tire.

When the wheel is called upon to exert longitudinal and transversal forces, the irregularities, both geometrical and structural, also introduce dynamic components in these directions. The tire-wheel assembly, however, is a complex mechanical element with given elastic and damping properties that can filter out some of the frequencies produced at the road-tire interface. High frequencies are primarily filtered out by the tire itself, before being further filtered by the suspension. These frequencies are felt onboard primarily as airborne vibration, i.e. noise.

The excitation due to driveline imbalance is usually transferred to the vehicle body through its soft mountings. The transmission is, however, made of flexible elements and, particularly at high frequency, these may have resonances. A long drive shaft has its own critical speeds, and in the case of a two-span shaft with a central joint (common in front-engine, rear-drive layouts), a critical speed, corresponding to a mode in which the two spans behave as rigid bodies on a compliant central support,

¹G. Genta, *Vibration of structures and machines*, Springer, New York, 1995, G. Genta, *Dynamics of rotating systems*, Springer, New York, 2005.

is usually located within the working range. If the balancing of the central joint is poor, strong vibration occurs when crossing this critical speed.

When Hooke's joints are present, torque pulsations occurring when the input and output shaft are at an angle can be a major problem. In modern front wheel drive cars, the joints near the wheels are of the constant-speed type to avoid vibration, but care must be taken to design the driveline layout to avoid excitations from these joints.

The engine is a major source of vibration and noise caused by imbalance of rotating parts, inertial forces from reciprocating elements and time variations of the driving torque. The excitation due to imbalance of rotating parts, mostly the crankshaft, has the frequency of the engine speed Ω . To reduce it, the crankshaft must be balanced accurately. The reciprocating masses produce forcing functions with frequencies that are equal to Ω and its multiples, in particular 2Ω and 4Ω .

The components with frequency Ω interact with those due to imbalance and can be reduced by using counter-rotating shafts with eccentric masses. Their compensation depends on the architecture of the engine, and above all on the number of cylinders; they are particularly strong in single cylinder engines, such as those used on many motor cycles. The simplest way to partially compensate for them is to use a counterbalance slightly larger than that used to compensate for the imbalance of rotating masses (this technique is usually referred to as *overbalancing*). To reduce components with frequency 2Ω , it is possible to use shafts counter-rotating at a speed twice the speed of the crankshaft, a practice fairly common on the engines of luxury cars.

Torsional vibration of the engine is another important source of vibration. Torsional vibrations of the engine were traditionally regarded as having little effect on comfort, important only for the structural survival of the mechanical components of the engine, in particular the crankshaft. This is, however, increasingly unrealistic, and the excitation caused by torsional vibration is increasingly seen as important for vehicle comfort.

The reason for this is the increasing number and mass of the ancillary devices, such as larger generators for coping with the increasing electrical needs of the vehicle, air conditioning compressors, power steering pumps, etc., that are located on brackets and driven by belts. Torsional vibration from the engine can set the system made by accessories, their brackets, belts covers, etc. into vibration. These vibrations are then transferred to both engine and structure, producing noise both inside the vehicle and outside, because these accessories are usually located close to the cooling air intakes.

The use of diesel engines makes things worse, because the more abrupt changes of pressure in the combustion chamber lead to strong high-order harmonics in torsional vibration. All vehicular diesel engines, and nowadays also spark ignition engines, have torsional vibration dampers, of the viscous (on industrial vehicles) or elastomeric type (passenger vehicles), but they may be not enough. More complex dampers have been introduced, both for reducing vibration of the crankshaft and for insulating the accessories. Moreover, the geometry of the engine is such that it is impossible to distinguish, at least as a first approximation, between torsional, axial and flexural vibration of the crankshaft.

Vibrations linked to the thermodynamic cycle have a fundamental frequency which, in four-stroke engines, is equal to half the rotational speed but a large number of harmonics are usually present. Because a reciprocating engine usually has a number of torsional critical speeds, its dynamics is quite complicated. It has been the object of many studies and the subject of many books.²

The harmonics whose order is equal to the number of cylinders and its multiples are usually referred to as major harmonics; these often are the most dangerous. In the case of a four-in-line engine the frequency of the lowest major harmonics is 2Ω , coinciding with one of the forcing functions due to reciprocating masses. A partial compensation is often performed by setting the shaft counter-rotating at a speed 2Ω in unsymmetrical position.

The design of the engine suspension system is a complex issue. The elimination of the sources of vibration, e.g., using dampers on the crankshaft or counterbalance shafts spinning at twice the rotational speed, properly insulating the engine from the vehicle structure by using adequate soft mountings and dampers, and insulating the passenger compartment for noise, are all useful provisions for increasing ride comfort. The engine suspension should be soft, to insulate the vehicle from vibration due to the engine, but must be stiff enough to avoid large relative motion between engine and vehicle.

The engine suspension is subject to a constant load, the weight of the engine, and to variable loads, such as inertia forces due to reciprocating parts and the motion of the vehicle, and a torque equal and opposite to the engine torque. The latter changes rapidly from zero to its maximum value, but can also change its sign when the engine is used to brake the vehicle.

Engine and gearbox are often in one piece, and in this case the torque acting on the engine suspension is the torque at the output of the gearbox (3–5 times the engine torque). If the differential is also inside the gearbox, the torque is that at the output of the final reduction, which may be as large as 10–14 times the engine torque.

The solution once universally accepted, based on three elastomeric supports, is nowadays often replaced by a solution based on two elastomeric supports plus a connecting rod, hinged at its ends by two elastomeric supports, that reacts to the driving torque

The engine suspension must be designed with the aim of reducing, as much as possible, the transmission of engine vibration to the vehicle, but also allowing for the fact that the stresses in the engine components are influenced by how the engine is attached to the vehicle. The transmission of commands to the engine and, in particular, to the gearbox, is important in reducing the transmission of vibration to the vehicle. Instead of using rigid rods to transfer commands to the gearbox, it is convenient to use flexible cables or even to avoid mechanical transmission of commands altogether (servo-controlled gearbox).

²See, for instance, W. Thompson, *Fundamentals of automobile engines balancing*, Mech. Eng. Publ. Ltd., 1978.

Together with the conventional solutions based on elastomeric supports, more advanced and even active solutions in which it is possible to change the relevant parameters are now used.

The engine suspension can be used as a kind of dynamic vibration absorber. The engine mass, the compliance and the damping of its support constitute a damped vibration absorber that can be tuned on the main wheel hop resonance, about 12–15 Hz, to control vertical shake vibration due to wheel excitation.

The contribution to overall noise due to aerodynamics can be large and often, as discussed in Chap. 21, has specific causes that may be different from those causing aerodynamic drag. Aerodynamic noise is primarily caused by vortices and detached flow on the front part of the vehicle, generally in the zone close to the windshield and the first strut (pillar A). The wake and aerodynamic field at the rear of the vehicle, important in causing aerodynamic drag, usually make a limited contribution to overall noise.

Active noise cancellation is a promising way to increase acoustic comfort. Already applied in aeronautics, the first automotive applications in the form of active engine mufflers and passenger compartment noise control are due to appear soon. With the introduction of active noise control, more advanced goals than pure noise suppression can be achieved. As an example, experience in the field of rail transportation has shown that complete noise suppression is not considered satisfactory by most passengers, as it decreases privacy by allowing others to listen to what people are saying. A completely noiseless machine may seem unnatural (in the field of domestic appliances there have been cases of dishwashers considered too quiet by their users), and may even be dangerous in some automotive applications. The ultimate goal may not be to suppress noise, but to achieve a noise that users find pleasant.

Similarly, absolute vibration suppression may be undesirable because vibration conveys useful information to the driver and can give warning symptoms of anomalies. Here again the goal seems more to supply a vibrational environment the user finds satisfactory than to completely suppress all vibrational input.

26.2 Road Excitation

Knowledge of the excitation due to motion on uneven roads is important for the study of riding comfort. Road excitation reduces the ability of the tires to exert forces in the x and y direction, because it causes a variable normal load F_z , and increases the stressing of the structural elements. Because such excitation cannot be studied with a deterministic approach, the methods used for random vibrations must be applied.

A number of studies have been devoted to characterizing road profiles experimentally and interpreting the results statistically. From experimental measurements of the road profile (Fig. 26.1), a law $h(x)$ can be defined and its power spectral density obtained through harmonic analysis. Note that the profile is a function of space and not of time, and the frequency referred to space $\bar{\omega}$ is expressed in rad/m or cycles/m

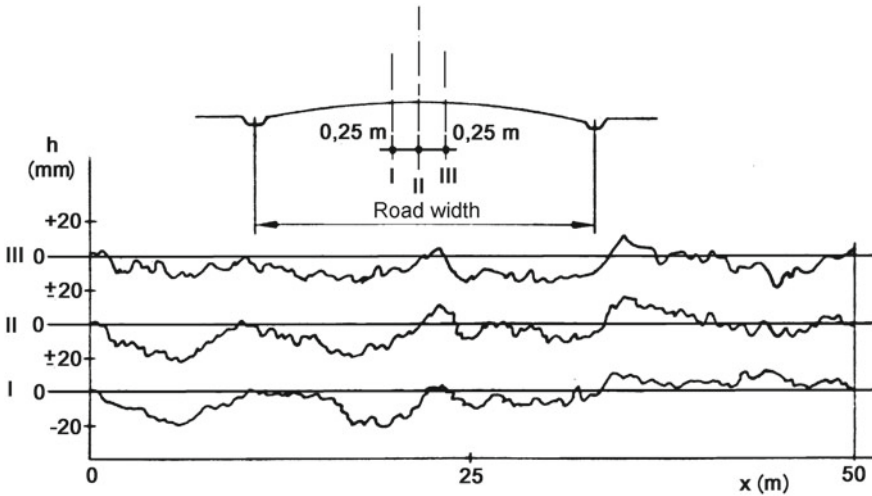


Fig. 26.1 Examples of road profiles

and not in rad/s or in Hz. The power spectral density \bar{S} of law $h(x)$ is thus expressed in $m^2/(rad/m)$ or in $m^2/(cycles/m)$.

The law $\bar{S}(\bar{\omega})$ can be expressed by a straight line on a logarithmic plot, i.e. by the law

$$\bar{S} = c\bar{\omega}^{-n} \tag{26.1}$$

where n is a nondimensional constant while the dimensions of c depend on n (if $n = 2$, c is expressed in $m^2(cycles/m)$, for instance).

An old I.S.O. proposal³ suggested $n = 2$ for road undulations, i.e. for disturbances with a wavelength greater than 6 m, and $n = 1.37$ for irregularities, with a wavelength smaller than the mentioned value. The proposal stated various values of c depending on the type of road.

A more recent approach is to abandon the distinction between undulations and irregularities. Often used values are

$$\begin{aligned} c &= 4.7 \times 10^{-6} \text{ m}^3 & n &= 2.1 & \text{highway,} \\ c &= 8.1 \times 10^{-7} \text{ m}^3 & n &= 2.1 & \text{road in poor conditions.} \end{aligned} \tag{26.2}$$

A⁴ recent ISO proposal subdivides road profiles into eight classes, indicated by letters from A to H, stating an exponent always equal to 2 for Eq. (26.1). The values of constant c for the various profiles are shown in Table 26.1. Classes from A to D are for hard-surfaced roads, with A for very smooth roads. Classes E and F are for

³B.S.I. Proposal for Generalized Road Inputs to Vehicles, ISO/TC 108/WG9 Document 5, 1972.

⁴ISO 8606:1995, Mechanical vibration—Road surface profiles—Reporting of measured data, 1/9/1995.

Table 26.1 Minimum, average and maximum values of constant c for the various classes of road following ISO 8606:1995 standard

Class	c_{min} (m ² cycles/m)	$c_{average}$ (m ² cycles/m)	c_{max} (m ² cycles/m)
A	—	1.6×10^{-7}	3.2×10^{-7}
B	3.2×10^{-7}	6.4×10^{-7}	1.28×10^{-6}
C	1.28×10^{-6}	2.56×10^{-6}	5.12×10^{-6}
D	5.12×10^{-6}	1.024×10^{-5}	2.048×10^{-5}
E	2.048×10^{-5}	4.096×10^{-5}	8.192×10^{-5}
F	8.192×10^{-5}	1.6384×10^{-4}	3.2768×10^{-4}
G	3.2768×10^{-4}	6.5536×10^{-4}	1.31072×10^{-3}
H	1.31072×10^{-3}	2.62144×10^{-3}	—

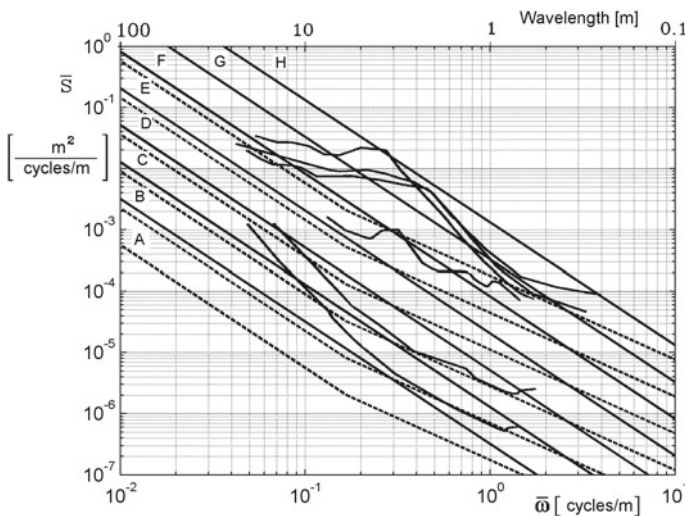


Fig. 26.2 Power spectral density of some road profiles, ISO/TC 108/RS9 Document 5, 1972 recommendation (dashed lines) and ISO 8606:1995 standard (full lines)

natural surface roads or roads in bad conditions, such as a badly maintained pavé. G and H are for highly irregular surfaces. The power spectral density is defined in a frequency range from 0.01 to 10 cycles/m (wavelength from 100 m to 100 mm).

Some examples of power spectral density \bar{S} for tarmac, concrete and pavé roads⁵ are shown in Fig. 26.2 as functions of $\bar{\omega}$ together with the old ISO recommendation and ISO 8606:1995 standard.

If the vehicle travels with velocity V , it is possible to transform the law $h(x)$ into a law $h(t)$ and compute a frequency ω and a power spectral density S (measured in m²/(rad/s) or m²/Hz) referred to time from $\bar{\omega}$ and \bar{S} defined with respect to space

⁵G.H. Tidbury, *Advances in Automobile Engineering*, part III, Pergamon Press, Londra, 1965.

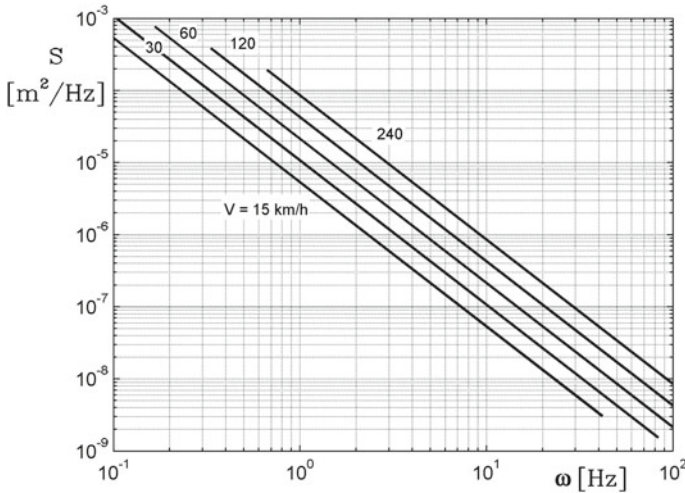


Fig. 26.3 Power spectral density of the displacement $h(t)$ as a function of the frequency ω at various speeds for road at the border between the B and C classes following ISO standards

$$\begin{cases} \omega = V\bar{\omega} , \\ S = \frac{\bar{S}}{V} . \end{cases} \tag{26.3}$$

The dependence of S on ω is thus

$$S = cV^{n-1}\omega^{-n} . \tag{26.4}$$

Remark 26.1 If $n = 2$, as is suggested by the most recent ISO standards, the power spectral density of the displacement is proportional to ω^{-2} and thus the power spectral density of the vertical velocity is constant: Road excitation is then equivalent to white noise in terms of vertical velocity of the contact point.

The law $S(\omega)$ at various speeds for a road at the limit between the B and C classes (a fair but not very good road) following ISO standards is plotted in Fig. 26.3.

Once the power spectral density $S(\omega)$ of the excitation (namely of function $h(t)$) and the frequency response $H(\omega)$ of the vehicle are known, the power spectral density of the response $S_r(\omega)$ is easily computed as

$$S_r(\omega) = H^2(\omega)S(\omega) . \tag{26.5}$$

The root mean square (r.m.s.) value of the response is the square root of the power spectral density integrated in the relevant frequency range. If, for instance, the frequency response $H(\omega)$ is the ratio between the amplitude of the acceleration

of the sprung mass and that of the displacement of the contact point, the response in terms of r.m.s. acceleration in the frequency range between ω_1 and ω_2 is

$$a_{rms} = \sqrt{\int_{\omega_1}^{\omega_2} S_r(\omega) d\omega} . \quad (26.6)$$

To summarize the quality of a road profile in a single figure an International Roughness Index (IRI), referring not to the road itself but to the way a given standard *quarter-car model* (see below) reacts to it, was introduced. Because it refers to a particular model, the so-called quarter-car with two degrees of freedom, it will be dealt with when we discuss suspension models.

26.3 Effects of Vibration on the Human Body

The ability of the human body to withstand vibration and related discomfort has been the object of countless studies and several standards on the subject have been stated. ISO 2631 standard (Fig. 26.4),⁶ distinguishes between vibrations with a frequency in the range between 0.5 and 80 Hz that may cause a reduction of comfort, fatigue, and health problems, and vibrations with a frequency in the range between 0.1 and 0.5 Hz that may cause motion sickness.

Standards refer to the acceleration due to vibration and suggest weighting functions of the frequency to compute the root mean square values of the acceleration. Such functions depend both on the point of the body where the acceleration is applied and the direction along which it acts.

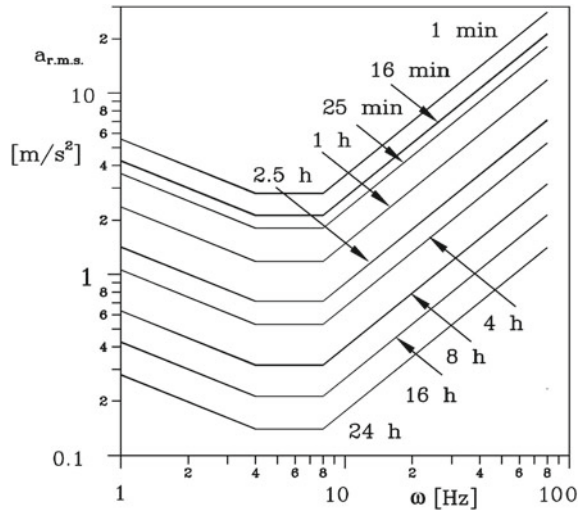
Figure 26.4, shows the r.m.s. value of the acceleration causing, in a given time, a reduction of physical efficiency. The exposure limits can be obtained by multiplying the values reported in the figure by 2, while the “reduced comfort boundary” is obtained by dividing the same values by 3.15 (i.e., by decreasing the r.m.s. value by 10 dB). From the plot it is clear that the frequency range in which humans are more affected by vibration lies between 4 and 8 Hz.

As already stated, frequencies lower than 0.5–1 Hz produce sensations that may be associated with motion sickness. They depend on many parameters other than acceleration and vary among individuals. Between 1 and 4 Hz, the ability of humans to tolerate acceleration decreases with the frequency, reaching a minimum between 4 and 8 Hz. Between 8 and 80 Hz this tolerance increases again in a practically linear law with frequency. In practice, what creates discomfort in that range is not so much acceleration, but the ratio between acceleration and frequency.

Above 80 Hz the effect of vibration depends upon the part of the body involved, as local vibrations become the governing factor, making it impossible to give general guidelines. There are also resonance fields at which some parts of the body

⁶ISO Standards 2631, 1997, Mechanical vibration and shock: Evaluation of human exposure to whole-body vibration. The standards are older, but were revised in 1997.

Fig. 26.4 rms value of the vertical acceleration causing reduced physical efficiency to a sitting subject as a function of the frequency. The curves for different exposure times have been reported (ISO 2631 standard)



vibrate with particularly large amplitudes. As an example, the thorax-abdomen system has a resonant frequency at about 3–6 Hz, although all resonant frequency values depend strongly upon individual characteristics. The head-neck-shoulder system has a resonant frequency at about 20–30 Hz, and many other organs have more or less pronounced resonances at other frequencies (e.g., the eyeball at 60–90 Hz, the lower jaw-skull system at 100–220 Hz, etc.).

Essentially similar results are plotted in Fig. 26.5. The plots are related to equal discomfort lines following BSI 6472 (a) and VDI 2057 (b).

Other curves related to vertical and horizontal vibration from various sources and reported by M.W. Sayers, S.M. Karamihas, *The Little Book of Profiling*, The University of Michigan, 1998, are plotted in Fig. 26.6.

Remark 26.2 The lower natural frequencies, those linked with the motion of the sprung mass, must be high enough to avoid motion sickness, but low enough to be well below 4 Hz. A common choice is to locate them in the range between 1.2 and 1.6 Hz. Higher frequencies, those due to the motion of unsprung masses, should be well above 8–10 Hz. A good choice could be to locate them around 15–20 Hz.

26.4 Quarter-Car Models

The simplest model for studying the suspension motions of a vehicle is the so-called *quarter-car model*, including a single wheel with related suspension and the part of the body whose weight is imposed on it. Often, in four-wheeled vehicles, the quarter vehicle including the suspension and the wheels is called a *corner* of the vehicle. The quarter-car model may be more or less complex, including not only the compliance

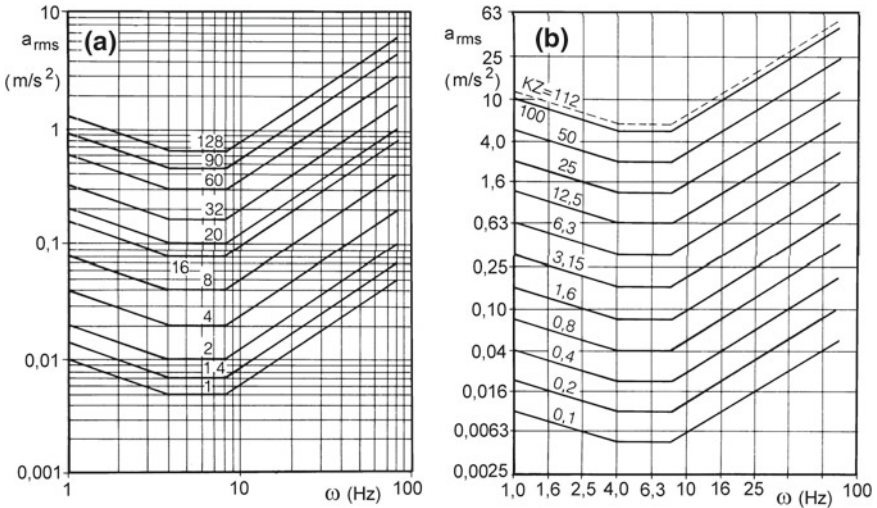


Fig. 26.5 Curves of constant discomfort, following BSI 6472 (a) and VDI 2057 (b)

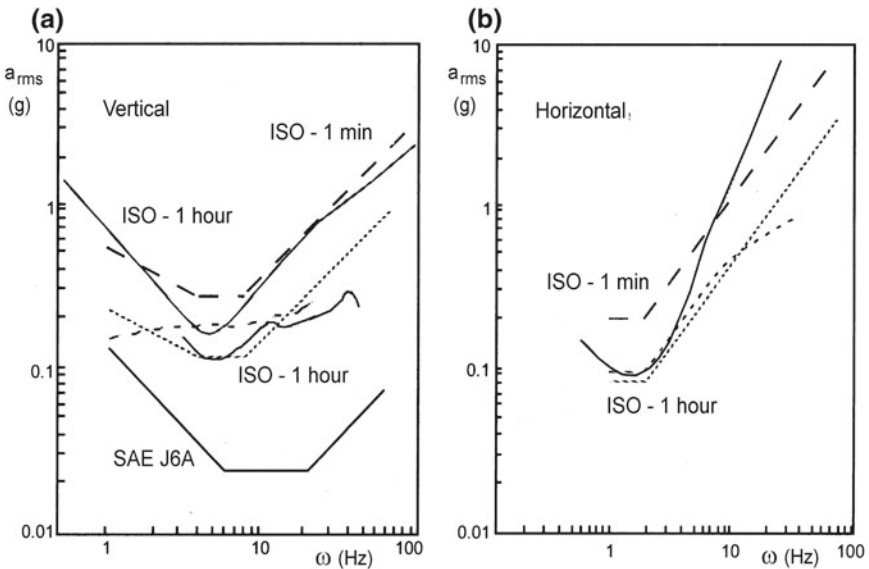


Fig. 26.6 Comparison between discomfort limits from ISO and other sources for vertical (a) and horizontal (b) vibration

of the suspension, but the compliance of the tire and also that of the rubber mounts connecting the frame carrying the suspension to the body. It may even include the inertia of the tire.

Three models based on the quarter-car approach are shown in Fig. 26.7.

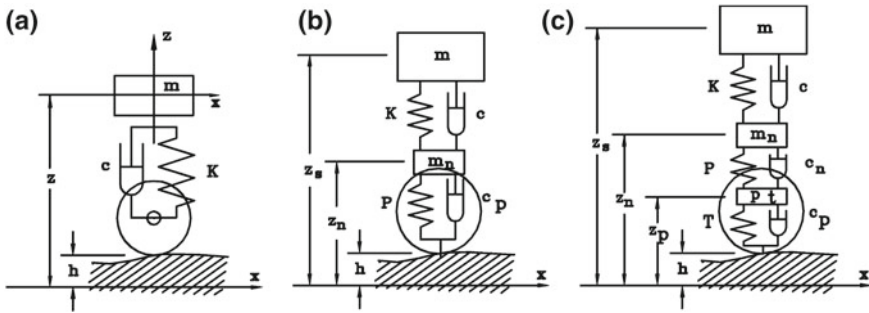


Fig. 26.7 Quarter-car models with one (a), two (b) and three (c) degrees of freedom

The first model has a single degree of freedom. The tires are considered rigid bodies and the only mass considered is the sprung mass. This model holds well for motions taking place at low frequency, in the range of the natural frequency of the sprung mass (in most cases, up to 3–5 Hz, in the range defined as *ride* by SAE).

The second model has two degrees of freedom. The tire is considered as a massless spring, and both the unsprung and the sprung masses are considered. This model holds well for frequencies up to the natural frequency of the unsprung mass and slightly over (in most cases, up to 30–50 Hz, including the ranges *ride*, *shake* and partially *harshness*).

The third model has three degrees of freedom. The tire is modelled as a spring-mass-damper system, representing its dynamic characteristics in the lowest mode. This model allows us to study motions taking place at frequencies in excess of the first natural frequency of the tires (up to 120–150 Hz, including then *harshness*).

If higher frequencies must be accounted for, it is possible to introduce a higher number of tire modes by inserting other masses. These models, essentially based on the modal analysis of the suspension-tire system, are clearly approximated because a tire can be considered a damped system and one that is usually nonlinear.

26.4.1 Quarter-Car with a Single Degree of Freedom

Consider the simplest quarter-car model shown in Fig. 26.7a. It is a simple mass-spring-damper system that, among other things, has been used in the past to demonstrate that the shock absorber must be a linear, symmetrical viscous damper.⁷

The equation of motion of the system is simple. Using the symbols shown in the figure it is

$$m\ddot{z} + c\dot{z} + Kz = c\dot{h} + Kh, \tag{26.7}$$

⁷Bourcier De Carbon C.: *Théorie mathématiques et réalisation pratique de la suspension amortie des vehicules terrestres*, Proceedings SIA Conference, Paris, 1950.

where $z(t)$ is the displacement from the static equilibrium position, referred to an inertial frame, and $h(t)$ is the vertical displacement of the supporting point due to road irregularities.⁸

The frequency response of the quarter-car can be obtained simply by stating a harmonic input of the type

$$h = h_0 e^{i\omega t} .$$

The output is itself harmonic and can be expressed as

$$z = z_0 e^{i\omega t} ,$$

where both amplitudes h_0 and z_0 are complex numbers to account for the different phasing of response and excitation due to damping.

By introducing the time histories of the forcing function and the excitation into the equation of motion, an algebraic equation is obtained:

$$(-\omega^2 m + i\omega c + K) z_0 = (i\omega c + K) h_0 . \tag{26.8}$$

It links the amplitude of the response to that of the excitation, and yields

$$z_0 = h_0 \frac{i\omega c + K}{-\omega^2 m + i\omega c + K} . \tag{26.9}$$

If h_0 is real (that is, if the equation is written in phase with the excitation), the real part of the response (the in-phase component of the response) can be separated easily from its imaginary part (in-quadrature component)

$$\begin{cases} \frac{\text{Re}(z_0)}{h_0} = \frac{K(K - m\omega^2) + c^2\omega^2}{(K - m\omega^2)^2 + c^2\omega^2} \\ \frac{\text{Im}(z_0)}{h_0} = \frac{-c m \omega^3}{(K - m\omega^2)^2 + c^2\omega^2} . \end{cases} \tag{26.10}$$

The amplification factor, i.e., the ratio between the absolute values of the amplitudes of the response and the excitation and the phase of the first with respect to the second, can be easily shown to be (Figs. 26.8a, c)

$$\begin{cases} \frac{|z_0|}{|h_0|} = \sqrt{\frac{K^2 + c^2\omega^2}{(K - m\omega^2)^2 + c^2\omega^2}} \\ \Phi = \arctan\left(\frac{-c m \omega^3}{K(K - m\omega^2) + c^2\omega^2}\right) . \end{cases} \tag{26.11}$$

⁸The z coordinate must be considered as the displacement from the static equilibrium position. By doing this, the static problem of finding the equilibrium position is separated from the dynamic problem here dealt with. This can only be done because of the linearity of the system.

More than the frequency response expressing the ratio between the amplitudes of response and excitation, what matters in motor vehicle suspensions is the ratio between the amplitudes of the acceleration of the sprung mass and that of the displacement of the supporting point. Because in harmonic motion the amplitude of the acceleration is equal to the amplitude of the displacement multiplied by the square of the frequency, it follows that:

$$\frac{|(\ddot{z})_0|}{|h_0|} = \omega^2 \frac{|z_0|}{|h_0|} .$$

Both frequency responses are plotted in Fig. 26.8 for different values of the damping of the shock absorber, together with the phase Φ . The responses are plotted as functions of the nondimensional frequency

$$\omega^* = \omega \sqrt{\frac{m}{K}}$$

and damping is expressed as a function of the optimum damping defined below.

All curves pass through point A, located at a frequency equal to $\sqrt{2K/m}$. Because the acceleration of the sprung mass must be kept to a minimum to produce a comfortable ride, a reasonable way to optimize the suspension is to choose a value of shock absorber damping that leads to a relative maximum, or at least a stationary point, at point A on the curve related to acceleration. By differentiating the expression of

$$\omega^2 \frac{|z_0|}{|h_0|}$$

with respect to ω and equating the derivative to zero at point A, the following value of the optimum damping is obtained:

$$c_{opt} = \sqrt{\frac{Km}{2}} = \frac{c_{cr}}{2\sqrt{2}} , \quad (26.12)$$

where

$$c_{cr} = 2\sqrt{Km}$$

is the critical damping of the suspension.

Although this method for optimizing the suspension can be readily criticized, because the comfort of a suspension is far more complex than simple reduction of the vertical acceleration (the so-called “jerk”, i.e., the derivative of the acceleration with respect to time d^3z/dt^3 also plays an important role), it nonetheless gives important indications.

The dynamic component of the force the tire exerts on the ground is

$$F_z = c(\dot{z} - \dot{h}) + K(z - h) = -m\ddot{z} . \quad (26.13)$$

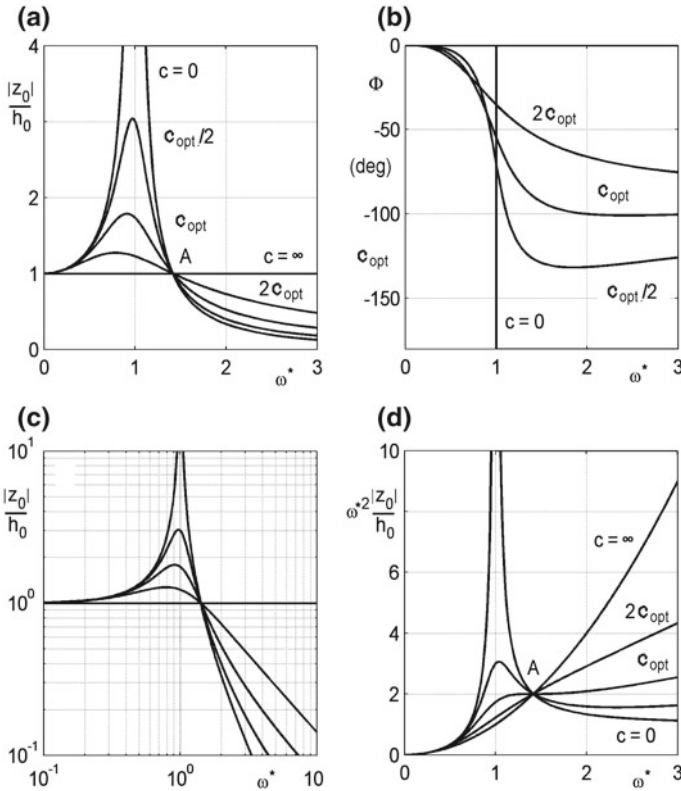


Fig. 26.8 Quarter-car with a single degree of freedom, response to harmonic excitation. Ratios between the amplitudes of the displacement (linear **(a)** and logarithmic **(c)** scales) and **d** the acceleration of the sprung mass, and the amplitude of the ground displacement and **b** phase, for different values of shock absorber damping. The responses are plotted as functions of the non-dimensional frequency $\omega^* = \omega\sqrt{m/K}$

Remark 26.3 Minimizing the vertical acceleration leads to minimizing the dynamic component of the vertical load on the tire, which has a negative influence on the ability of the tire to exert cornering forces. The condition leading to optimum comfort seems, then, to coincide with that leading to optimum handling performance.

Equation (26.12) allows one to choose the value of the damping coefficient c . For the value of the stiffness K there is no such optimization: To minimize both the acceleration and the dynamic component of the force, K should be kept as low as possible. The only limit to the softness of the springs is the space available.

Remark 26.4 This reasoning has, however, the following limitation: The softer the springs, the larger the oscillations of the sprung mass. Large displacements must be avoided because they may cause large errors in the working angles of the tire, causing the tires to work in conditions that may be far from optimal.

An empirical rule states that soft suspensions improve comfort while hard suspensions improve handling. This is even more true if aerodynamic devices are used to produce negative lift: suspensions allowing a large degree of travel cause major changes of vehicle position with respect to the airflow, producing changes of the aerodynamic force that are detrimental.

Moreover, at a fixed value of the sprung mass, the lower the stiffness of the spring, the lower the natural frequency. Very soft suspensions easily lead to natural frequencies of about 1 Hz or even less, which may cause motion sickness and a reduction in comfort that varies from person to person. Cars with soft suspensions with large travel, typical of some manufacturers, are popular with some customers but considered uncomfortable by others.

The optimum value of the damping expressed by Eq. (26.12) is lower than the critical damping. The quarter-car is then underdamped and may undergo free oscillations, even if these generally damp out quickly because the damping ratio $\zeta = c/c_{cr}$ is not very low:

$$\frac{c_{opt}}{c_{cr}} = \frac{1}{2\sqrt{2}} \approx 0.354. \quad (26.14)$$

Example 26.1 Consider a quarter-car model with the following characteristics: sprung mass $m = 250$ kg; stiffness $K = 25$ kN/m; damping coefficient $c = 2,150$ Ns/m.

Compute the natural frequency of the suspension and its frequency response. Assume that the vehicle travels at 30 m/s on a road that may be classified, following ISO standards, at the limit between class B and class C, and compute the power spectral density of the acceleration of the sprung mass and its root mean square value. Assess the performance of the quarter car in these conditions.

Frequency response. The natural frequency is

$$\omega = \sqrt{\frac{K}{m}} = 10 \text{ rad/s} = 1.59 \text{ Hz}$$

The value of the optimum damping is

$$c_{opt} = \sqrt{\frac{mK}{2}} = 1,770 \text{ Ns/m}$$

and thus the suspension has a damping higher than the optimum value.

The dynamic compliance, that is the ratio between the displacement of the sprung mass and that of the supporting point,

$$|H(\omega)| = \frac{|z_0|}{|h_0|} = \sqrt{\frac{K^2 + c^2\omega^2}{(K - m\omega^2)^2 + c^2\omega^2}}, \quad (26.15)$$

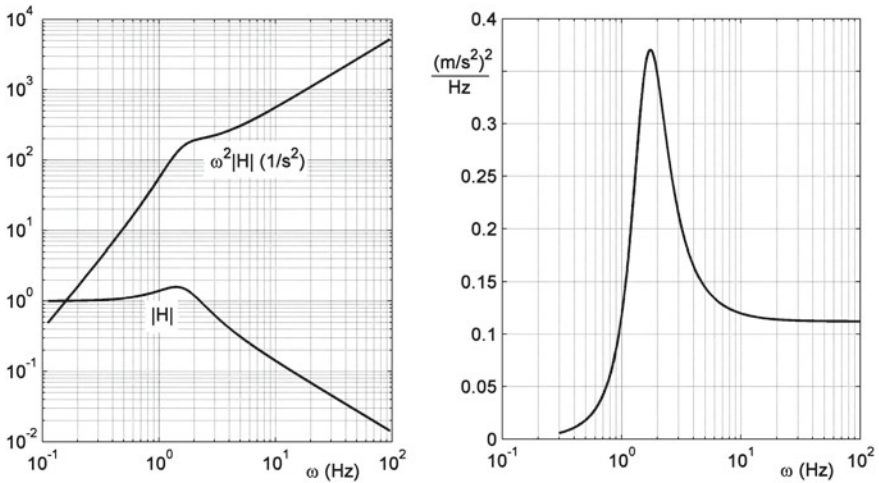


Fig. 26.9 Dynamic compliance and inertance of the quarter-car model with a single degree of freedom. Power spectral density of the acceleration due to motion on a road at the boundary between ISO classes B and C at a speed of 30 m/s

is plotted in Fig. 26.9, together with the inertance $\omega^2 H$, that is the ratio between the acceleration of the sprung mass and the displacement of the supporting point. Note the logarithmic scales.

Response to road excitation. The power spectral density is plotted in Fig. 26.2 in $m^2/(\text{cycles/m})$ as a function of the frequency ω' in cycles/m. The equation of the line dividing zone B from zone C is

$$S' = c\omega'^n,$$

where the frequency with respect to space is expressed in cycles/m and the power spectral density in $m^2/(\text{cycles/m})$; constants c and n are

$$c = 1.28 \times 10^{-6} \text{ m}, \quad n = -2$$

Computing the quantities referred to time from those referred to space at a speed of 30 m/s, it follows that

$$S = c'\omega^n$$

where, expressing ω in Hz and S in m^2/Hz ,

$$c' = \frac{c}{V^{n+1}} = 3.84 \times 10^{-5} \text{ m}^3 \text{ s}^{-2}.$$

The power spectral density of the acceleration of the sprung mass can thus be immediately computed by multiplying the square of the inertance by the power spectral density of the road profile, obtaining the result reported in Fig. 26.2. The r.m.s. value of the acceleration can be computed by integrating the power spectral density. The limits of integration referred to the space frequency are 0.01 and 10 cycles/m. By referring them to time, the frequency range extends from 0.3 to 300 Hz, obtaining

$$a_{rms} = 5.84 \text{ m/s}^2 = 0,60 \text{ g}.$$

This is a high value that causes reduced physical efficiency in less than 1 s at a frequency between 1 and 2 Hz, where the resonance of the sprung mass is located. This result should not surprise us, for the quarter car model has only one degree of freedom and no tire. From the power spectral density it is clear that the largest contribution to the integral is due to the range between 10 and 300 Hz, because the response is still quite high even with increasing frequency. The computation, performed by neglecting the ability of the tire to filter out the excitation at medium-high frequency, has little meaning.

What the example shows is that the suspension alone is unable to filter out road excitation, and that the presence of the tire is compulsory.

Because the quarter-car model is linear, the damper was assumed to be acting both in the jounce and in the rebound stroke (double effect damper) and to be symmetrical (having the same damping coefficient for motion in both directions). Dampers used in early automotive suspensions acted only in rebound and are today double effect, but they are not symmetrical because the damping coefficient in the jounce stroke is much lower than in the rebound stroke.

To understand the advantages of symmetrical double-effect dampers,⁹ consider a quarter-car with a single degree of freedom, passing at high speed over a bump or pothole (Fig. 26.10). If the time needed to cross the road irregularity is far shorter than the period of oscillation of the sprung mass (for instance, a bump 0.3 m long is crossed in 0.01 s at a speed of 30 m/s), an impulsive model can be used to compute the trajectory of the sprung mass. The effects of the perturbation to its motion can be considered as a variation of the vertical component of the momentum applied instantly. The trajectory of the sprung mass deviates by an angle α :

$$\tan(\alpha) = \frac{w}{u} ,$$

where w is the vertical component of the velocity. It can be computed using the momentum theorem

$$mw = \int_{t_1}^{t_2} F dt . \quad (26.16)$$

⁹Bourcier De Carbon C.: *Théorie mathématiques et réalisation pratique de la suspension amortie des vehicules terrestres*, Proceedings SIA Conference, Paris, 1950.

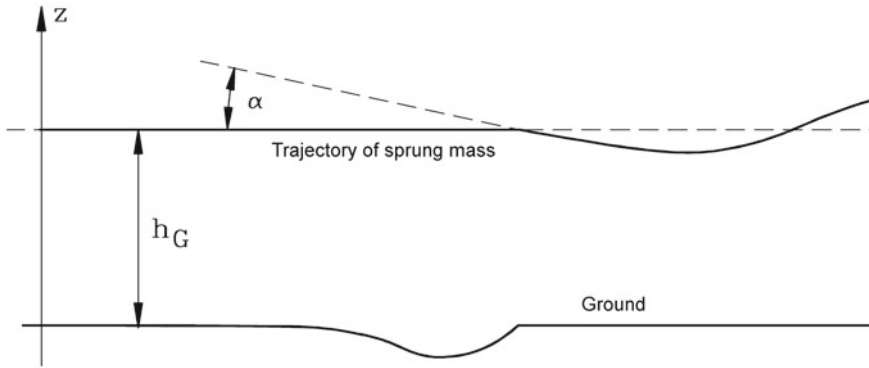


Fig. 26.10 Quarter-car with a rigid wheel crossing a ditch

The integral in Eq. (26.16) is the impulse of the forces due to the spring and to the damper from time t_1 , when the wheel enters the ditch, to time t_2 when it gets out

$$w = \frac{1}{m} \left(\int_{t_1}^{t_2} F_m dt + \int_{t_1}^{t_2} F_a dt \right). \tag{26.17}$$

The force due to the spring is the part exceeding the static value compensating for the weight. If the integrals on the right-hand side of Eq. (26.17) vanish, the suspension completely absorbs the irregularity, without any perturbation being transmitted to the sprung mass. The first of the two integrals is assumed to be far smaller than the second, because in a small amplitude, high frequency disturbance the force due to the spring, which is proportional to the displacement, is negligible compared to the force due to the shock absorber, which is proportional to the velocity. By neglecting the first integral and assuming that the damper is symmetrical, the expression for the vertical velocity becomes

$$w = \frac{1}{m} \int_{t_1}^{t_2} -c \dot{h} dt = -\frac{c}{m} (h_2 - h_1), \tag{26.18}$$

where $h(x)$ is the law expressing the road profile.

From Eq. (26.18) it is clear that if $h_2 = h_1$ the suspension is able to insulate the sprung mass perfectly from the road irregularity, a result that is due to the fact that the damping coefficient in rebound is equal to that in jounce.

This result, however, is compromised by the oversimplification of the model. It is well known that, while the shock absorber must act in both the up- and the down-stroke, the damping coefficients must be unequal for best performance. This is easily explained by noting that while the instant value of the force due to the shock absorber is larger than that due to the spring, the same inequality does not hold for the integrals, particularly when the first one vanishes. Another factor is that the road-wheel constraint is unilateral. The disturbance when crossing a bump at high speed

is higher than when crossing over a hole. In the first case, the force due to the spring acts upwards; in the second a damping coefficient higher in the downstroke gives a negative value of the second integral of Eq. (26.17), which may compensate for the positive value of the first one. Some approximations are also linked to the use of the impulsive model, particularly because if the unsprung mass and its natural frequency are accounted for, the time needed to cross the obstacle is no longer much smaller than the period of the free oscillations of the system.

Example 26.2 Consider the quarter-car with a single degree of freedom studied in Example 26.1, crossing at a speed $V = 30$ m/s over an obstacle with harmonic profile similar to the usual obstacles (Fig. 26.11c). Let the profile be

$$h = h_0 \sin \left[\pi \frac{x - x_1}{x_2 - x_1} \right] \quad (26.19)$$

with $h_0 = 100$ mm and a length $(x_2 - x_1)$ of 300 mm. Because

$$x = Vt, \quad (26.20)$$

the vertical velocity is

$$\dot{h} = \frac{\pi V h_0}{x_2 - x_1} \cos \left[\pi \frac{x - x_1}{x_2 - x_1} \right]. \quad (26.21)$$

Equation (26.7) was numerically integrated, with the results shown in Fig. 26.11a in terms of displacements and in Fig. 26.11b in terms of velocity. The quarter-car with symmetric damper (full line curve) succeeds well at filtering out the obstacle, with a maximum displacement of 6 mm. (6% of the displacement of the supporting point). The plot of the velocity shows that the negative impulse in the second part of the obstacle practically balances the positive impulse in the first one.

The dashed line was computed by neglecting the contribution of the spring to the impulse.

The dotted line was computed assuming that the damper has a coefficient in the jounce stroke equal to 80% of that in the rebound stroke. It is clear that the best performance is obtained with a symmetric damper. This consideration is, however, dependent on the extreme simplification of the model. Among other simplifications, the mono-lateral nature of the road-wheel contact has been neglected.

26.4.2 Quarter-Car with Two Degrees of Freedom

The following model is that shown in Fig. 26.7b. It is well suited for the study of the behavior of vehicle suspensions in a frequency range beyond the natural frequency of the unsprung mass.

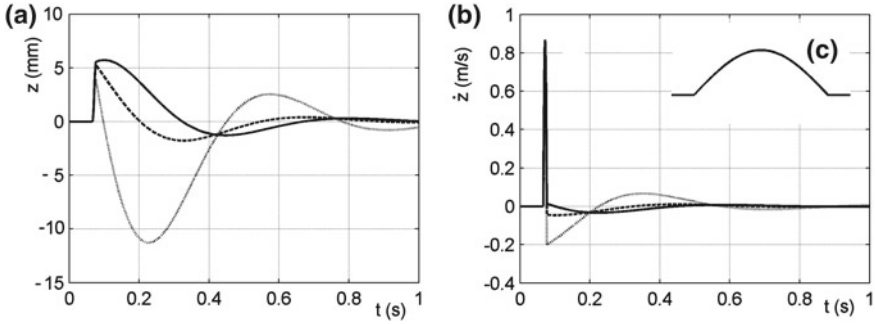


Fig. 26.11 Response in terms of displacement (a) and velocity (b) of a single degree of freedom quarter-car model crossing at 30 m/s a bump 300 mm wide and 100 mm high (c). Full line: symmetric damper; dashed line: the contribution of the spring to the impulse has been neglected; dotted line: asymmetric damper

With reference to Fig. 26.7b, the equation of motion of the model is

$$\begin{aligned}
 & \begin{bmatrix} m_s & 0 \\ 0 & m_u \end{bmatrix} \begin{Bmatrix} \ddot{z}_s \\ \ddot{z}_u \end{Bmatrix} + \begin{bmatrix} c & -c \\ -c & c + c_p \end{bmatrix} \begin{Bmatrix} \dot{z}_s \\ \dot{z}_u \end{Bmatrix} + \\
 & + \begin{bmatrix} K & -K \\ -K & K + P \end{bmatrix} \begin{Bmatrix} z_s \\ z_u \end{Bmatrix} = \begin{Bmatrix} 0 \\ c_p \dot{h} + Ph \end{Bmatrix}, \tag{26.22}
 \end{aligned}$$

where z_s and z_u are the displacements from the static equilibrium position and are referred to an inertial frame.

The response to a harmonic excitation $h(t)$ is readily obtained in the same way used for the previous model and yields a harmonic oscillation, not in phase with the excitation. The relationship linking the complex amplitudes of the response and the excitation is

$$\begin{aligned}
 & \left\{ -\omega^2 \begin{bmatrix} m_s & 0 \\ 0 & m_u \end{bmatrix} + i\omega \begin{bmatrix} c & -c \\ -c & c + c_p \end{bmatrix} + \right. \\
 & \left. + \begin{bmatrix} K & -K \\ -K & K + P \end{bmatrix} \right\} \begin{Bmatrix} z_{s0} \\ z_{u0} \end{Bmatrix} = h_0 \begin{Bmatrix} 0 \\ i\omega c_p + P \end{Bmatrix}. \tag{26.23}
 \end{aligned}$$

By neglecting the damping of the tire c_p , which is usually small, the amplification factors of the sprung and unsprung masses are

$$\begin{cases} \frac{|z_{s0}|}{|h_0|} = P \sqrt{\frac{k^2 + c^2\omega^2}{f^2(\omega) + c^2\omega^2 g^2(\omega)}} \\ \frac{|z_{u0}|}{|h_0|} = P \sqrt{\frac{(k - m\omega^2)^2 + c^2\omega^2}{f^2(\omega) + c^2\omega^2 g^2(\omega)}} \end{cases}, \tag{26.24}$$

where

$$\begin{cases} f(\omega) = m_s m_u \omega^4 - [P m_s + K(m_s + m_u)] \omega^2 + K P \\ g(\omega) = (m_s + m_u) \omega^2 - P . \end{cases}$$

The dynamic component of the force exerted by the tire on the ground in the z direction may be easily computed in a similar way. The force in the z direction is

$$F_z = -P (z_u - h) \quad (26.25)$$

and thus

$$|F_{z0}| = P (|z_u - h|) . \quad (26.26)$$

The modulus of $z_u - h$ is not coincident with the difference between the modulus of z_u and that of h because the two time histories are out of phase with each other. By performing the relevant computations, it follows that

$$\frac{|F_{z0}|}{|h_0|} = P \omega^2 \sqrt{\frac{[K(m_s + m_u) - m_s m_u \omega^2]^2 + c^2(m_s + m_u) \omega^2}{f^2(\omega) + c^2 \omega^2 g^2(\omega)}} . \quad (26.27)$$

The frequency responses related to both the sprung and the unsprung masses are plotted in Fig. 26.12a, b for a system with $P = 4K$ and $m_s = 10m_u$. The plots, shown using the non-dimensional frequency

$$\omega^* = \omega \sqrt{\frac{m}{K}} , \quad (26.28)$$

include curves obtained with different values of damping c ; all curves lie in the non-shaded region of the graph.

If $c = 0$ the natural frequencies are two and the peaks are infinitely high. Also for $c \rightarrow \infty$ the peak, corresponding to the natural frequency of the whole system, which is now rigid, over the spring simulating the tire, goes to infinity.

The frequency responses of Fig. 26.12a, b multiplied by ω^{*2} are shown in Fig. 26.12c, d; they give the non-dimensional ratio between the accelerations of the two masses and the displacement of the supporting point (suitably made non-dimensional). All curves pass through points O, A, B and C. Between O and A and between B and C the maximum acceleration of the sprung mass increases with decreasing damping, while between A and B and from C upwards it increases with damping.

An optimum value of damping can be found by trying to keep the acceleration as low as possible in a large range extending up to the natural frequency of the unsprung mass, i.e. by looking for a curve having a relative maximum or a stationary point in A. Operating as seen with the previous model, the following value is obtained

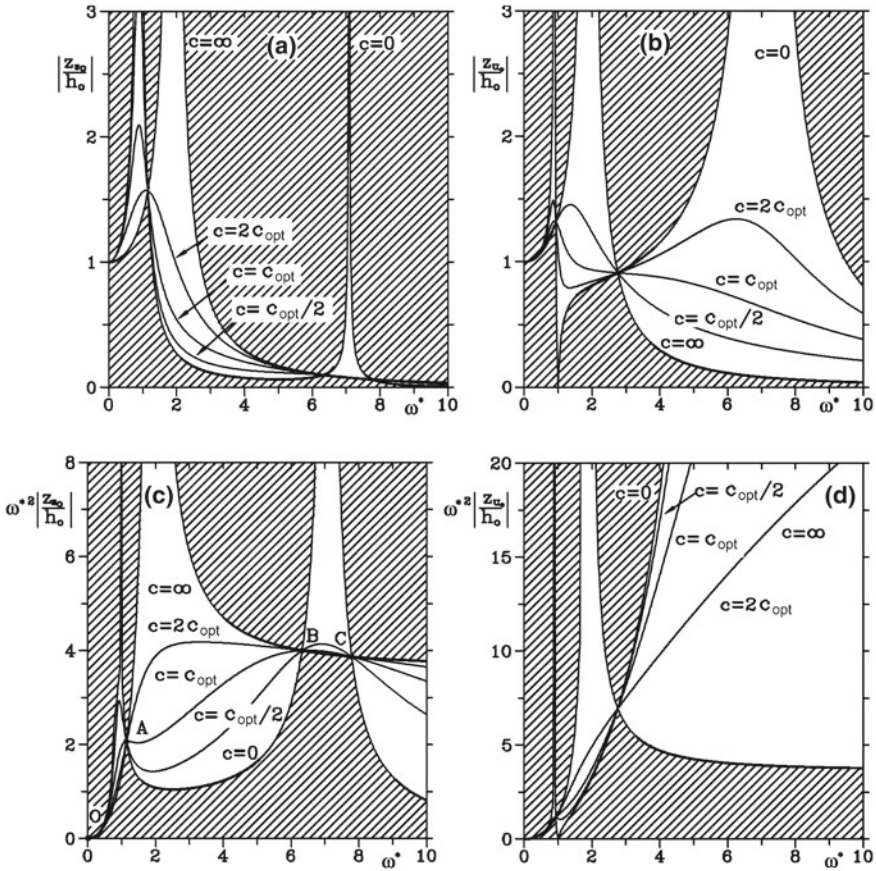


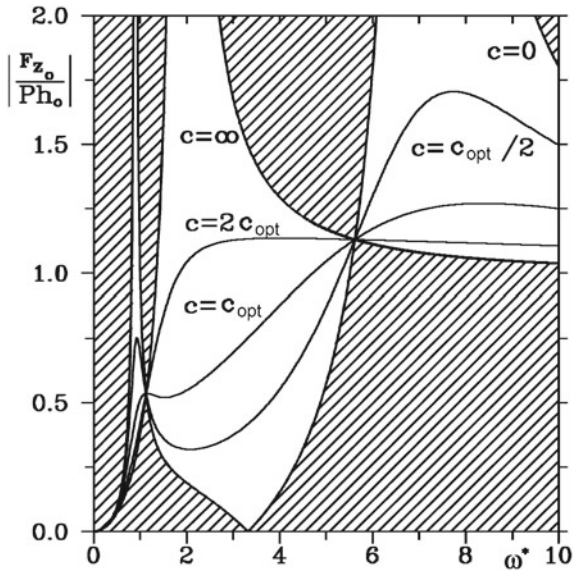
Fig. 26.12 Quarter-car with two degrees of freedom, response to harmonic excitation. Ratios between the amplitudes of the displacements of the sprung and the unsprung masses (**a, b**) and of the accelerations (**c, d**) to the amplitude of the displacement of the ground, for different values of the damping of the shock absorber. The responses are plotted as functions of the nondimensional frequency $\omega^* = \omega\sqrt{m/K}$

$$c_{opt} = \sqrt{\frac{Km}{2}} \sqrt{\frac{P + 2K}{P}} \tag{26.29}$$

Because P is much larger than K , the value of $\sqrt{(P + 2K)/P}$ is close to unity (in the case of Fig. 26.12 $\sqrt{(P + 2K)/P} = 1.22$) and the optimum damping is only slightly larger than that computed for the model with a single degree of freedom (Eq. (26.12)). From Fig. 26.12c it is clear that this value of damping is effective in keeping the acceleration low in a wide frequency range.

The amplitude of the dynamic component of force F_z (Eq. (26.29)) is plotted in non-dimensional form (divided by $P|h_0|$) as a function of the nondimensional

Fig. 26.13 Quarter-car with two degrees of freedom, response to harmonic excitation. Ratio between the amplitude of the dynamic component of force F_z between tire and road and the displacement of the ground, made non-dimensional by dividing it by the stiffness of the tire P , for different values of the damping of the shock absorber. The response is plotted as a function of the non-dimensional frequency $\omega^* = \omega\sqrt{m/K}$



frequency in Fig. 26.13. The value of the optimum damping expressed by Eq. (26.29) is also effective in keeping the maximum value of the dynamic component of force F_z as low as possible, at least at low frequencies. At higher frequencies, a slightly higher value of damping could be effective, even if it would result in a larger acceleration of the sprung mass.

The maximum value of the non-dimensional amplitude of force F_z has been plotted as a function of ratio c/c_{opt} in Fig. 26.14a. When the damping goes beyond the optimum value computed above, a certain decrease of the maximum amplitude of the force at high frequency is clearly obtained.

The minimum value of the force on the ground (computed as the static component minus the amplitude of the dynamic component) has been plotted as a function of ratio c/c_{opt} in Fig. 26.14b, using data similar to those related to the front suspension of a small car. The curves refer to different amplitudes of the excitation h_0 . If the damping is small enough the wheel can bounce on the road. Clearly, when this occurs the present linear model is no longer applicable.

Example 26.3 Repeat the computations of example 26.1 using a quarter-car model with two degrees of freedom. To the data already considered (sprung mass $m_s = 250$ kg; stiffness of the spring $K = 25$ kN/m; damping coefficient of the damper $c = 2,150$ Ns/m.) add the following: unsprung mass $m_u = 25$ kg; stiffness of the tire $k_t = 100$ kN/m.

Compute the r.m.s. value of the acceleration as a function of the speed.

Natural frequencies. The optimum damping is

$$c_{opt} = 2,170 \text{ Ns/m,}$$

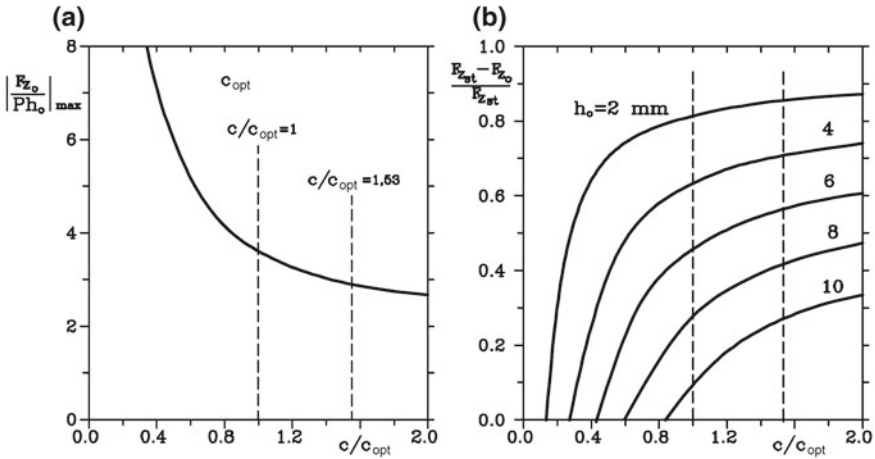


Fig. 26.14 **a** Maximum value of the amplitude of the dynamic component of force F_z in a frequency range between 0 and $30 \sqrt{K/m}$ as a function of ratio c/c_{opt} . Same characteristics as the system studied in the previous figures. **b** Minimum value of the ground force (static force minus amplitude of the dynamic component) as a function of ratio c/c_{opt} for a quarter car model with parameters typical for a small car: $m_s = 238$ kg; $m_u = 38$ kg; $K = 15.7$ kN/m; $P = 135$ kN/m; actual value of c/c_{opt} equal to 1.53

a value very close to the actual one.

The characteristic equation allowing the natural frequencies of the undamped system to be computed is

$$\omega^4 - 5.100\omega^2 + 400.000 = 0.$$

The values of the natural frequencies are then

$$\begin{cases} \omega_1 = 8.93 \text{ rad/s} = 1.421 \text{ Hz} \\ \omega_2 = 70.85 \text{ rad/s} = 11.28 \text{ Hz.} \end{cases}$$

Frequency response. The dynamic compliance $H(\omega)$ and the inertance are plotted in Fig. 26.15.

Response to road excitation. The power spectral density can be computed in a way similar to what was seen in the previous example. The result is plotted in Fig. 26.15.

The r.m.s. value of the acceleration is

$$a_{rms} = 1.34 \text{ m/s}^2 = 0.136 \text{ g.}$$

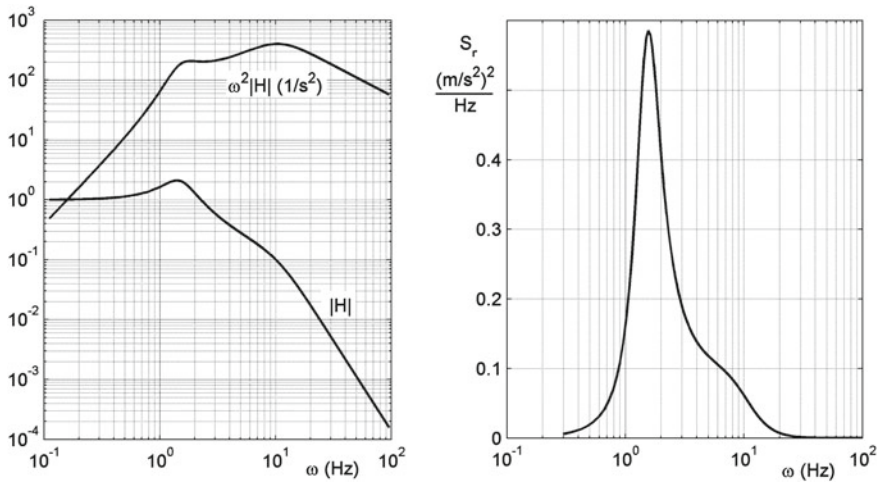


Fig. 26.15 Dynamic compliance and inertance of the quarter-car model with two degrees of freedom. Power spectral density of the acceleration due to motion on a road at a speed of 30 m/s

By comparing the results of the two examples it is clear that the presence of the tire is effective in filtering out high frequency disturbances, while the transmissibility at the natural frequency is slightly higher. At any rate, the r.m.s. value of the acceleration is now acceptable, even if it is not optimal. From the plot of Fig. 26.4, it is clear that this value causes reduced physical efficiency in 3 h; however, the driver and the passengers are also insulated from vibration from the road by the seats.

Considering the integral between a wavelength of 0.1 and 100m is practically equivalent to considering the whole spectrum from 0 to infinity, because the power spectral density vanishes outside this range.

The computation has been repeated for various values of the speed and the results are shown in Fig. 26.16. The r.m.s. value of the acceleration grows with increasing speed.

From the considerations above it is possible to draw the conclusion that the value of the damping coefficient expressed in Eq. (26.29) is optimal both from the viewpoint of comfort and of handling, because it leads to low variations in the forces on the ground. A slightly higher damping may, however, somewhat improve handling because it slightly reduces the variable component of the force on the ground.

This conclusion, obtained from a highly simplified model, is not in good accordance with experimental evidence stating that the value of damping for optimizing riding comfort is lower than that for optimizing handling.

To optimize the value of the damping coefficient of the suspension it is possible to consider motion on a road profile of the type defined by ISO 8606:1995 standard and expressed by Eq. (26.1) with $n = 2$. An excitation of this type may be considered, as already stated, as a white noise in terms of velocity, defined in the frequency range between 0.01 and 10 cycles/m.

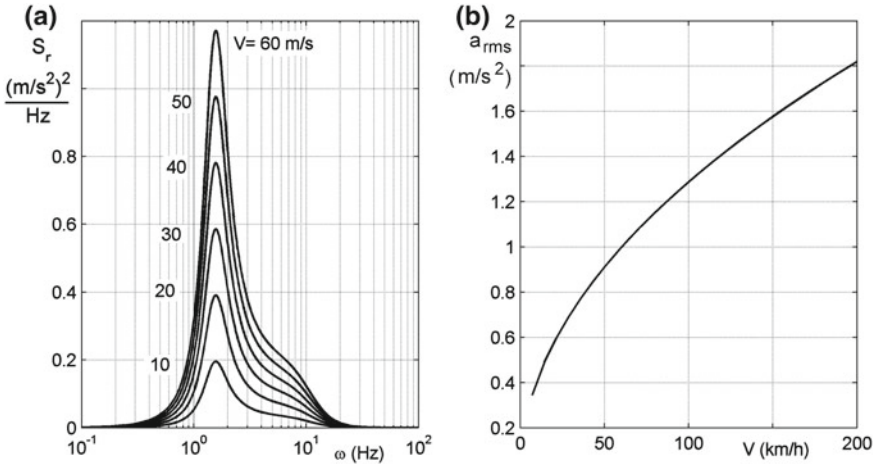


Fig. 26.16 Power spectral density of the acceleration of the sprung mass (a) and its r.m.s. value (b) at different values of the speed of the vehicle

The power spectral density of the vertical displacement of the contact point with the ground can be expressed as

$$S = cV\omega^{-2} . \tag{26.30}$$

In S.I. units (rad/s), the value of coefficient c is that reported in Table 26.1 multiplied by 2π . The frequency range in which the spectrum is defined is between frequencies ω_1 and ω_2 , where:

$$\omega_1 = 0,01 * 2\pi V , \quad \omega_2 = 10 * 2\pi V . \tag{26.31}$$

The r.m.s. value of the vertical acceleration of the sprung mass is

$$a_{rms} = \sqrt{\int_{\omega_1}^{\omega_2} \omega^4 H^2 S d\omega} = \sqrt{cV} \sqrt{\int_{\omega_1}^{\omega_2} \omega^2 H^2 d\omega} , \tag{26.32}$$

where H is the frequency response yielding the displacement of the sprung mass.

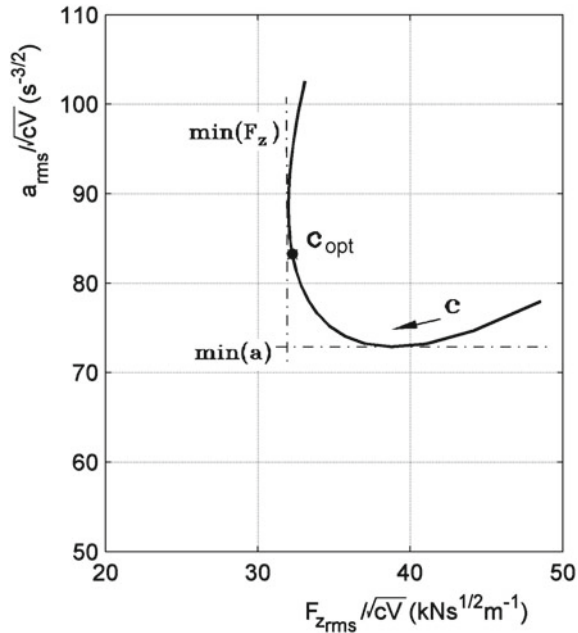
In a similar way the r.m.s. value of the variable component of the vertical road-tire force on the ground is

$$F_{z_{rms}} = \sqrt{\int_{\omega_1}^{\omega_2} H_F^2 S d\omega} = \sqrt{cV} \sqrt{\int_{\omega_1}^{\omega_2} \frac{H_F^2}{\omega^2} d\omega} , \tag{26.33}$$

where H_F is the frequency response yielding the variable component of the force.

The r.m.s. values of the acceleration and of the dynamic component of force F_z are easily computed for different values of the damping coefficient of the shock absorber.

Fig. 26.17 Ratio a_{rms}/\sqrt{cV} versus $F_{z,rms}/\sqrt{cV}$ for the quarter-car model with two degrees of freedom with the same data as in Fig. 26.14b ($m_s = 238$ kg; $m_u = 38$ kg; $K = 15.7$ kN/m; $P = 135$ kN/m). Computation referred to a speed of 30 m/s



The plot of the former versus the latter allows some interesting conclusions to be drawn on the choice of the value of the damping (Fig. 26.17).

It must be remembered that ratios a_{rms}/\sqrt{cV} and $F_{z,rms}/\sqrt{cV}$ are independent from c , that is from the characteristics of the road, but not completely independent from the speed. Actually they would be so if the integrals were computed in a frequency range from 0 to infinity, but the speed is included in the integration limits here defined.

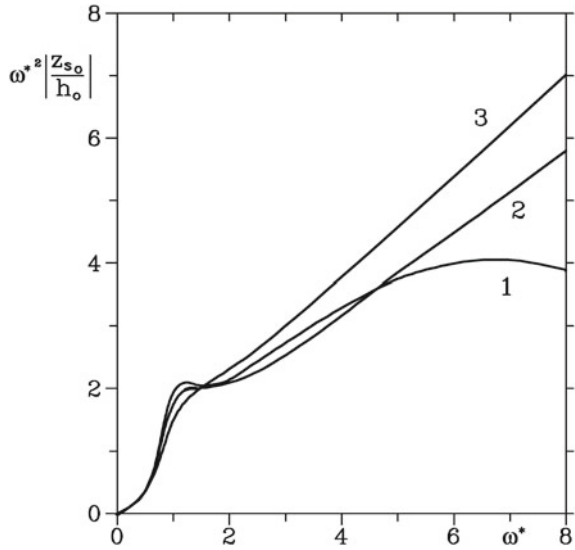
Remark 26.5 The conditions leading to optimum comfort (in the sense of minimum acceleration) and to optimum handling (in the sense of minimum force variations) are readily identified: The first is obtained with a damping lower than the optimum damping defined above, while the second for a damping value that is higher. This result is in better accordance with experimental results than the previous one.

As already stated, the presence of the tires has a negligible effect on the frequency response at low frequency, while at higher frequencies their stiffness must be accounted for. A comparison between the results obtained using the quarter-car models with one and two degrees of freedom is shown in Fig. 26.18.

26.4.3 International Roughness Index

As already stated, the International Roughness Index (IRI) is defined with reference to a particular quarter-car with two degrees of freedom moving at a specified speed.

Fig. 26.18 Acceleration of the sprung mass as a function of the frequency for a unit displacement input. Comparison between the quarter-car model with one and two degrees of freedom (in the latter case $P = 4K$, $m_s = 10m_u$). (1): Two degrees of freedom; (2): One degree of freedom, damping defined by Eq. (26.29); (3): One degree of freedom, damping defined by Eq. (26.12)



The data of the quarter-car, often defined as *golden car*, are:

$$\frac{K}{m_s} = 63, 3 \text{ s}^{-2}, \frac{P}{m_s} = 653 \text{ s}^{-2}, \frac{m_u}{m_s} = 0, 15, \frac{c}{m_s} = 6 \text{ s}^{-1} .$$

The value of the optimum damping is

$$\frac{c_{opt}}{m_s} = 6, 147 \text{ s}^{-1}$$

and thus the model has a damping that is close to optimal.

The reference speed is 80 km/h.

To define the Roughness Index of a given road profile, the motion of the quarter-car is simulated and the cumulative travel of the sprung mass with respect to the unsprung mass is calculated over time. The index is the total value of the travel divided by the distance travelled by the vehicle

$$IRI = \frac{1}{VT} \int_0^T |\dot{z}_s - \dot{z}_s| dt . \tag{26.34}$$

The index so defined is a non-dimensional quantity, but one that is often measured in non-consistent units, [m/km] or [in/mi]. A correlation between the road characteristics and the roughness index is shown in Fig. 26.19.

Remark 26.6 The Roughness Index may also be interpreted as the average value of the absolute value of the relative speed of the two masses divided by the vehicle speed.

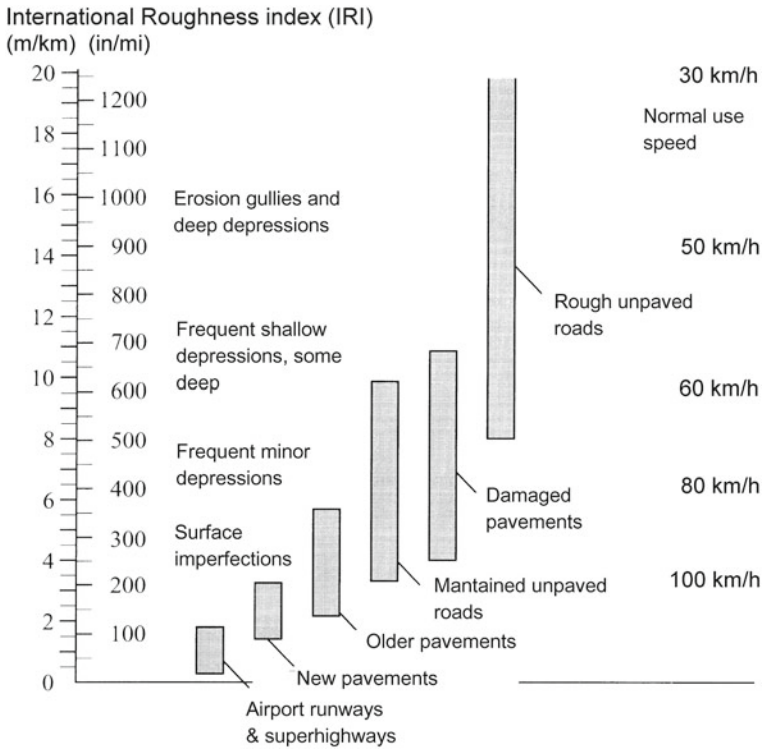


Fig. 26.19 Correlation between the road characteristics and the roughness index

The use of an index to define the quality of the road surface, one based on the ratio between the total motion of the suspension and the distance travelled, dates back to the 1940s. It is used at present by many international organizations. Since 1982 the World Bank has used it to compare road conditions in various countries. It has been shown that a good correlation exists between the index and both the vertical acceleration and the variation of the force on the ground; this property allows the comfort and the performance on a given road to be understood.

26.4.4 *Quarter-Car with Secondary Suspension (Three Degrees of Freedom)*

In many vehicles the suspensions are not assembled directly to the body, but are mounted on a secondary frame, one that often carries other elements with a non-negligible mass as well. This auxiliary frame is connected to the chassis with a

secondary suspension made by elastomeric mounts. A quarter car of this type is shown in Fig. 26.7c).

Its equation of motion is

$$\begin{aligned} & \begin{bmatrix} m_s & 0 & 0 \\ 0 & m_t & 0 \\ 0 & 0 & m_u \end{bmatrix} \begin{Bmatrix} \ddot{z}_s \\ \ddot{z}_t \\ \ddot{z}_u \end{Bmatrix} + \begin{bmatrix} c & -c & 0 \\ -c & c + c_t & -c_t \\ 0 & -c_t & c_t + c_p \end{bmatrix} \begin{Bmatrix} \dot{z}_s \\ \dot{z}_t \\ \dot{z}_u \end{Bmatrix} + \\ & + \begin{bmatrix} K & -K & 0 \\ -K & K + K_t & -K_t \\ 0 & -K_t & K_t + P \end{bmatrix} \begin{Bmatrix} z_s \\ z_t \\ z_u \end{Bmatrix} = \begin{Bmatrix} 0 \\ 0 \\ c_p \dot{h} + Ph \end{Bmatrix}. \end{aligned} \tag{26.35}$$

The response to a harmonic excitation can be computed as with previous models.

Example 26.4 Repeat the computations of the previous example assuming that a secondary suspension is located between the sprung and unsprung masses. The data are: sprung mass $m_s = 250$ kg; mass of the auxiliary frame $m_t = 10$ kg; unsprung mass $m_u = 25$ kg; stiffness of the spring $K = 25$ kN/m; stiffness of the spring of the auxiliary suspension $K_t = 100$ kN/m; stiffness of the tire $k_t = 100$ kN/m; damping coefficient of the damper $c = 2,150$ Ns/m; damping coefficient of the auxiliary suspension $c_t = 5,000$ Ns/m.

The values of the natural frequencies are

$$\begin{cases} \omega_1 = 8.30 \text{ rad/s} = 1.32 \text{ Hz} \\ \omega_2 = 59.68 \text{ rad/s} = 9.50 \text{ Hz} \\ \omega_3 = 130.28 \text{ rad/s} = 20.73 \text{ Hz}. \end{cases}$$

The dynamic compliance $H(\omega)$ and the inertance $\omega^2 H$ are plotted in Fig. 26.20, along with the power spectral density of the acceleration of the sprung mass when the vehicle travels at 30 m/s on a road defined as in-between classes B and C ISO 8606: 1995.

The r.m.s. value of the acceleration is

$$a_{rms} = 1.21 \text{ m/s}^2 = 0.12 \text{ g}.$$

The auxiliary suspension improves comfort slightly. By comparing the plots, however, it is clear that the improvement is concentrated in the medium-high frequency range. If the comparison were done at a higher speed, in a condition in which high frequency excitation were more significant, the improvement would be larger.

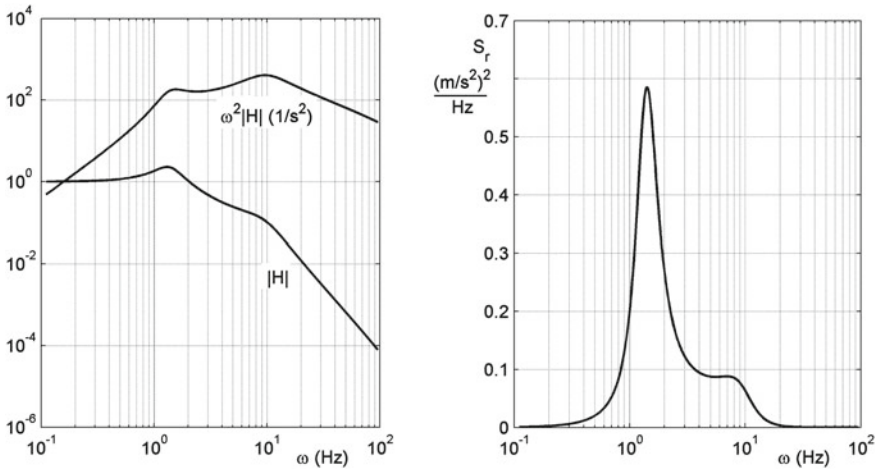


Fig. 26.20 Dynamic compliance and inertance of the quarter-car model with three degrees of freedom. Power spectral density of the acceleration due to motion on a road at a speed of 30 m/s

26.4.5 Quarter-Car Model with Dynamic Vibration Absorber

A dynamic vibration absorber essentially consists of a mass connected to the system through a spring and possibly a damper (Fig. 26.21a). If properly tuned, it can reduce the amplitude substantially at one of the resonances of the original system, but it introduces an additional resonance whose peak amplitude is controlled by the value of its damping c_d .

The frequency response of the system of Fig. 26.21a is shown in Fig. 26.21c for three different values of damping: If c_d is low, two resonance peaks are present, while if c_d is high, there is only one peak. If the damping tends to zero the two peaks have an infinite height, while if it tends to infinity the system reduces to an undamped system with a single degree of freedom and thus a single peak with infinite height. It is possible to demonstrate that the stiffness k_d which reduces the amplitude of the motion of mass m to a minimum is¹⁰

$$(K_d)_{opt} = K \frac{mm_d}{(m + m_d)^2} . \tag{26.36}$$

The value $(c_d)_{opt}$ of the damping necessary to obtain such a minimum and the peak amplitude are respectively

$$(c_d)_{opt} = \frac{m_d}{m + m_d} \sqrt{K \frac{3mm_d}{2(m + m_d)}} , \quad \left| \frac{z_0}{h_0} \right|_{max} = \sqrt{1 + \frac{2m}{m_d}} . \tag{26.37}$$

¹⁰J.P. Den Hartog, *Mechanical vibrations*, McGraw Hill, New York, 1956.

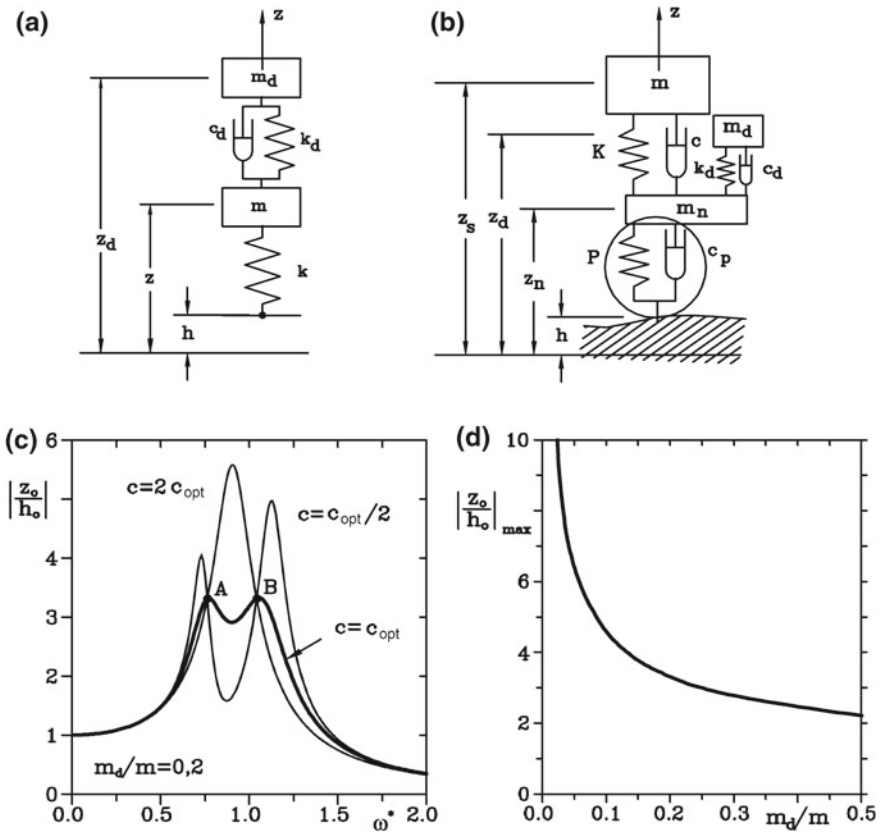


Fig. 26.21 Dynamic vibration absorber, applied to a spring-mass system (a) and to a quarter-car model (b). Frequency response of the first of the two systems for different values of c_d and with $m_d/m = 0.2$ (c) and value of the peak amplitude with optimum damping as a function of the mass ratio m_d/m (d)

Sometimes the vibration absorber may have no elastic element or may be provided with a damper whose behavior is modelled better by dry friction than by viscous damping.

Dynamic vibration absorbers are sometimes used in motor vehicle suspensions, as in the quarter-car model of Fig. 26.21b, in which a standard shock absorber is also represented. The equation of motion of the system is

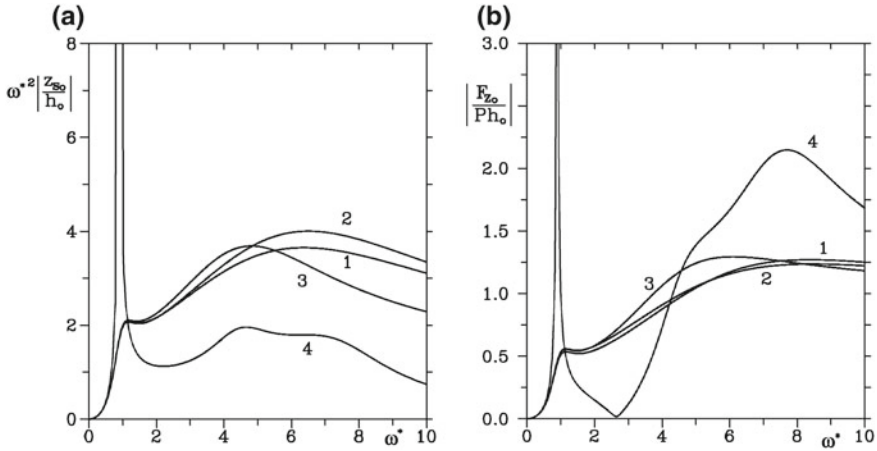


Fig. 26.22 Quarter-car model with dynamic vibration absorber: Non-dimensional amplitude of the acceleration (a) and of the dynamic component of the force F_z (b) as functions of the non-dimensional frequency ω^* ($P = 4K$; $m_s = 10m_u$; $c = \sqrt{6mK/8}$). Line 1: quarter-car without vibration absorber; line 2: $m_d = 0.05m_s$, $\sqrt{k_d/m_d} = 0.89$, $c_d = 2\sqrt{k_d m_d}$; line 3: $m_d = 0.05m_s$, $\sqrt{k_d/m_d} = 7.09$, $c_d = 2\sqrt{k_d m_d}$; line 4: $m_d = 0.05m_s$, $c = 0$, $\sqrt{k_s/m_s} = 4.8$, $c_s = 0.8\sqrt{k_s m_s}$

$$\begin{aligned}
 & \begin{bmatrix} m_s & 0 & 0 \\ 0 & m_d & 0 \\ 0 & 0 & m_u \end{bmatrix} \begin{Bmatrix} \ddot{z}_s \\ \ddot{z}_d \\ \ddot{z}_u \end{Bmatrix} + \begin{bmatrix} c & 0 & -c \\ 0 & c_d & -c_d \\ -c & -c_d & c + c_d + c_p \end{bmatrix} \begin{Bmatrix} \dot{z}_s \\ \dot{z}_d \\ \dot{z}_u \end{Bmatrix} + \\
 & + \begin{bmatrix} K & 0 & -K \\ 0 & K_d & -K_d \\ -K & -K_d & K + K_d + P \end{bmatrix} \begin{Bmatrix} z_s \\ z_d \\ z_u \end{Bmatrix} = \begin{Bmatrix} 0 \\ 0 \\ c_p \dot{h} + Ph \end{Bmatrix}. \tag{26.38}
 \end{aligned}$$

The various frequency responses may be obtained immediately as with the other quarter-car models. Some results are reported in Fig. 26.22. Because no attempt has been made to optimize the suspension, the figure has only a qualitative interest.

Curve 1 deals with a conventional quarter-car model as studied in the previous section. Curves 2 and 3 refer to a system in which a vibration absorber is applied to the unsprung mass, tuned on the first and the second natural frequency ($\sqrt{k_d/m_d} = 0.89$ and $\sqrt{k_d/m_d} = 7.09$). The mass of the vibration absorber is 1/20 of the sprung mass and the damping c_d is $2\sqrt{k_d m_d}$.

To add a vibration absorber to a conventional suspension changes its performance only slightly, both in terms of acceleration of the sprung mass and of forces on the ground. But vibration absorbers are interesting because of the possibility of using them instead of conventional shock absorbers, as in the case shown by curve 4.

In the case shown, in which the values of the parameters were obtained by trial and error without a true optimization, the acceleration of the sprung mass is quite low in the entire frequency range, except for a strong resonance peak at low frequency.

Remark 26.7 The height of the peak is obviously limited, however, because some damping is present, and in practice is further limited by the other forms of damping present in the actual system, such as that due to the tire.

If the stiffness of the springs K is low, the peak occurs at very low frequency, where its importance may be marginal, and the advantages of the vibration absorber, primarily linked to lower cost and complexity of the system due to elimination of the need for an element mounted between the body and the wheel, add to its excellent suspension performance.

Dynamic vibration absorbers, used instead of conventional shock absorbers, proved advantageous on several low cost small cars with soft suspensions; they may also, however, be added to conventional luxury cars to further increase ride comfort.

26.4.6 *Quarter-Car with Many Degrees of Freedom to Study the Suspension-Tire Interaction*

In the model of Fig. 26.7c, an additional degree of freedom has been included to account for the compliance of the tire. To proceed in a more comprehensive way it is possible to use the component mode synthesis approach, which is theoretically applicable only if the tire is a linear elastic system, or at least a lightly damped but nonetheless linear system.

The part of the system that may be considered a substructure can be identified. When the system is discretized and the generalized coordinates are the displacements of a certain number of points (the nodes), it is possible to subdivide the nodes into two groups: the connection nodes, that are common to the substructure and to other parts of the system, and the internal nodes. The vector of the generalized coordinates and the stiffness matrix of the substructure may be accordingly partitioned

$$\mathbf{q} = \begin{Bmatrix} \mathbf{q}_1 \\ \mathbf{q}_2 \end{Bmatrix}, \quad \mathbf{K} = \begin{bmatrix} \mathbf{K}_{11} & \mathbf{K}_{12} \\ \mathbf{K}_{21} & \mathbf{K}_{22} \end{bmatrix}, \quad (26.39)$$

where subscripts 1 and 2 refer respectively to the boundary and the internal degrees of freedom. The other matrices (mass and damping matrices) may be partitioned in the same way.

In the present case, if the tire is a substructure, the connection nodes are located on the wheel rim and the internal nodes are all others. If the rim is a rigid body and, as in the case of the quarter-car model, only the vertical displacement is considered, the only generalized coordinate that is common to the tire and the other parts of the system is displacement z_u (\mathbf{q}_1 has just one element).

Consider the tire in its deformed configuration under the static forces due to the load applied to the suspension and linearize its behavior about this configuration. Neglecting the forces applied to the internal nodes in the static configuration, vector \mathbf{q}_2 is

$$\mathbf{q}_2 = \mathbf{K}_{22}^{-1} \mathbf{K}_{21} \mathbf{q}_1. \quad (26.40)$$

To express the dynamic deflected configuration it is ideally possible to lock the boundary nodes (in this case by constraining the rim of the wheel) and perform dynamic analysis. The natural frequencies and the mode shapes of the tire are then obtained by solving the eigenproblem related to matrices \mathbf{K}_{22} and \mathbf{M}_{22} :

$$\det(-\omega^2 \mathbf{M}_{22} + \mathbf{K}_{22}) = 0.$$

Once the eigenproblem has been solved, it is possible to use the eigenvector matrix Φ to perform the modal transformation

$$\mathbf{q}_2 = \Phi \eta_2.$$

The generalized coordinates of the substructure can thus be expressed as

$$\begin{aligned} \begin{Bmatrix} \mathbf{q}_1 \\ \mathbf{q}_2 \end{Bmatrix} &= \begin{Bmatrix} \mathbf{q}_1 \\ -\mathbf{K}_{22}^{-1} \mathbf{K}_{21} \mathbf{q}_1 + \Phi \eta_2 \end{Bmatrix} = \\ &= \begin{bmatrix} \mathbf{I} & \mathbf{0} \\ -\mathbf{K}_{22}^{-1} \mathbf{K}_{21} & \Phi \end{bmatrix} \begin{Bmatrix} \mathbf{q}_1 \\ \eta_2 \end{Bmatrix} = \Psi \begin{Bmatrix} \mathbf{q}_1 \\ \eta_2 \end{Bmatrix}. \end{aligned} \quad (26.41)$$

Equation (26.41) is a coordinate transform, allowing the deformation of the internal part of the substructure to be expressed in terms of constrained and internal modes. Matrix Ψ expressing this transformation can be used to compute new mass, stiffness and, if needed, damping matrices and a force vector

$$\mathbf{K}^* = \Psi^T \mathbf{K} \Psi, \quad \mathbf{M}^* = \Psi^T \mathbf{M} \Psi, \quad \mathbf{C}^* = \Psi^T \mathbf{C} \Psi, \quad \mathbf{f}^* = \Psi^T \mathbf{f}. \quad (26.42)$$

If the constrained coordinates are m (in the present case $m = 1$) and the internal coordinates are n and only k modes of the constrained substructure are considered ($k < n$), the size of the original \mathbf{M} , \mathbf{K} , etc. matrices is $m + n$, while that of matrices \mathbf{M}^* , \mathbf{K}^* , etc. is $m + k$.

Remark 26.8 If all internal modes are considered ($k = n$) the method does not introduce errors, but there is no simplification. Both approximation and simplification increase while decreasing the number of modes considered.

The substructure so obtained can be easily assembled to the other parts of the system. If, for instance, only one boundary degree of freedom (the vertical displacement of the unsprung mass) and only one vibration mode of the tire are considered, the quarter-car model has three degrees of freedom, two ‘physical’ ones (displacements of the sprung and unsprung masses) plus a modal one.

Example 26.5 Consider the quarter-car model of the previous examples, taking into account the inertia of the tire as well. A realistic model of the tire not being available,

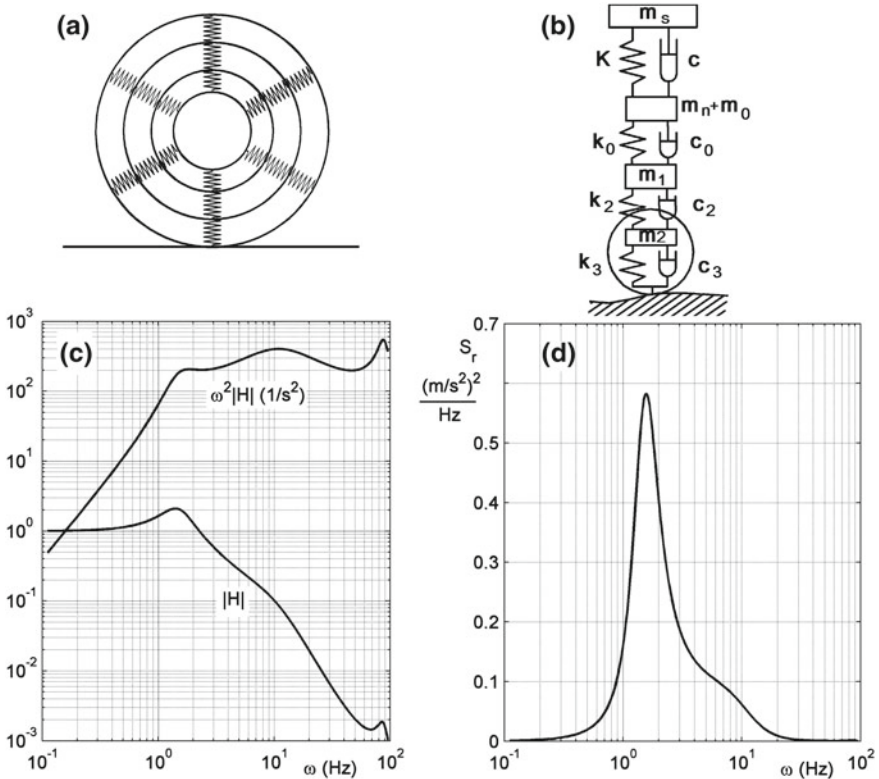


Fig. 26.23 **a** Simplified dynamic model of a tire made of four rigid rings connected to each other by springs. **b** Dynamic model of a quarter-car with the tire simulated as in **a**. **c** and **d** Response of the quarter-car model with three degrees of freedom based on the model in **b**)

consider it as made of a number of rigid rings, the first being attached to the rim and the last connected to the ground, connected to each other by linear springs and dampers (Fig. 26.23a, where the rigid rings are 4). The dynamic model of the quarter-car is shown in Fig. 26.23b.

Assume the following data: sprung mass $m_s = 250$ kg; unsprung mass $m_u = 23$ kg; masses of the 4 rings modelling the tire $m_i = 1$ kg ($i = 0, \dots, 3$), stiffness of the suspension spring $K = 25$ kN/m; stiffness of the springs simulating the tire $k_i = 300$ kN/m ($i = 0, \dots, 3$); damping coefficient of the shock absorber $c = 2,150$ Ns/m; damping coefficient of the dampers simulating the tire $c_i = 100$ Ns/m ($i = 0, \dots, 3$).

The values of k_i were chosen so that, in static conditions, the stiffness of the tire (that is, the stiffness of the three springs in series) is the same as in the previous examples. A certain damping of the tire must be introduced in the present model; otherwise, the response tends to infinity at the resonance of the latter. The value

chosen is, however, low enough not to influence the results at other frequencies, and it allows the tire to be studied with the assumption of small damping.

The tire is a system with three degrees of freedom; its mass, stiffness and damping matrices and the forcing vector due to the motion of the contact point are

$$\mathbf{M} = m_0 \begin{bmatrix} 1 & 0 & 0 \\ 0 & 1 & 0 \\ 0 & 0 & 1 \end{bmatrix}, \quad \mathbf{K} = k_0 \begin{bmatrix} 1 & -1 & 0 \\ -1 & 2 & -1 \\ 0 & -1 & 2 \end{bmatrix},$$

$$\mathbf{C} = c_0 \begin{bmatrix} 1 & -1 & 0 \\ -1 & 2 & -1 \\ 0 & -1 & 2 \end{bmatrix}, \quad \mathbf{f} = h \begin{Bmatrix} 0 \\ 0 \\ i\omega c_0 + k_0 \end{Bmatrix}.$$

The first degree of freedom coincides with the vertical displacement of the unsprung mass and is thus a constrained degree of freedom; the other two are internal degrees of freedom of the tire. The stiffness matrix must then be partitioned as

$$K_{11} = k_0, \quad K_{12} = [-k_0 \ 0], \quad K_{21} = \begin{bmatrix} -k_0 \\ 0 \end{bmatrix}, \quad K_{22} = k_0 \begin{bmatrix} 2 & -1 \\ -1 & 2 \end{bmatrix}.$$

The other matrices are partitioned in the same way. Modal analysis of the internal modes yields the following values for the natural frequencies and the eigenvectors

$$\begin{cases} \omega_1 = 457 \text{ rad/s} = 87 \text{ Hz} \\ \omega_2 = 949 \text{ rad/s} = 151 \text{ Hz} \end{cases} \quad \Phi = \begin{bmatrix} \frac{\sqrt{2}}{2} & \frac{-\sqrt{2}}{2} \\ \frac{\sqrt{2}}{2} & \frac{\sqrt{2}}{2} \end{bmatrix}.$$

The transformation matrix Ψ is

$$\Psi = \begin{bmatrix} 1 & 0 & 0 \\ \frac{2}{3} & \frac{\sqrt{2}}{2} & \frac{-\sqrt{2}}{2} \\ \frac{1}{3} & \frac{\sqrt{2}}{2} & \frac{\sqrt{2}}{2} \end{bmatrix}.$$

The transformed matrices are then

$$\mathbf{M}^* = m_0 \left[\begin{array}{c|cc} 1.556 & 0.7071 & -0.2357 \\ \hline 0.7071 & 1 & 0 \\ -0.2357 & 0 & 1 \end{array} \right],$$

$$K^* = k_0 \left[\begin{array}{c|cc} 0.3333 & 0 & 0 \\ \hline & 0 & 1 & 0 \\ & 0 & 0 & 3 \end{array} \right],$$

$$C^* = c_0 \left[\begin{array}{c|cc} 0.3333 & 0 & 0 \\ \hline & 0 & 1 & 0 \\ & 0 & 0 & 3 \end{array} \right], \quad \mathbf{f}^* = h(i\omega c_0 + k_0) \begin{Bmatrix} \frac{1}{3} \\ -\frac{\sqrt{2}}{2} \\ \frac{2}{2} \\ \frac{2}{2} \end{Bmatrix}.$$

If a model with three degrees of freedom is required, just one of the internal modes of the tire is needed. The third row and column of the transformed matrices may then be cancelled and the tire can be assembled to the quarter-car model, obtaining

$$\begin{bmatrix} m_s & 0 & 0 \\ 0 & m_u + 1.556m_0 & 0.7071m_0 \\ 0 & 0.7071m_0 & m_0 \end{bmatrix} \begin{Bmatrix} \ddot{z}_s \\ \ddot{z}_u \\ \ddot{\eta} \end{Bmatrix} +$$

$$+ \begin{bmatrix} c & -c & 0 \\ -c & c + 0.3333c_0 & 0 \\ 0 & 0 & c_0 \end{bmatrix} \begin{Bmatrix} \dot{z}_s \\ \dot{z}_u \\ \dot{\eta} \end{Bmatrix} +$$

$$+ \begin{bmatrix} K & -K & 0 \\ -K & K + 0.3333k_0 & 0 \\ 0 & 0 & k_0 \end{bmatrix} \begin{Bmatrix} z_s \\ z_u \\ \eta \end{Bmatrix} = h(i\omega c_0 + k_0) \begin{Bmatrix} 0 \\ \frac{1}{3} \\ -\frac{\sqrt{2}}{2} \\ \frac{2}{2} \end{Bmatrix}.$$

The values of the natural frequencies are

$$\begin{cases} \omega_1 = 8.93 \text{ rad/s} = 1.42 \text{ Hz} \\ \omega_2 = 72.97 \text{ rad/s} = 11.61 \text{ Hz} \\ \omega_3 = 553.74 \text{ rad/s} = 88.13 \text{ Hz} . \end{cases}$$

The dynamic compliance $H(\omega)$ and the inertance $\omega^2 H$ are reported in Fig. 26.23 together with the power spectral density of the acceleration of the sprung mass.

The r.m.s. value of the acceleration is

$$a_{rms} = 1.36 \text{ m/s}^2 = 0.14 \text{ g}.$$

The inertia of the tire has no major effect on the results, except in a narrow frequency range about its natural frequency, where a small peak can be seen in

the frequency responses. The r.m.s. value of the acceleration is slightly higher and, because of the presence of high frequency components, an auxiliary suspension may be useful. Because of the approximate tire model here used, this example is simply an indication of how the component modes synthesis approach can be used.

26.4.7 *Effect of the Suspension Kinematics*

In the previous cases the motion of the unsprung mass is only a vertical translation, as if the suspension kinematism were a prismatic guide with axis parallel to the body-fixed z -axis. This model for an independent suspension is, however, quite rough, because no actual suspension is made with a prismatic guide. Each type of suspension has its own kinematics, or better elasto-kinematics because the various linkages are rigid only as a first approximation.

Usually the deviations of the trajectory of the unsprung mass from a straight line parallel to the z -axis are considered shortcomings of the guiding kinematic arrangement, as if straight motion were the ideal situation. But it is actually advisable, on the contrary, that when the wheel gets a shock in the horizontal direction the suspension allows it to move backwards, reducing the excitation in the x -direction transferred to the vehicle body. Moreover, as seen in Part I and in a later section, only by accepting that the wheel does not move exactly in the z -direction is it possible to counteract the *dive* effects that occur when braking, and the *lift* (or *squat*) effects found when driving.

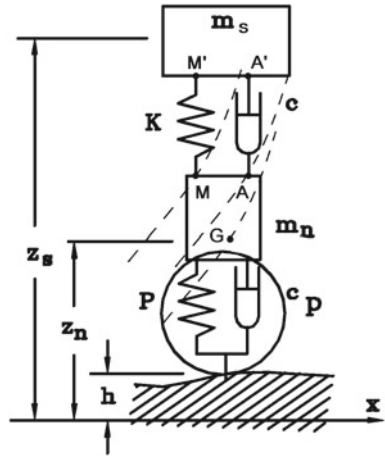
The first of these effects, the ability to absorb horizontal shocks, may be obtained in two ways: by using a kinematic arrangement to produce a suitable trajectory, as in the case of trailing arms (note that the opposite arrangements, which could be defined as leading arms, cause a forward displacement of the wheel when the latter moves upwards and for this reason are seldom used today); or by giving a suitable horizontal compliance to the suspension.

In the first case, it is still possible to use the quarter-car model, while in the second the model must include a further degree of freedom for each wheel, namely horizontal displacement.

While a knowledge of the exact elasto-kinematics of the suspension is essential for stating the position of the wheel with respect to the ground and thus for assessing contact forces, its actual effect on the inertial forces acting on the elements of the suspension and on the forces due to the spring and the shock absorber is limited. Thus it is possible to neglect the compliance of the guiding elements and proceed to a first approximation study related to comfort by using models based on the quarter-car approach.

It is possible to define the trajectories of points G, M and A (Fig. 26.24), i.e. of the center of mass of the unsprung mass and the attachment points of the spring and of the shock absorber in a reference frame $x_1y_1z_1$ fixed to the sprung mass. The trajectory of a generic point P of the unsprung mass is

Fig. 26.24 quarter-car model with two degrees of freedom. The dashed lines are the trajectories of points G, A and M in the xz plane (functions f_G, f_A and f_M)



$$\begin{cases} f_{1P}(x_1, y_1, z_1) = 0 \\ f_{2P}(x_1, y_1, z_1) = 0 \end{cases} \quad (26.43)$$

The motion of the unsprung mass occurs mostly in the z_1 direction, and thus it is expedient to transform Equations (26.43) by solving them in x_1 and y_1 . The coordinates of point P are then linked to each other by the relationships

$$\begin{cases} x_{1P} = f_P(z_{1P}) \\ y_{1P} = g_P(z_{1P}) \end{cases} \quad (26.44)$$

Using geometrical considerations it is possible to obtain a third equation expressing coordinate z_{1P} of point P as a function of the coordinate z_{1G} of the center of mass of the unsprung mass

$$z_{1P} = h_P(z_{1G}) \quad (26.45)$$

The inertial coordinate z_u of the center of mass of the unsprung mass is

$$z_u = z_s + z_{1G} \quad (26.46)$$

The kinematics of the suspension is then completely defined.

To write a linearized equation of motion for studying small oscillations about a reference position (for instance, that of static equilibrium), the equations expressing the trajectory of the generic point P may be linearized as

$$\begin{cases} x_{1P} = x_{1P0} + \left(\frac{df_P}{dz_{1P}} \right)_0 z_{1P} \\ y_{1P} = y_{1P0} + \left(\frac{dg_P}{dz_{1P}} \right)_0 z_{1P} \\ z_{1P} = z_{1P0} + \left(\frac{dh_P}{dz_{1G}} \right)_0 z_{1G} \end{cases} \quad (26.47)$$

that is

$$\begin{cases} x_{1P} = x_{1P_0} + \left(\frac{df_P}{dz_{1P}}\right)_0 z_{1P_0} + \left(\frac{df_P}{dz_{1P}}\right)_0 \left(\frac{dh_P}{dz_{1G}}\right)_0 z_{1G} \\ y_{1P} = y_{1P_0} + \left(\frac{dg_P}{dz_{1P}}\right)_0 z_{1P_0} + \left(\frac{dg_P}{dz_{1P}}\right)_0 \left(\frac{dh_P}{dz_{1G}}\right)_0 z_{1G} \\ z_{1P} = z_{1P_0} + \left(\frac{dh_P}{dz_{1G}}\right)_0 z_{1G} . \end{cases} \quad (26.48)$$

The velocity of point P can be expressed in $x_1 y_1 z_1$ reference frame as

$$V_P = \begin{Bmatrix} \left(\frac{df_P}{dz_{1P}}\right)_0 \left(\frac{dh_P}{dz_{1G}}\right)_0 \dot{z}_{1G} \\ \left(\frac{dg_P}{dz_{1P}}\right)_0 \left(\frac{dh_P}{dz_{1G}}\right)_0 \dot{z}_{1G} \\ \left(\frac{dh_P}{dz_{1G}}\right)_0 \dot{z}_{1G} \end{Bmatrix} , \quad (26.49)$$

where

$$\dot{z}_{1G} = \dot{z}_u - \dot{z}_s . \quad (26.50)$$

In the case of point G, function h_G and its derivative are

$$h_G(z_{1G}) = z_{1G} , \quad \frac{dh_G}{dz_{1G}} = 1 \quad (26.51)$$

and thus the velocity of the unsprung mass is

$$V_G = \begin{Bmatrix} \left(\frac{df_G}{dz_{1G}}\right)_0 (\dot{z}_u - \dot{z}_s) \\ \left(\frac{dg_G}{dz_{1G}}\right)_0 (\dot{z}_u - \dot{z}_s) \\ \dot{z}_u \end{Bmatrix} . \quad (26.52)$$

The translational kinetic energy of the quarter-car with two degrees of freedom is then

$$\mathcal{T} = \frac{1}{2} m_s \dot{z}_s^2 + \frac{1}{2} m_u \dot{z}_u^2 + \frac{1}{2} m_u \left[\left(\frac{df_G}{dz_{1G}}\right)^2 + \left(\frac{dg_G}{dz_{1G}}\right)^2 \right] (\dot{z}_u - \dot{z}_s)^2 , \quad (26.53)$$

i.e.:

$$\mathcal{T} = \frac{1}{2} (m_s + m_u \beta) \dot{z}_s^2 + \frac{1}{2} m_u (1 + \beta) \dot{z}_u^2 + m_u \beta \dot{z}_u \dot{z}_s , \quad (26.54)$$

where β is a constant whose value is

$$\beta = \left(\frac{df_G}{dz_{1G}}\right)_0^2 + \left(\frac{dg_G}{dz_{1G}}\right)_0^2 . \quad (26.55)$$

The mass matrix can be immediately obtained from the kinetic energy

$$\mathbf{M} = \begin{bmatrix} m_s + m_u \beta & m_u \beta \\ m_u \beta & m_u (1 + \beta) \end{bmatrix}. \quad (26.56)$$

Distance MM' must be computed to obtain the potential energy of the spring. The coordinates of point M' are constant in the $x_1 y_1 z_1$ frame. They can be written as $x_{0M'}$, $y_{0M'}$, $z_{0M'}$. The potential energy of the spring is then

$$\mathcal{U} = \frac{1}{2} K [(x_M - x_{M'})^2 + (y_M - y_{M'})^2 + (z_M - z_{M'})^2], \quad (26.57)$$

where the system has been assumed to behave linearly about its static equilibrium position. Only the quadratic terms of the potential energy enter the stiffness matrix. The linear terms actually produce constant terms (generalized forces) in the equation of motion that do not affect the dynamic behavior about the equilibrium position, and these constant terms are arbitrary. Taking into account only the quadratic terms, the potential energy reduces to

$$\mathcal{U} = \frac{1}{2} K \gamma z_{1G}^2 = \frac{1}{2} K \gamma (z_u - z_s), \quad (26.58)$$

where

$$\gamma = \left(\frac{dh_M}{dz_{1G}} \right)_0^2 \left[1 + \left(\frac{df_M}{dz_{1M}} \right)_0^2 + \left(\frac{dg_M}{dz_{1M}} \right)_0^2 \right]. \quad (26.59)$$

Taking into account also the deformation potential energy of the tire,

$$\mathcal{U}_P = \frac{1}{2} P z_u^2$$

(after neglecting constant and linear terms), the stiffness matrix of the system is

$$\mathbf{K} = \begin{bmatrix} K\gamma & -K\gamma \\ -K\gamma & K\gamma + P \end{bmatrix}. \quad (26.60)$$

By substituting subscript M with subscript A , Eq. (26.49) yields directly the relative velocity of point A with respect to the sprung mass, i.e., to point A' . However, what matters for the computation of the forces due to the shock absorber is not the relative velocity but only its component in the direction AA' . Distance AA' is:

$$\overline{AA'} = \sqrt{(x_A - x_{A'})^2 + (y_A - y_{A'})^2 + (z_A - z_{A'})^2}. \quad (26.61)$$

The Raleigh dissipation function of the shock absorber is then

$$\mathcal{F} = \frac{1}{2}c \left(\frac{d\overline{AA'}}{dt} \right)^2. \quad (26.62)$$

The dissipation function can be simplified by linearizing it about the equilibrium position, as

$$\mathcal{F} = \frac{1}{2}c\delta (\dot{z}_u - \dot{z}_s)^2, \quad (26.63)$$

where

$$\delta = \left(\frac{dh_A}{dz_{1G}} \right)_0^2 \frac{\left[(x_{A_0} - x_{A_0'}) \left(\frac{df_A}{dz_{1A}} \right)_0 + (y_{A_0} - y_{A_0'}) \left(\frac{dg_A}{dz_{1A}} \right)_0 + (z_{A_0} - z_{A_0'}) \right]^2}{(x_{A_0} - x_{A_0'})^2 + (y_{A_0} - y_{A_0'})^2 + (z_{A_0} - z_{A_0'})^2}. \quad (26.64)$$

By also inserting the term due to the damping of the tire into the expression of the dissipation function, the damping matrix of the system is obtained,

$$\mathbf{C} = \begin{bmatrix} c\delta & -c\delta \\ -c\delta & c\delta + c_P \end{bmatrix}. \quad (26.65)$$

As far as the elastic and damping terms are concerned, the linearized equation of motion is still Eq. (26.22), except for the values of the stiffness of the spring or the damping coefficient of the shock absorber which are *reduced* through coefficients γ and δ . The mass matrix is, on the other hand, different, because it is not diagonal. An inertial coupling proportional to the value of the unsprung mass is then present. It will cause a larger motion of the sprung mass at frequency ranges typical of the motion of the unsprung mass.

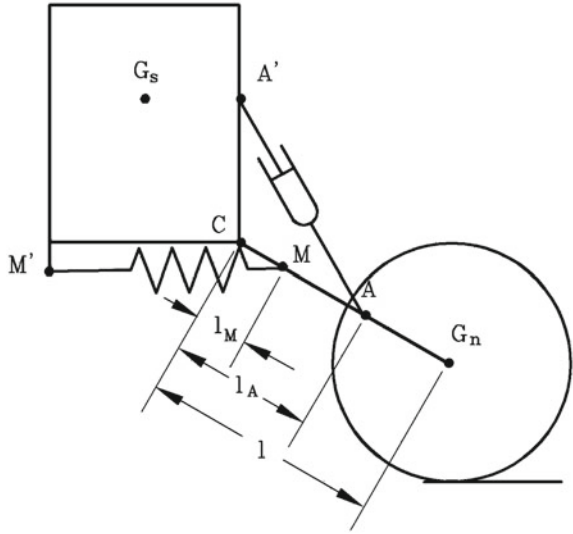
In any case, the quarter-car model assumes that the sprung mass moves along the z direction, an approximation that is increasingly unrealistic with increasing coupling of horizontal and vertical motion of the unsprung mass due to the kinematics of the suspension. In particular, a motion of the sprung mass in the x direction due to a motion in the z direction may be detrimental to comfort, and cannot be studied using such simple models.

Example 26.6 Consider the quarter-car with two degrees of freedom shown in Fig. 26.25. The trailing arm suspension is hinged about an axis parallel to the y -axis of the vehicle. The data are: sprung mass $m_s = 250$ kg; unsprung mass $m_u = 25$ kg; stiffness of the spring $K = 700$ kN/m; damping coefficient $c = 19.35$ kNs/m; Data of the tire: $P = 100$ kN/m; $c_P = 0$. Geometrical data: $l = 500$ mm, $l_A = 300$ mm, $l_M = 100$ mm; position of C: $[200 \ 0 \ -300]^T$ mm; position of M': $[-200 \ 0 \ -360]^T$ mm; position of A': $[200 \ 0 \ 0]^T$ mm.

The functions f_1 and f_2 defining the trajectory of a point P of the suspension are

$$\begin{cases} (x_1 - x_0)^2 + (z_1 - z_0)^2 - l_P^2 = 0 \\ y_1 - y_0 = 0, \end{cases}$$

Fig. 26.25 Trailing arm quarter-car: geometrical definitions



where x_0 , y_0 and z_0 are the coordinates of point C. The corresponding functions f_P and g_P are

$$\begin{cases} f_P = x_0 \pm \sqrt{l_P^2 - (z_{1P} - z_0)^2} \\ g_P = y_0 . \end{cases}$$

The double sign does not give problems, because it is determined by the geometry of the system: Sign (+) must be used if point P is forward of the axis of the hinge. Because the suspension lies in a plane parallel to the xz plane, coordinate y of all points can be assumed as zero ($y_0 = 0$).

The derivative $\left(\frac{df}{dz}\right)_0$ is then

$$\left(\frac{df_P}{dz_{1P}}\right)_0 = \left(\frac{- (z_{1P} - z_0)}{\sqrt{l_P^2 - (z_{1P} - z_0)^2}}\right)_0 .$$

The static equilibrium position is defined by

$$\begin{cases} x_{1G_0} = x_0 + l \cos(\theta_0) = 633 \text{ mm} \\ z_{1G_0} = z_0 - l \sin(\theta_0) = -550 \text{ mm} \end{cases}$$

and thus

$$\left(\frac{df_G}{dz_{1G}}\right)_0 = 0.577 , \quad \beta = 0.333 .$$

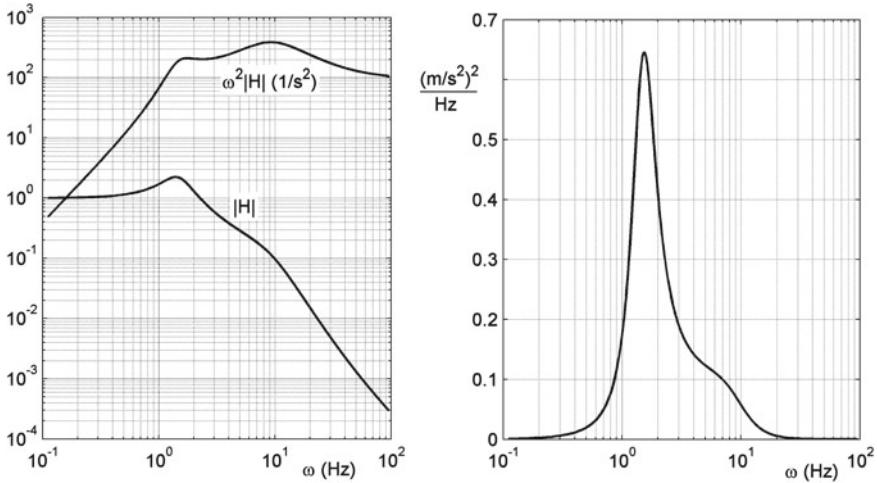


Fig. 26.26 Dynamic compliance and inertia of the trailing arm quarter-car model. Power spectral density of the acceleration due to motion on a road at a speed of 30 m/s

The mass matrix is then

$$\mathbf{M} = \begin{bmatrix} 258,33 & 8,33 \\ 8,33 & 33,33 \end{bmatrix} .$$

By remembering that triangles CMH' are CGH similar, the coordinate z_1 of point M is obtained:

$$z_{1M} = z_0 - \frac{l_M}{l} \sqrt{l^2 - (z_{1G} - z_0)^2}$$

and then

$$\left(\frac{dh_M}{dz_{1G}} \right)_0 = -\frac{l_M}{l} \left(\frac{(z_{1G} - z_0)}{\sqrt{l^2 - (z_{1G} - z_0)^2}} \right)_0 .$$

Thus it follows that

$$\left(\frac{df_M}{dz_{1P}} \right)_0 = 1.732 , \quad \left(\frac{dh_M}{dz_{1G}} \right)_0 = 0.116 , \quad \gamma = 0.0364 .$$

The coordinate of point A is obtained in a similar way,

$$z_{1A} = z_0 + \frac{l_A}{l} (z_{1G} - z_0)$$

and thus

$$\left(\frac{dh_A}{dz_{1G}}\right)_0 = \frac{l_A}{l} = 0.6.$$

Finally, it follows that

$$\left(\frac{df_M}{dz_{1G}}\right)_0 = 0.577, \quad \delta = 0.111.$$

Note that the values of K and c were chosen in such a way that the reduced values $K\gamma$ and $c\delta$ were practically identical to those of Example 26.3.

The dynamic compliance $H(\omega)$ and the inertance $\omega^2 H$ are plotted in Fig. 26.26 together with the power spectral density of the acceleration of the sprung mass.

The r.m.s. value of the acceleration is

$$a_{rms} = 1.34 \text{ m/s}^2 = 0.14 \text{ g}.$$

By comparing the plot with that obtained for the simple two degrees of freedom quarter-car model, it will be noted that the peak of the response is higher, and also that the response is in general higher at frequencies close to the resonances of both sprung and unsprung masses. At higher frequencies the response is lower, primarily because the inertia is in some way increased by the coupling of longitudinal and vertical motion, causing the suspension to behave as if it were softer. The reduction of the r.m.s. value of the acceleration is, however, minimal.

26.5 Heave and Pitch Motion

26.5.1 Simplified Models with Rigid Tires

The heave motion of the vehicle is strictly coupled with pitch motion. The simplest model for studying the heave-pitch coupling is shown in Fig. 26.27a. Its equation of motion is that of a beam on two elastic and damped supports

$$\begin{aligned} & \begin{bmatrix} m_S & 0 \\ 0 & J_y \end{bmatrix} \begin{Bmatrix} \ddot{Z}_s \\ \ddot{\theta} \end{Bmatrix} + \begin{bmatrix} c_1 + c_2 & -ac_1 + bc_2 \\ -ac_1 + bc_2 & a^2c_1 + b^2c_2 \end{bmatrix} \begin{Bmatrix} \dot{Z}_s \\ \dot{\theta} \end{Bmatrix} + \\ & + \begin{bmatrix} K_1 + K_2 & -aK_1 + bK_2 \\ -aK_1 + bK_2 & a^2K_1 + b^2K_2 \end{bmatrix} \begin{Bmatrix} Z_s \\ \theta \end{Bmatrix} = \\ & = \begin{Bmatrix} c_1\dot{h}_A + c_2\dot{h}_B + K_1h_A + K_2h_B \\ -ac_1\dot{h}_A + bc_2\dot{h}_B - aK_1h_A + bK_2h_B \end{Bmatrix}. \end{aligned} \tag{26.66}$$

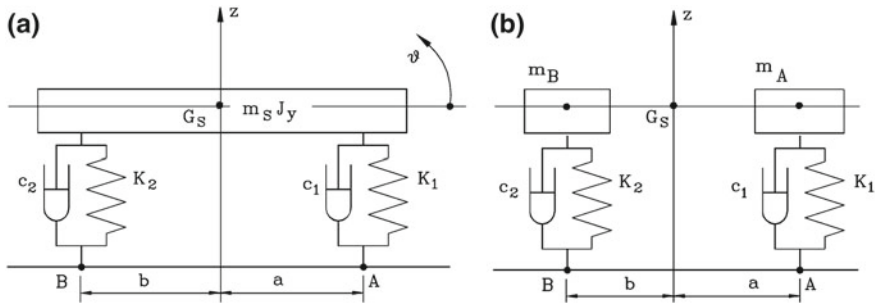


Fig. 26.27 Beam models for heave and pitch motions

The overturning moment due to weight (term $-m_s g h$ to be added in position 22 in the stiffness matrix) is not included in Eq. (26.66), because no assumption has been made on the height of the pitch center over the road plane. Nor is any aerodynamic term introduced into the equation of motion. The longitudinal position of the springs and the shock absorbers has been assumed to be the same.

The forcing functions were written in a form that considers only the vertical motion of points A and B, neglecting horizontal forces at the ground-wheels interface and the possible coupling between vertical and horizontal motions due to suspensions.

If mass m_s and moment of inertia J_y are those of the whole sprung mass, the stiffnesses K_i and the damping coefficients c_i are those of a whole axle and are then twice those of a single spring or shock absorber.

The compliance of the tires was neglected in the beam model shown in Fig. 26.27a. It may thus be considered an evolution of the quarter-car with a single degree of freedom. In some cases it can be reduced to a pair of quarter-cars, as shown in Fig. 26.27b. To compare the two models, it is possible to use the coordinates Z_A and Z_B instead of Z_s and θ to describe the motion of the beam. The coordinate transformation may be expressed as:

$$\begin{Bmatrix} Z_s \\ \theta \end{Bmatrix} = \frac{1}{l} \begin{bmatrix} b & a \\ -1 & 1 \end{bmatrix} \begin{Bmatrix} Z_A \\ Z_B \end{Bmatrix} \quad (26.67)$$

The mass matrix to be included in the equation of motion when using the new coordinates is

$$\mathbf{M}' = \mathbf{T}^T \mathbf{M} \mathbf{T},$$

where \mathbf{T} is the transformation matrix defined by Eq. (26.67). All other matrices can be obtained in the same way. Equation (26.66) then becomes

$$\begin{aligned} \frac{m_S}{l^2} \begin{bmatrix} b^2 + r_y^2 & ab - r_y^2 \\ ab - r_y^2 & a^2 + r_y^2 \end{bmatrix} \begin{Bmatrix} \dot{Z}_A \\ \dot{Z}_B \end{Bmatrix} + \begin{bmatrix} c_1 & 0 \\ 0 & c_2 \end{bmatrix} \begin{Bmatrix} \dot{Z}_A \\ \dot{Z}_B \end{Bmatrix} + \\ + \begin{bmatrix} K_1 & 0 \\ 0 & K_2 \end{bmatrix} \begin{Bmatrix} Z_A \\ Z_B \end{Bmatrix} = \begin{Bmatrix} c_1 \dot{h}_A + K_1 h_A \\ c_2 \dot{h}_B + K_2 h_B \end{Bmatrix}, \end{aligned} \quad (26.68)$$

where r_y is the radius of gyration of the sprung mass about the y -axis.

A *dynamic index* I_d of the sprung mass can thus be defined as

$$I_d = \frac{r_y^2}{ab}. \quad (26.69)$$

If I_d is equal to unity, i.e., if

$$J_y = m_S ab,$$

that is

$$r_y^2 = ab,$$

the two equations uncouple from each other, yielding the two equations of motion of two separate quarter-cars with sprung masses

$$m_S \frac{b}{l} \text{ and } m_S \frac{a}{l},$$

and the model of Fig. 26.27a reduces to that of Fig. 26.27b.

This condition is usually not verified in practice. The tendency to increase the wheelbase for stability reasons leads to values of the dynamic index usually smaller than 1, even smaller than 0.8.

The natural frequencies of the undamped system may be computed using the homogeneous equation associated with Eq. (26.66) or (26.68), after cancelling the damping term. If the solution

$$\begin{Bmatrix} Z_A \\ Z_B \end{Bmatrix} = \begin{Bmatrix} Z_{A_0} \\ Z_{B_0} \end{Bmatrix} e^{i\omega t}, \quad (26.70)$$

is introduced in the second of the mentioned equations, the characteristic equation

$$\det \left[-\omega^2 \frac{m_S}{l^2} \begin{bmatrix} b^2 + r_y^2 & ab - r_y^2 \\ ab - r_y^2 & a^2 + r_y^2 \end{bmatrix} + \begin{bmatrix} K_1 & 0 \\ 0 & K_2 \end{bmatrix} \right] = 0 \quad (26.71)$$

is obtained.

The natural frequencies are then the roots of equation

$$\omega^4 - \omega^2 \frac{K_1(r_y^2 + a^2) + K_2(r_y^2 + b^2)}{m_S r_y^2} + K_1 K_2 \frac{l^2}{m_S^2 r_y^2} = 0, \quad (26.72)$$

that yields

$$\omega_i = \frac{\sqrt{(b^2 + r_y^2) K_2 + (a^2 + r_y^2) K_1 \pm \Delta}}{r_y \sqrt{2m_S}}, \quad (26.73)$$

where

$$\Delta = \sqrt{(b^2 + r_y^2)^2 K_2^2 + 2K_1 K_2 [(ab - r_y^2)^2 - r_y^2 l^2] + (a^2 + r_y^2)^2 K_1^2}.$$

The corresponding eigenvectors are

$$\mathbf{q}_i = \left\{ \begin{array}{c} \frac{(b^2 + r_y^2) K_2 - (a^2 + r_y^2) K_1 \mp \Delta}{2K_1 (ab - r_y^2)} \\ 1 \end{array} \right\}.$$

The solution with (+) sign yields two positive values, that generally are not equal to each other. The motion of the beam is neither a rotation about its center of mass (pitch) nor a translational motion in the z direction (heave), but the very fact that the displacements at the front and rear axles have the same sign means that the node (the point with zero displacement) lies outside of the wheelbase, and thus the motion is primarily translational (heave, Fig. 26.28a). The solution with (−) sign (Fig. 26.28b) yields a positive and a negative value: the displacements of the front and rear axles are one positive and one negative and the node is within the wheelbase. The motion is primarily rotational, even if not about the center of mass, and it is primarily a pitching motion.

If the dynamic index I_d has a unit value (Fig. 26.28c, e, d), it follows that

$$\Delta = (b^2 + r_y^2) K_2 - (a^2 + r_y^2) K_1 = l(bK_2 - aK_1)$$

and then

$$\omega_1 = \sqrt{\frac{lK_2}{am_S}}, \quad \omega_2 = \sqrt{\frac{lK_1}{bm_S}}. \quad (26.74)$$

As previously stated, the natural frequencies in this case are those of the two separate quarter-cars of Fig. 26.27b. The corresponding eigenvectors are

$$\mathbf{q}_1 = \begin{Bmatrix} 0 \\ 1 \end{Bmatrix}, \quad \mathbf{q}_2 = \begin{Bmatrix} 1 \\ 0 \end{Bmatrix},$$

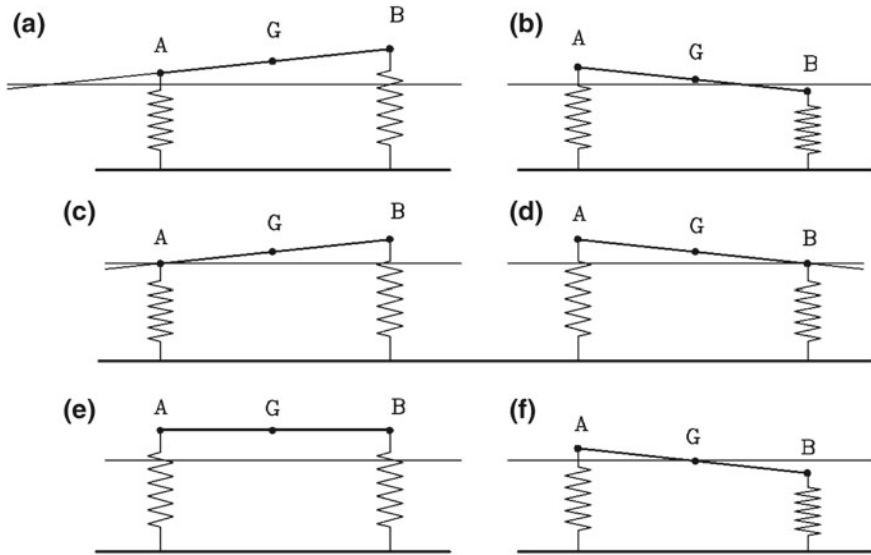


Fig. 26.28 Heave and pitching motions. **a** and **b** General case; primarily heave (**a**) and primarily pitching **b** motions. **c** and **d** Case with $I_d = 1$. **e** and **f** Case with $aK_1 = bK_2$

and the free oscillations of the sprung mass are rotations about the points where the suspensions are connected to the body. It is impossible to identify a heave and a pitch mode; it is more accurate to speak about a front-axle and a rear-axle mode. The limiting case is where the node internal to the wheelbase and that external to it tend to the ends of the wheelbase.

The other limiting case (Fig. 26.28e, f) is when

$$aK_1 = bK_2. \tag{26.75}$$

From Eq. (26.66) without damping terms it is clear that the two equations of motion uncouple: the heave motion uncouples from the pitch motion. The first is translational, while the second is rotational and occurs about the center of mass. The natural frequencies are then

$$\left\{ \begin{array}{l} \omega_1 = \sqrt{\frac{lK_1}{bm_S}} \quad \text{bounce,} \\ \omega_2 = \sqrt{\frac{laK_1}{r_y^2 m_S}} = \omega_1 \sqrt{\frac{ab}{r_y^2}} \quad \text{pitch.} \end{array} \right. \tag{26.76}$$

The two limiting cases may also occur simultaneously. From Eq. (26.76) it follows that when this is the case the two natural frequencies have the same value.

Remark 26.9 This solves an apparent inconsistency; if

$$aK_1 = bK_2,$$

the centers of rotation are one in the centre of mass (pitch mode) and one at infinity (heave mode), while when the dynamic index has a unit value they are at the end of the wheelbase. When both conditions occur simultaneously, the two natural frequencies coincide; in this case, any linear combination of the eigenvectors is itself an eigenvector. Thus in the case of a rigid beam, any point of the beam (or better, of the straight line constituting the beam axis) may be considered as a center of rotation.

Example 26.7 Consider a vehicle having the following characteristic: sprung mass $m_s = 1,080$ kg; pitching moment of inertia $J_y = 1,480$ kg m²; stiffness of the suspensions (referred to the axles) $K_1 = 45$ kN/m; $K_2 = 38$ kN/m; $a = 1.064$ m; $b = 1.596$ m, ($l = 2.66$ m). Study the pitching oscillations of the vehicle, using a beam model.

The pitching radius of gyration and the dynamic index are

$$r_y = \sqrt{\frac{J_y}{m}} = 1.17 \text{ m}, \quad I_d = \frac{r_y^2}{ab} = 0.807. \quad (26.77)$$

The sprung mass may be subdivided into two masses, one at the front axle and one at the rear

$$m_1 = \frac{bm_s}{l} = 648 \text{ kg}, \quad m_2 = \frac{am_s}{l} = 432 \text{ kg}. \quad (26.78)$$

The two natural frequencies of the independent quarter-car models are

$$\omega_1 = 1.33 \text{ Hz}, \quad \omega_2 = 1.49 \text{ Hz}. \quad (26.79)$$

Because the dynamic index is different from 1, the approximation so obtained is a rough one. By solving the characteristic equation, the correct natural frequencies are obtained

$$\omega_1 = 1.36 \text{ Hz}, \quad \omega_2 = 1.62 \text{ Hz}. \quad (26.80)$$

The corresponding eigenvectors, normalized so that the largest element has a unit value, are

$$\mathbf{q}_1 = \begin{Bmatrix} 1 \\ -0.32 \end{Bmatrix}, \quad \mathbf{q}_2 = \begin{Bmatrix} 0.44 \\ 1 \end{Bmatrix},$$

The node of the first mode lies within the wheelbase and, because it is 2.015 m from the front axle, is behind the center of mass. This is essentially a pitching mode. The node of the second mode, a heave mode, is in front of the vehicle, 2.09 m from the front axle.

26.5.2 Pitch Center

No guiding linkage is considered in the model of Fig. 26.27a, but it is implicitly assumed that the connection points of the suspension to the body may move only in a vertical direction. The wheelbase of the vehicle is then not affected either by bounce or pitch motion. Moreover, it is assumed that the inertia of the unsprung masses does not affect the motion of the body.

It is, in any case, possible to find a point along the x -axis such that a vertical force applied to it produces a vertical motion but no pitching. This point is the pitch center.

To define the position of the pitch center, a static force F can be applied to the body in a vertical direction at a point on the x -axis at a generic distance d from the center of mass. Equation (26.66) becomes

$$\begin{bmatrix} K_1 + K_2 & -aK_1 + bK_2 \\ -aK_1 + bK_2 & a^2K_1 + b^2K_2 \end{bmatrix} \begin{Bmatrix} Z_s \\ \theta \end{Bmatrix} = F \begin{Bmatrix} 1 \\ d \end{Bmatrix}. \quad (26.81)$$

Solving for the pitch angle θ , it follows that

$$\theta = \frac{aK_1 - bK_2 - d(K_1 + K_2)}{K_1K_2l^2}. \quad (26.82)$$

Equating the numerator to zero, it follows that if

$$d = \frac{aK_1 - bK_2}{K_1 + K_2} \quad (26.83)$$

angle θ vanishes. This value of d is the distance in the x direction of the pitch center from the center of mass; it is positive if the pitch center is forward of the mass center. In the majority of cases, d is positive. If Eq. (26.75) holds, $d = 0$ and the mass center is above or below the mass center.

The presence of kinematic guides for suspensions does not change things: Eq. (26.66) still holds, even if the meaning of the terms may vary. Consider, for instance, a vehicle with longitudinal swing arm suspensions and springs located below the floor. Linearize the equations of motion about a reference position (Fig. 26.29).

Assume that the suspended mass moves vertically by a distance Δz and rotates in pitch by an angle θ . Points A and B move vertically by

$$\begin{cases} \Delta z_A = \Delta z - c\theta \\ \Delta z_B = \Delta z + d\theta \end{cases}. \quad (26.84)$$

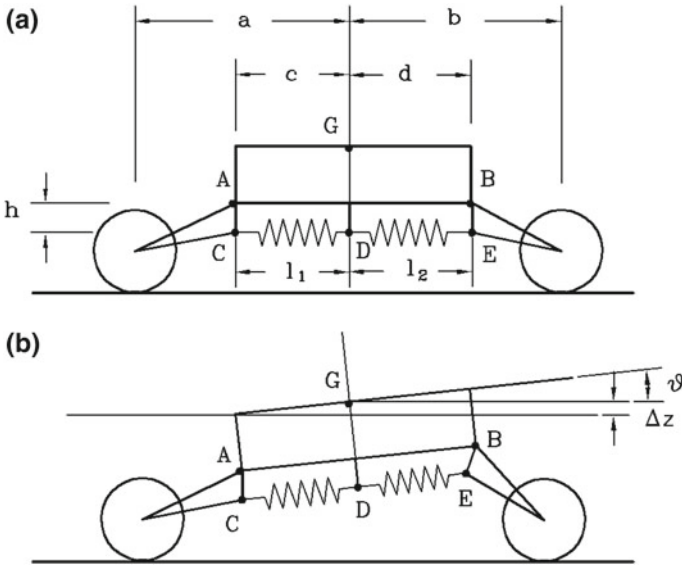


Fig. 26.29 Vehicle with longitudinal swing arm suspensions. **a** Sketch of the system; **b** position during bounce and pitch motion

By linearizing the system about the horizontal position, rotations ϕ_i of the two swing arms are

$$\begin{cases} \Delta\phi_1 = \frac{\Delta z_A}{a-c} \Delta x_A = \frac{\Delta z - c\theta}{a-c} \\ \Delta\phi_2 = -\frac{\Delta z_B}{b-d} \Delta x_A = -\frac{\Delta z + d\theta}{b-d} \end{cases} \quad (26.85)$$

The springs stretch by

$$\begin{cases} \Delta l_1 = -\Delta\phi_1 h = -h \frac{\Delta z - c\theta}{a-c} \\ \Delta l_2 = \Delta\phi_2 h = -h \frac{\Delta z + d\theta}{b-d} \end{cases} \quad (26.86)$$

The change in elastic potential energy is then

$$\begin{aligned} \Delta\mathcal{U} &= \frac{1}{2} K_1 \Delta l_1^2 + \frac{1}{2} K_2 \Delta l_2^2 = \\ &= \frac{1}{2} K_1 \left(h \frac{\Delta x - c\theta}{a-c} \right)^2 + \frac{1}{2} K_2 \left(h \frac{\Delta x + d\theta}{b-d} \right)^2 \end{aligned} \quad (26.87)$$

By differentiating the potential energy with respect to the generalized displacements, the following relationships linking the vertical force and the pitching moment applied to the vehicle body with the generalized displacements emerge

$$\begin{Bmatrix} F_z \\ M_y \end{Bmatrix} = \begin{bmatrix} K_1^* + K_2^* & -cK_1^* + dK_2^* \\ -cK_1^* + dK_2^* & c^2K_1^* + d^2K_2^* \end{bmatrix} \begin{Bmatrix} \Delta z_s \\ \theta \end{Bmatrix}, \quad (26.88)$$

where:

$$K_1^* = K_1 \left(\frac{h}{a-c} \right)^2, \quad K_2^* = \left(\frac{h}{b-d} \right)^2.$$

As clearly seen, the structure of the stiffness matrix is identical to the general case, even if it includes terms that are typical of the particular type of suspension. The damping matrix may be obtained along the same lines.

The suspension type also affects the mass matrix to be introduced into Eq. (26.66), because heave and pitch motions also cause some movements of the unsprung masses, causing their inertial parameters to enter the mass matrix as well.

The height of the pitch center becomes important when the wheels exert longitudinal forces, because the coupling between driving (or braking) and pitching depend on it. The *antidive* and *antilift* (or *antisquat*) characteristics of the suspensions also depend on the height of the pitch center.

If the wheels do not exert longitudinal forces, the pitch center is assumed to lie roughly at the height of the centers of the wheels, which amounts to assuming that the wheels travel at constant speed even when the body oscillates in heave or pitch.¹¹

26.5.3 Empirical Rules for the Design of Suspensions

As already stated, the bounce and pitch dynamics of the suspended mass are strictly related to each other. Some empirical criteria for the choice of the relevant parameters are here reported: They date back to the 1930s and were introduced by Maurice Olley.¹²

- The vertical stiffness of the front suspension must be about 30% lower than that of the rear suspension;
- The pitch and bounce frequencies must be close to each other; the bounce frequency should be less than 1.2 times the pitch frequency;
- Neither frequency should be greater than 1.3 Hz;
- The roll frequency should be approximately equal to the bounce and pitch frequency.

¹¹Milliken W.F., Milliken D.L., *Chassis Design*, Professional Engineering Publishing, Bury St. Edmunds, 2002.

¹²T. D. Gillespie, *Fundamentals of vehicle dynamics*, SAE, Warrendale, 1992.

The first rule states that the natural frequency of the rear suspension is higher than that of the front, at least if the weight distribution is not such that the rear wheels are far more loaded than those in front. The importance of having a lower natural frequency for the front suspension may be explained by observing that any road input reaches the front suspension first and then, only after a certain time, the rear one. If the natural frequency of the latter is higher, when the vehicle rides over a bump the rear part quickly “catches up” to the motion of the front and, after the first oscillation, the body of the vehicle moves in bounce rather than pitch, a favorable factor for ride comfort. Then the rear part of the vehicle should lead the motion, but by that time damping has caused the amplitude to decrease.

The second rule is easily fulfilled in modern cars. The problem here may be that of having the pitch frequency much higher than the bounce one, and higher than 1.3 Hz (third rule), as may happen when the dynamic index is smaller than unity (vehicle with long wheelbase and small front/rear overhang). Generally speaking, a dynamic index close to unity is considered a desirable condition for good ride properties, while a complete bounce-ride uncoupling as occurs when $aK_1 = bK_2$ is considered a nuisance. Coupling between bounce and pitching is good as it tends to avoid strong pitch oscillations.

The fourth rule has nothing to do with pitch motion, and will be discussed later.

Example 26.8 Check whether the vehicle studied in the previous example complies with the criteria defined by Olley. Study the response of the vehicle when crossing a road irregularity at a speed of 100 km/h = 27.8 m/s by using an impulsive model, assuming that the impulse given by the irregularity first to the front axle and then to the rear axle has a unit value.

To study the motion of the body after crossing the irregularity, assume that both suspensions are damped with a damping coefficient equal to the optimum value computed using a quarter-car model with a single degree of freedom.

The natural frequencies of the suspensions, computed using the model with two independent quarter-cars, are 1.33 (front axle) and 1.49 Hz (rear axle). The second is higher than the first by about 12%. By considering that the natural frequencies are proportional to the square root of the stiffness, this corresponds to a stiffness of the rear axle 24% greater than that of the front, a value not much different from the suggested 30%.

Because the dynamic index has no unit value ($I_d = 0.807$), the model made by two quarter-cars is not accurate. If the system is considered as a coupled system, the frequencies for bounce and pitch motions are 1.36 and 1.62 Hz, which does not coincide with those previously computed (the first is not much different, while the second is greater by about 8%). The first is smaller than 1.2 times the second (actually smaller than that) and the frequencies are relatively similar. However, the natural frequency in pitch is greater than 1.3 Hz, and is higher than what has been suggested, even if not by much.

The values of the damping of the shock absorbers, computed using the quarter-car model with a single degree of freedom, are

$$c_1 = \sqrt{\frac{K_1 m_1}{2}} = 3,820 \text{ Ns/m}, \quad c_2 = \sqrt{\frac{K_2 m_2}{2}} = 2,865 \text{ Ns/m}. \quad (26.89)$$

The delay between the instant the front axle is excited and that when the rear axle is on the irregularity is, at 100 km/h,

$$\tau = \frac{l}{V} = 0.096 \text{ s}. \quad (26.90)$$

To compute the response of the model made by two independent quarter-car models to a unit impulse, it is enough to compute the free responses of the two systems with the initial conditions due to the impulse. The front suspension will start with the initial conditions

$$(z_A)_0 = 0, \quad (\dot{z}_A)_0 = \frac{I}{m_A} \text{ for } t = 0. \quad (26.91)$$

In the same way, the initial conditions for the rear suspension are

$$(z_B)_0 = 0, \quad (\dot{z}_B)_0 = \frac{I}{m_B} \text{ for } t = \tau. \quad (26.92)$$

The result is reported in Fig. 26.30a in terms of time histories. The vertical displacement at the center of mass and the pitch angle may be computed through Eq. (26.67) from the displacements of the points where the suspensions are attached. The result is plotted in Fig. 26.30b, dashed curves. Because the natural frequency of the rear axle is greater than that of the front axle, the two masses move synchronously after a single oscillation is completed: pitch motions extinguish faster than bounce.

To avoid the approximations due to the model with two independent quarter-cars, it is possible to numerically integrate the system's equations of free motion (homogeneous equation associated to Eq. (26.66)) in two distinct intervals of time, between $t = 0$ and $t = \tau$ and after $t = \tau$. In the first interval the initial conditions are those following the first impulse.

$$\left\{ \begin{array}{c} z_G \\ \theta \end{array} \right\}_0 = \left\{ \begin{array}{c} 0 \\ 0 \end{array} \right\}, \quad \left\{ \begin{array}{c} \dot{z}_G \\ \dot{\theta} \end{array} \right\}_0 = \left\{ \begin{array}{c} \frac{I}{m} \\ -\frac{aI}{J} \end{array} \right\} \text{ for } t = \tau. \quad (26.93)$$

For the second interval, that following the second impulse, the initial conditions are

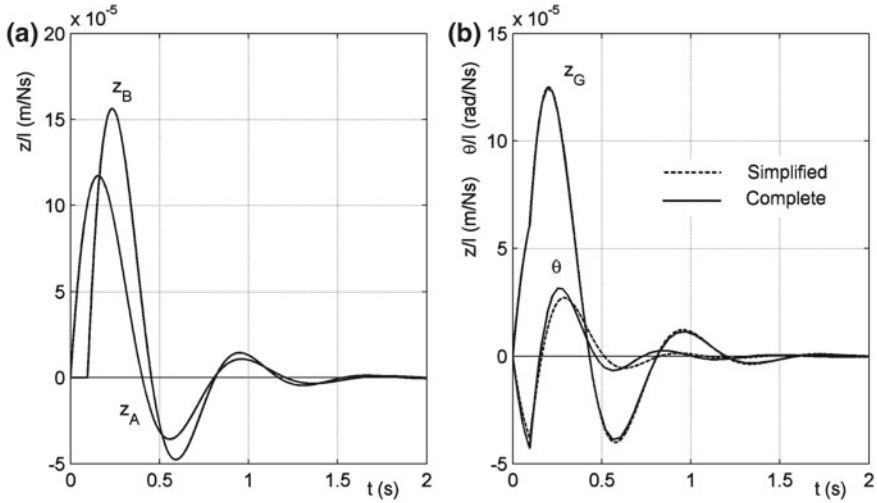


Fig. 26.30 Bounce and pitch response for a vehicle crossing an obstacle with the front and the rear axle at 100 km/h. The obstacle causes a unit vertical impulse. Displacements of points A and B (a) and of the center of mass and rotation (b) computed using the simplified (Fig. 26.27b) and complete (Fig. 26.27a) model

$$\begin{Bmatrix} z_G \\ \theta \end{Bmatrix}_0 = \begin{Bmatrix} z_G \\ \theta \end{Bmatrix}_1, \quad \begin{Bmatrix} \dot{z}_G \\ \dot{\theta} \end{Bmatrix}_0 = \begin{Bmatrix} \dot{z}_G \\ \dot{\theta} \end{Bmatrix}_1 + \begin{Bmatrix} \frac{l}{m} \\ \frac{bl}{J} \end{Bmatrix} \text{ for } t = \tau, \quad (26.94)$$

where subscript 1 designates the condition at the end of the first part of the integration, just before receiving the second impulse. The result is shown in Fig. 26.30b, full lines. The errors due to the model made by two independent quarter-cars are small, even if the dynamic index is smaller than 1.

26.5.4 Frequency Response of the Model with Two Degrees of Freedom

If, when using the quarter-car model road, roughness excites only bounce motions, in a complete vehicle it excites both bounce and pitching motions, as already seen. Neglecting roll, it is possible to use a model of the type seen in Fig. 26.27a, assuming that laws $h_A(t)$ and $h_B(t)$ are identical, except for the fact that the second is delayed with respect to the first by time

$$\tau = \frac{l}{V}, \quad (26.95)$$

needed to travel a distance equal to the wheelbase. To compute the frequency response of the vehicle, the forcing functions to be introduced into Eq. (26.68) are then

$$\begin{cases} h_A = h_o \sin(\omega t) \\ h_B = h_o \sin[\omega(t + \tau)] = h_o[\sin(\omega t) \cos(\omega \tau) + \cos(\omega t) \sin(\omega \tau)] \end{cases} \quad (26.96)$$

Term $\omega \tau$ is proportional to the ratio between the wheelbase l of the vehicle and the wavelength of road irregularities λ . The frequency $\bar{\omega}$ related to space instead of time is linked with the wavelength by the relationship

$$\lambda = \frac{2\pi}{\bar{\omega}} \quad (26.97)$$

and to the frequency related to time by the relationship

$$\bar{\omega} = \frac{\omega}{V} \quad (26.98)$$

It follows then that

$$\omega \tau = \frac{\omega l}{V} = 2\pi \frac{l}{\lambda} \quad (26.99)$$

At low frequency, the excitation at the two axles occurs almost in phase, with the result that pitch motions are little excited. In a similar way, if l is a whole multiple of the wavelength λ (the wavelength is equal to the wheelbase or to one of its whole sub-multiples), $\omega \tau$ is a whole multiple of 2π and then $\cos(\omega \tau) = 1$ and $\sin(\omega \tau) = 0$. The two axles are excited in phase: if the equations of motion were uncoupled and the center of mass were at mid-wheelbase, only bounce motion would be excited and no pitching would occur. Although this is not exactly true due to coupling, the result is that the vehicle pitches much less than it bounces.

If, on the contrary, l is an odd multiple of $\lambda/2$ (the wavelength of the irregularities is twice the wheelbase or is a whole multiple of twice the wheelbase), it follows that $\cos(\omega \tau) = -1$ and $\sin(\omega \tau) = 0$, and the two axles are excited with 180° phasing. In this case, if the center of mass were at mid-wheelbase and the system uncoupled, no bouncing would occur and the vehicle would only pitch. This consideration holds qualitatively for actual cases.

This phenomenon, usually referred to as wheelbase filtering, introduces a dependence between the response of the system and speed. If, for instance, the wheelbase is 2 m and the speed is 20 m/s, the delay τ is 0,1 s. The maximum pitch response, with a very low bounce, occurs when the irregularities have a wavelength equal to twice the wheelbase or one of the odd submultiples of twice the wheelbase, that is 4, 4/3, 4/5, ...m. At 20 m/s, the corresponding frequencies at which bounce motions are minimal are 5, 15, 25, ...Hz. In the same way, the maximum bounce motions with little pitching occur at wavelengths equal to the wheelbase and its whole sub-multiples, 2, 1, 0,5, ...m. At a speed of 20 m/s, the corresponding frequencies are

10, 20, 30, ...Hz. Moreover, little pitch excitation occurs at very low frequency, as already stated, and as a consequence pitch excitation is minimal in highway driving.

The situation may be different for industrial vehicles owing to the larger wheelbase and lower speed coupled with high spring stiffness: wheelbase filtering may lead to strong pitch response, accompanied by low bounce. The effect is further worsened by the fact that in tall vehicles pitch excitation causes longitudinal oscillation in points above the center of mass that may prove quite inconvenient.

In general, the expression of the excitation vector is

$$h_0 \left\{ \begin{array}{l} \left[K_1 + K_2 \cos(\omega\tau) - c_2\omega \sin(\omega\tau) \right] \sin(\omega t) + \\ \quad + \left[c_1\omega + c_2\omega \cos(\omega\tau) + K_2 \sin(\omega\tau) \right] \cos(\omega t) \\ \left[-aK_1 + bK_2 \cos(\omega\tau) - bc_2\omega \sin(\omega\tau) \right] \sin(\omega t) + \\ \quad + \left[-ac_1\omega + bc_2\omega \cos(\omega\tau) + bK_2 \sin(\omega\tau) \right] \cos(\omega t) \end{array} \right\} . \quad (26.100)$$

The equation of motion (26.66) for vertical and pitch oscillations can then be written as

$$\begin{aligned} & \begin{bmatrix} m_s & 0 \\ 0 & J_y \end{bmatrix} \begin{Bmatrix} \ddot{Z}_s \\ \ddot{\theta} \end{Bmatrix} + \begin{bmatrix} c_1 + c_2 & -ac_1 + bc_2 \\ -ac_1 + bc_2 & a^2c_1 + b^2c_2 \end{bmatrix} \begin{Bmatrix} \dot{Z}_s \\ \dot{\theta} \end{Bmatrix} + \\ & + \begin{bmatrix} K_1 + K_2 & -aK_1 + bK_2 \\ -aK_1 + bK_2 & a^2K_1 + b^2K_2 \end{bmatrix} \begin{Bmatrix} Z_s \\ \theta \end{Bmatrix} = \\ & = h_0 \begin{Bmatrix} f_1(\omega\tau) \sin(\omega t) + g_1(\omega\tau) \cos(\omega t) \\ f_2(\omega\tau) \sin(\omega t) + g_2(\omega\tau) \cos(\omega t) \end{Bmatrix} , \end{aligned} \quad (26.101)$$

where:

$$\begin{aligned} f_1(\omega\tau) &= K_1 + K_2 \cos(\omega\tau) - c_2\omega \sin(\omega\tau) , \\ f_2(\omega\tau) &= -aK_1 + bK_2 \cos(\omega\tau) - bc_2\omega \sin(\omega\tau) , \\ g_1(\omega\tau) &= c_1\omega + c_2\omega \cos(\omega\tau) + K_2 \sin(\omega\tau) , \\ g_2(\omega\tau) &= -ac_1\omega + bc_2\omega \cos(\omega\tau) + bK_2 \sin(\omega\tau) . \end{aligned} \quad (26.102)$$

Functions $f_i(\omega\tau)$ and $g_i(\omega\tau)$ may be considered as filters that, applied to the sine and cosine components of the excitation due to the road profile, yield the bounce and pitch excitation. However, because of coupling between the equations of motion, all terms of the excitation contribute to both bouncing and pitching.

To obtain a first approximation evaluation of the effect of wheelbase filtering, assume that the equations of motion are uncoupled ($aK_1 = bK_2$ and $bc_2 = ac_1$) and that the center of mass is at mid wheelbase ($a = b$). To comply with both these conditions the front and rear suspensions must have the same elastic and damping characteristics ($K_1 = K_2$ and $c_2 = c_1$).

The two equations of motion uncouple, reducing to

$$m_s \ddot{Z}_s + 2c_1 \dot{Z}_s + 2K_1 Z_s = h_0 [f_1(\omega\tau) \sin(\omega t) + g_1(\omega\tau) \cos(\omega t)], \quad (26.103)$$

where

$$\begin{aligned} f_1(\omega\tau) &= K_1 [1 + \cos(\omega\tau)] - c_1 \omega \sin(\omega\tau), \\ g_1(\omega\tau) &= c_1 \omega [1 + \cos(\omega\tau)] + K_1 \sin(\omega\tau), \end{aligned} \quad (26.104)$$

for vertical motions, and

$$J_y \ddot{\theta} + 2a^2 c_1 \dot{\theta} + 2a^2 K_1 \theta = h_0 [f_2(\omega\tau) \sin(\omega t) + g_2(\omega\tau) \cos(\omega t)], \quad (26.105)$$

where

$$\begin{aligned} f_2(\omega\tau) &= aK_1 [-1 + \cos(\omega\tau)] - ac_1 \omega \sin(\omega\tau), \\ g_2(\omega\tau) &= ac_1 \omega [-1 + \cos(\omega\tau)] + aK_1 \sin(\omega\tau), \end{aligned} \quad (26.106)$$

for pitching motions.

If the phasing between bounce and pitch motion is not to be computed, it is useless to obtain the sine and cosine components of the response separately: what matters is solely its amplitude. The amplitude of the excitation for bouncing motions is

$$h_0 \sqrt{2(K_1^2 + c_1^2 \omega^2)} \sqrt{1 + \cos(\omega\tau)}. \quad (26.107)$$

The corresponding frequency response is then

$$\left| \frac{Z_{s0}}{h_0} \right| = \sqrt{\frac{4(K_1^2 + c_1^2 \omega^2)}{(2K_1 - m\omega^2)^2 + 4c_1^2 \omega^2}} \sqrt{\frac{1 + \cos(\omega\tau)}{2}}. \quad (26.108)$$

The first square root is nothing else than the amplification factor of a quarter-car with a single degree of freedom with mass $m/2$, stiffness K_1 and damping c_1 . The second term gives the wheelbase filtering effect for vertical motions. Function

$$\sqrt{\frac{1 + \cos(\omega\tau)}{2}}$$

is plotted in Fig. 26.31a versus the frequency, together with the frequency response for the acceleration (inertance) of the quarter-car model and their product. The values of the speed and the wheelbase used to plot the figure are 30 m/s and 2.16 m respectively.

In a similar way, the amplitude of the excitation entering the second equation, that for pitching motions, is

$$h_0 \sqrt{2a^2(K_1^2 + c_1^2 \omega^2)} \sqrt{1 - \cos(\omega\tau)}. \quad (26.109)$$

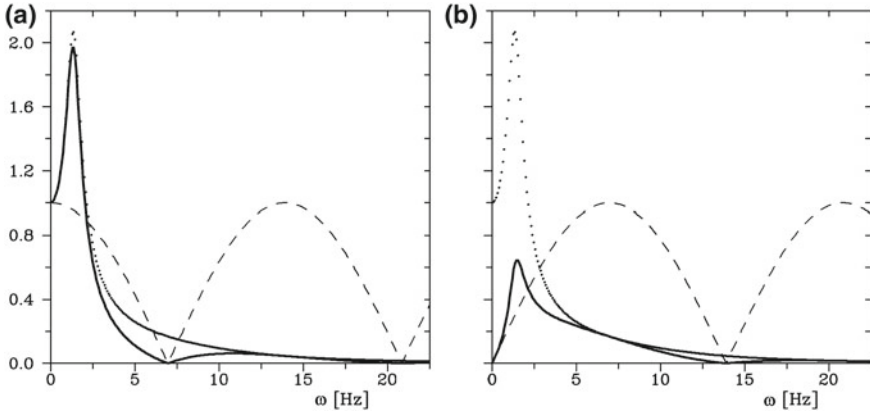


Fig. 26.31 Wheelbase filtering. **a** Function $\sqrt{2[1 + \cos(\omega\tau)]}$ (dotted line), inertance of the quarter-car model and product of the two; **b** Same as in (a), but for function $\sqrt{2[1 - \cos(\omega\tau)]}$. $V = 30$ m/s; $l = 2.16$ m

The frequency response for pitch motion is

$$\left| \frac{\theta_0}{h_0} \right| = \sqrt{\frac{4a^2 (K_1^2 + c_1^2\omega^2)}{(2a^2 K_1 - J_y\omega^2)^2 + 4a^2 c_1^2\omega^2}} \sqrt{\frac{1 - \cos(\omega\tau)}{2}}, \tag{26.110}$$

that is, introducing the dynamic index I_d ,

$$\left| \frac{\theta_0}{h_0} \right| = \sqrt{\frac{4 (K_1^2 + c_1^2\omega^2)}{(2K_1 - mI_d\omega^2)^2 + 4c_1^2\omega^2}} \sqrt{\frac{1 - \cos(\omega\tau)}{2}}. \tag{26.111}$$

If the dynamic index has a unit value, the first square root coincides with that seen for vertical motions, that is, it coincides with the amplification factor of a quarter-car with a single degree of freedom with mass $m/2$, stiffness K_1 and damping c_1 ; reference must otherwise be made directly to the pitching oscillations of the beam constituting the model of the vehicle. The second term yields the wheelbase filtering effect for pitching motions. Function

$$\sqrt{\frac{1 - \cos(\omega\tau)}{2}}$$

is plotted in Fig. 26.31b versus the frequency, together with the inertance of the quarter-car and their product, using the same values of V and l , as in Fig. 26.31a.

Remark 26.10 The subjective feeling of riding comfort is also affected by the position of the passengers; when they are close to the centre of mass, pitching oscillations

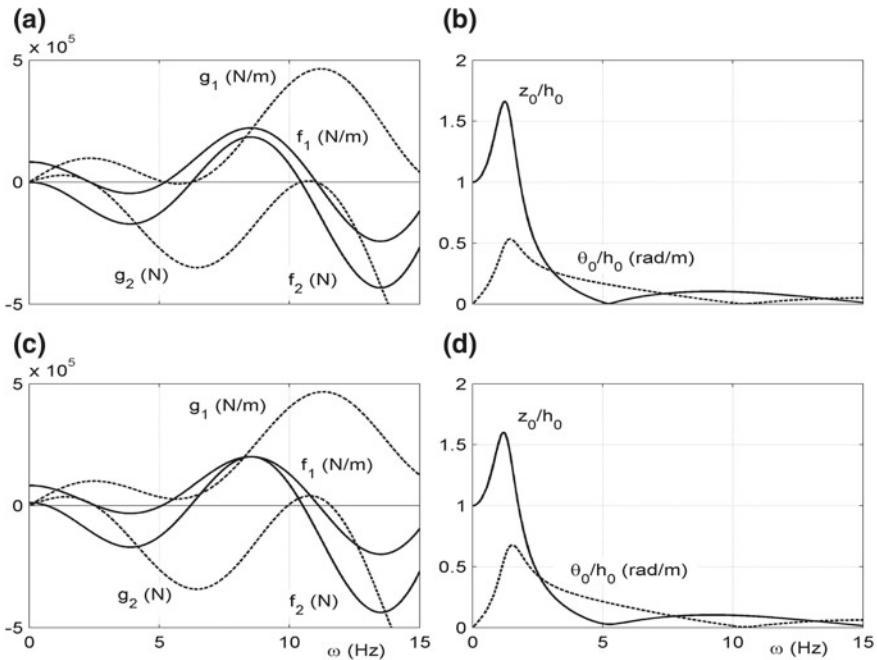


Fig. 26.32 Functions $f_i(\omega\tau)$ and $g_i(\omega\tau)$ and frequency responses for bounce and pitch motions for the vehicle of the previous examples at 100 km/h. **a** and **b** simplified uncoupled model. **c** and **d** actual value of the parameters

are slight, but they may be a nuisance in points located a greater distance from it. Bounce—pitch coupling due to suspensions may severely reduce riding comfort.

Example 26.9 Compute functions $f_i(\omega\tau)$ and $g_i(\omega\tau)$ for the vehicle of the previous examples at a speed of 100 km/h = 27.8 m/s and plot the frequency responses for bounce and pitch oscillations.

The computation will be performed initially using a first approximation model (uncoupling between bounce and pitch and unit dynamic index), and then factoring in the actual value of the parameters.

To uncouple the equations, the actual values of a and b are substituted by $l/2$ and those of K_1, K_2, c_1 and c_2 by the mean values of the stiffnesses and damping coefficients. Moreover, J_y is assumed to be equal to mab .

The results are plotted in Fig. 26.32a, b. As expected, at vanishing frequency and when l is equal to a whole multiple of λ ($\omega = 0, \omega = 10.44$ Hz, ...) the pitching response vanishes and only bounce is present. If l is an odd multiple of $\lambda/2$ ($\omega = 5.22$ Hz, $\omega = 15.66$ Hz, ...) the bounce response vanishes and only pitch is present.

The results obtained from the actual values of the parameters are shown in Fig. 26.32c, d. As is clear from the figure, the results differ from those obtained

by uncoupling the equations, but the difference is not large. In particular, the bounce response never vanishes, even if at about 5 and 15 Hz it becomes quite small.

It must be noted that the model with stiff tires used here should not be used for frequencies higher than 4–6 Hz.

26.5.5 Effect of Tire Compliance

If the compliance of tires is accounted for, the model must contain also the unsprung masses. The minimum number of degrees of freedom needed to study bounce and pitch motions is four (Fig. 26.33a). If the dynamic index has a unit value, the model of Fig. 26.33a may be substituted by that of Fig. 26.33b.

Remembering that the excitation due to the vertical motion of points A and B can be expressed by Eq. (26.96), the equation of motion can be written in the form

$$\begin{aligned}
 & \begin{bmatrix} m_s & 0 & 0 & 0 \\ 0 & J_y^* & 0 & 0 \\ 0 & 0 & m_1 & 0 \\ 0 & 0 & 0 & m_2 \end{bmatrix} \begin{Bmatrix} \ddot{Z}_s \\ \ddot{\theta} \\ \ddot{Z}_1 \\ \ddot{Z}_2 \end{Bmatrix} + \\
 & + \begin{bmatrix} c_1 + c_2 & -ac_1 + bc_2 & -c_1 & -c_2 \\ & a^2c_1 + b^2c_2 & ac_1 & -bc_2 \\ & & c_1 + 2c_{p1} & 0 \\ \text{symm.} & & & c_2 + 2c_{p2} \end{bmatrix} \begin{Bmatrix} \dot{Z}_s \\ \dot{\theta} \\ \dot{Z}_1 \\ \dot{Z}_2 \end{Bmatrix} + \\
 & + \begin{bmatrix} K_1 + K_2 & -aK_1 + bK_2 & -K_1 & -K_2 \\ & a^2K_1 + b^2K_2 & aK_1 & -bK_2 \\ & & K_1 + 2P_1 & 0 \\ \text{symm.} & & & K_2 + 2P_2 \end{bmatrix} \begin{Bmatrix} Z_s \\ \theta \\ Z_1 \\ Z_2 \end{Bmatrix} = \\
 & = h_0 \begin{Bmatrix} 0 \\ 0 \\ 2P_1 \sin(\omega t) + 2\omega c_{p1} \cos(\omega t) \\ 2f(\omega\tau) \sin(\omega t) + 2g(\omega\tau) \cos(\omega t) \end{Bmatrix}, \tag{26.112}
 \end{aligned}$$

where m_1 and m_2 are the unsprung masses of the two axes.

$$\begin{aligned}
 f(\omega\tau) &= P_2 \cos(\omega\tau) - c_{p2}\omega \sin(\omega\tau), \\
 g(\omega\tau) &= c_{p2}\omega \cos(\omega\tau) + P_2 \sin(\omega\tau). \tag{26.113}
 \end{aligned}$$

Example 26.10 Compute the frequency responses for bounce and pitch motion using the model with four degrees of freedom. Compare the results with those obtained from the model with two degrees of freedom.

Data of the unsprung masses: $m_{n1} = m_{n2} = 65$ kg, $P_1 = P_2 = 125$ kN/m, $c_{p1} = c_{p2} = 0$.

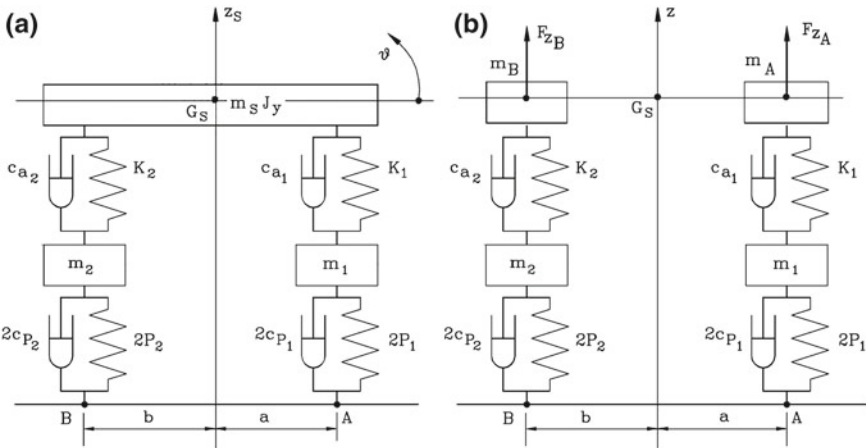


Fig. 26.33 Beam models with four degrees of freedom for the study of pitch and bounce motions taking into account the compliance of tires

The results obtained using the model with two degrees of freedom are reported in Fig. 26.34a, b, while those obtained using the model of four degrees of freedom are reported in Fig. 26.34c, d. The values of the natural frequencies of the undamped system are 1.25, 1.51, 10.61 e 10.74 Hz, while those of the simplified model are 1.36 e 1.62 Hz.

At low frequency the results obtained from the two models are similar, while at frequencies higher than those of the unsprung masses the filtering effect of the tires reduces the amplitude of the response.

26.5.6 Interconnected Suspensions

If the value of the pitch natural frequency is too high when compared with that of the bounce motions, ride comfort may be affected. To control the natural frequencies of pitch and bounce independently, without changing the wheel positions and the inertial properties of the body, the suspensions can be interconnected. Pitching frequencies can be raised without increasing those in bounce if the front and rear wheels are connected by a spring opposing pitching motions, similar to the anti-roll bars used for rolling motions. This is however the opposite of what is usually needed and, moreover, has the effect of decreasing the damping of pitch.

Various types of mechanical, hydraulic or pneumatic interconnections may be used, the latter particularly in the presence of air or hydraulic springs. A mechanical solution is shown in Fig. 26.35a. The vehicle is based on longitudinal swing arm suspensions, with springs located longitudinally under the sprung mass. The springs are connected to a further element, itself elastically connected to the vehicle body.

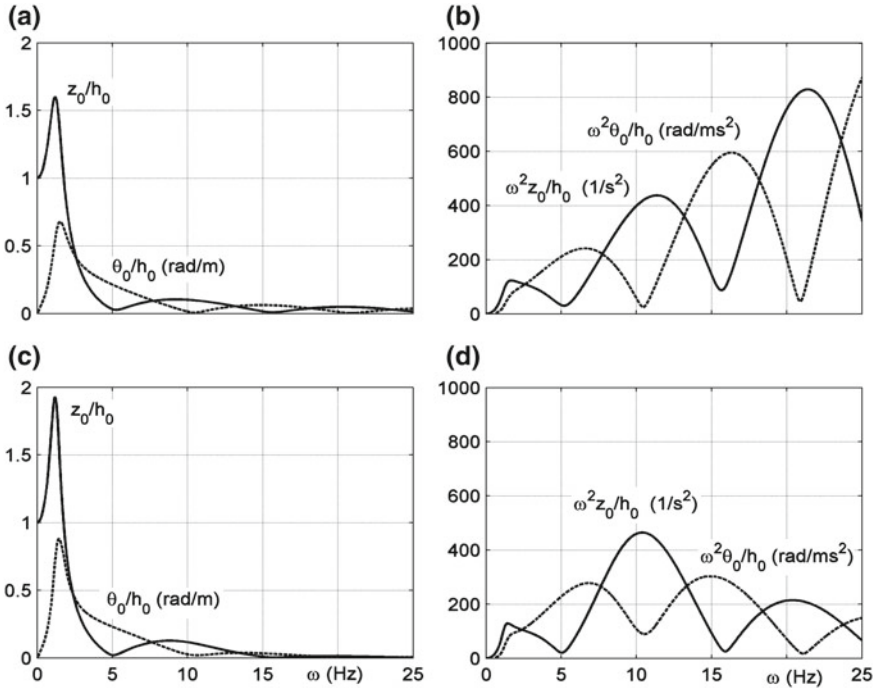


Fig. 26.34 Frequency responses for displacements and accelerations in bounce and pitch motions for the vehicle of the previous examples at 100 km/h. **a** and **b** model with two degrees of freedom; **c** and **d** model with four degrees of freedom

The system is functionally similar (even if simpler) to the model shown in Fig. 26.35b, in which the intermediate element is a beam, hinged to the vehicle body and connected to the unsprung masses through springs. The tires are considered here as rigid bodies and have not been included in the model.

If the beam and springs with stiffness χ_1 and χ_2 were not included, the equation of motion would have been Eq. (26.66), without the damping matrix, as in the figure, if damping is neglected. If the inertia of the beam is neglected, no further degree of freedom is needed, because the position of the beam is determined by the displacement z and the rotation θ of the sprung mass. The stiffness matrix may be obtained simply by adding the potential energy of springs χ_1 and χ_2 and performing the relevant derivatives.

The positions of points P and Q are simply

$$\begin{cases} z_P = z + c\theta - l_1\gamma \\ z_Q = z + c\theta + l_2\gamma \end{cases}, \tag{26.114}$$

where γ is the angle between line PQ and the horizontal and all relevant angles are assumed to be small.

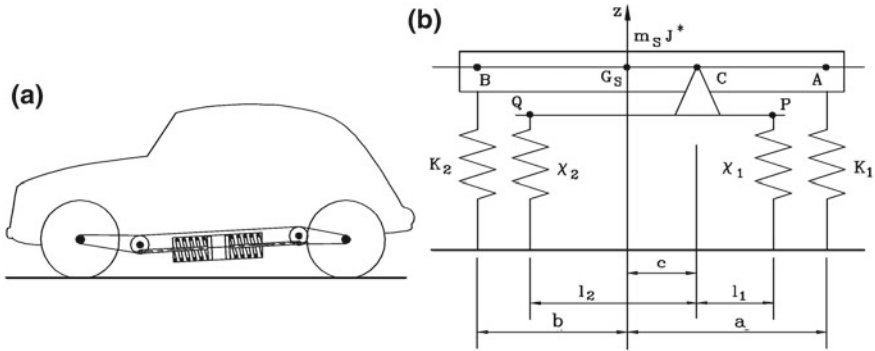


Fig. 26.35 Longitudinal interconnection of the suspensions. **a** Sketch of an application; **b** model in which the interconnection is implemented using a beam hinged to the sprung mass. The tires are considered as rigid bodies and not included in the model

The potential energy due to the two added springs is

$$\begin{aligned}
 2\mathcal{U} &= \chi_1 z_P^2 + \chi_2 z_Q^2 = (\chi_1 + \chi_2) (z^2 + c^2\theta^2 + 2c\theta z) + \\
 &+ \gamma^2 (l_1^2 \chi_1 + l_2^2 \chi_2) + 2\gamma (z + c\theta) (l_1 \chi_1 - l_2 \chi_2) .
 \end{aligned}
 \tag{26.115}$$

The value of γ can be easily computed by stating

$$\frac{\partial \mathcal{U}}{\partial \gamma} = 0 ,$$

which yields

$$\gamma = -(z + c\theta) \frac{l_1 \chi_1 - l_2 \chi_2}{l_1^2 \chi_1 + l_2^2 \chi_2} .
 \tag{26.116}$$

The final expression for the potential energy is then

$$\mathcal{U} = \frac{1}{2} (z + c\theta)^2 \frac{\chi_1 \chi_2 (l_1 + l_2)^2}{l_1^2 \chi_1 + l_2^2 \chi_2} .
 \tag{26.117}$$

By performing the relevant derivatives, the stiffness matrix becomes

$$\mathbf{K} = \begin{bmatrix} K_1 + K_2 + \chi & -aK_1 + bK_2 + \chi c \\ -aK_1 + bK_2 + \chi c & a^2 K_1 + b^2 K_2 + \chi c^2 \end{bmatrix} ,
 \tag{26.118}$$

where

$$\chi = \frac{\chi_1 \chi_2 (l_1 + l_2)^2}{l_1^2 \chi_1 + l_2^2 \chi_2} .$$

From Eq. (26.118) it is clear that the terms due to the interconnection between front and rear suspensions affect in a different way the various elements of the stiffness matrix and allow us to modify independently the values of the bounce and pitch natural frequencies, possibly lowering the latter without affecting the former.

26.6 Roll Motion

26.6.1 Model with a Single Degree of Freedom

As already stated, roll is coupled with handling and not with ride comfort. However it is also true that rolling can affect strongly the subjective feeling of riding comfort.

The simplest model for studying roll motion is a rigid body, simulating the sprung mass, free to rotate about the roll axis, constrained to the ground by a set of springs and damper with a stiffness and a damping coefficient equal to those of the suspensions (Fig. 26.36). If J_x , m_s , χ_i and Γ_i are respectively the moment of inertia about the roll axis, the sprung mass, the torsional stiffness and the damping coefficient of the i th suspension, the equation of motion is

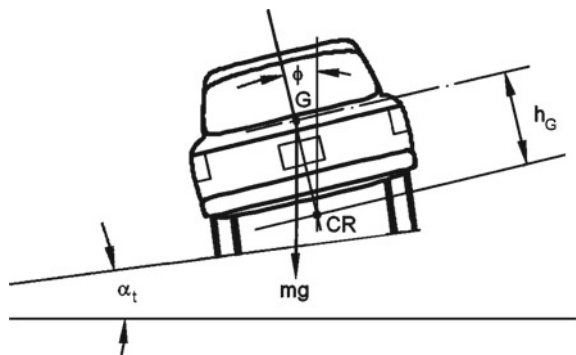
$$\begin{aligned}
 J_x \ddot{\phi} + (\Gamma_1 + \Gamma_2) \dot{\phi} + (\chi_1 + \chi_2) \phi - m_s g h_G \sin(\phi) &= & (26.119) \\
 &= \Gamma_1 \dot{\alpha}_{t_1} + \Gamma_2 \dot{\alpha}_{t_2} + \chi_1 \alpha_{t_1} + \chi_2 \alpha_{t_2} ,
 \end{aligned}$$

where the forcing functions are those due to the transversal inclination of the road α_{t_i} at the i th suspension.

The inertia of the unsprung masses and the compliance of the tires are not included in such a simple model, which is formally identical to the quarter-car with a single degree of freedom.

For small values of the roll angle, the model may be linearized, stating $\sin(\phi) \approx \phi$. The roll natural frequency is then

Fig. 26.36 Model with a single degree of freedom for the study of roll motion. Cross section in a plane containing the center of mass G of the sprung mass. The roll axis goes through point CR



$$\omega_{roll} = \sqrt{\frac{\chi_1 + \chi_2 - m_s g h_G}{J_x}} . \quad (26.120)$$

The optimum damping value may be obtained from Eq. (26.12):

$$\Gamma_{opt} = \sqrt{\frac{J_x (\chi_1 + \chi_2 - m_s g h_G)}{2}} . \quad (26.121)$$

This condition is generally not satisfied, particularly if the vehicle has anti-roll bars. The torsional damping of the suspensions is supplied by the same shock absorbers normally designed to optimize vertical motion; the roll damping they supply is usually lower than needed. The increase in stiffness due to anti-roll bars is not accompanied by an increase in damping. The effect causes a decrease of the damping ratio, together with an increase of the natural frequency.

The stiffer the suspension in torsion, the more underdamped the roll behavior, if the increase in stiffness is due to anti-roll bars. Although reducing rolling in stationary conditions, they may increase it in dynamic conditions. An overelongation in the step response, as when roll is due to a moment abruptly applied (steering step input, wind gusts or other similar instances), may then result. A large roll in dynamic conditions may cause rollover.

The stationary value of the roll angle on a road with transversal slope $\alpha_t = \alpha_{t_1} = \alpha_{t_2}$ is

$$\phi = \alpha_t \frac{\chi_1 + \chi_2}{\chi_1 + \chi_2 - m_s g h_G} . \quad (26.122)$$

The importance of a center of mass not too high on the roll axis and stiff suspensions (in roll) is then clear. The last condition contradicts the need for a small roll in dynamic conditions.

Example 26.11 Consider the vehicle studied in Example 26.7, and assume that the moment of inertia J_x is equal to 388.8 kg m^2 and the sprung mass is $1,080 \text{ kg}$. Compute the time history of the roll angle when the vehicle encounters a ramp leading from a horizontal road to a transversal slope $\alpha_t = 5^\circ$ in a distance of 10 m at a speed of 30 m/s .

Other data: stiffnesses of the axles $K_1 = 45 \text{ kN/m}$, $K_2 = 38 \text{ kN/m}$, damping of the axles $c_1 = 3,820 \text{ Ns/m}$, $c_2 = 2,865 \text{ Ns/m}$, distance of the springs and dampers from the symmetry plane $d = 0.5 \text{ m}$, wheelbase $l = 2.66 \text{ m}$. Repeat the computation, adding an anti-roll bar at the front axle, with a stiffness $\chi_b = 4,000 \text{ Nm/rad}$.

Computation without anti-roll bar.

The stiffnesses and damping coefficients of the axles can be computed using formulae of the type

$$\chi_i = K_i d_i^2 . \quad (26.123)$$

It then follows that: $\chi_1 = 11.25 \text{ kNm/rad}$, $\chi_2 = 9.5 \text{ kNm/rad}$, $\Gamma_1 = 955 \text{ Nms/rad}$, $\Gamma_2 = 716 \text{ Nms/rad}$. The total roll damping $\Gamma_1 + \Gamma_2 = 1.671 \text{ Nms/rad}$ is then smaller than the optimum damping computed by neglecting the gravitational effect (2.008 Nms/rad), while only slightly smaller than that computed by taking it into account (1.733 Nsm/rad).

The roll natural frequencies are then $\omega = 1.00 \text{ Hz}$ (gravitational effect included) or $\omega = 1.16 \text{ Hz}$.

The linearized, state space equation

$$\begin{Bmatrix} \dot{v}_\phi \\ \dot{\phi} \end{Bmatrix} = \begin{bmatrix} -\frac{(\Gamma_1+\Gamma_2)}{J_x} & -\frac{\chi}{J_x} \\ 1 & 0 \end{bmatrix} \begin{Bmatrix} v_\phi \\ \phi \end{Bmatrix} + \frac{1}{J_x} \begin{bmatrix} \Gamma_1 & \Gamma_2 & \chi_1 & \chi_2 \\ 0 & 0 & 0 & 0 \end{bmatrix} \begin{Bmatrix} \dot{\alpha}_{t_1} \\ \dot{\alpha}_{t_2} \\ \alpha_{t_1} \\ \alpha_{t_2} \end{Bmatrix} \quad (26.124)$$

where $v_\phi = \dot{\phi}$, can be written and then solved numerically to compute the time history of the response.

The input to the system is given by angles α_i and their derivatives. If the excitation is due to motion at a speed V on a ramp having a length l_r leading linearly to a transversal slope α_t , assuming that at time $t = 0$ the front axle meets the ramp, it follows that

$$\alpha_{t_1} = \begin{cases} 0 & \text{for } t \leq 0 \\ \alpha_t t \frac{V}{l_r} & \text{for } 0 < t < \frac{l_r}{V} \\ \alpha_t & \text{for } t \geq \frac{l_r}{V}, \end{cases} \quad \alpha_{t_2} = \begin{cases} 0 & \text{for } t \leq \frac{l_r}{V} \\ \alpha_t \left(t - \frac{l_r}{V}\right) \frac{V}{l_r} & \text{for } \frac{l_r}{V} < t < \frac{l_r+l}{V} \\ \alpha_t & \text{for } t \geq \frac{l_r+l}{V}, \end{cases} \quad (26.125)$$

$$\dot{\alpha}_{t_1} = \begin{cases} 0 & \text{for } t \leq 0 \\ \alpha_t \frac{V}{l_r} & \text{for } 0 < t < \frac{l_r}{V} \\ \alpha_t & \text{for } t \geq \frac{l_r}{V}, \end{cases} \quad \dot{\alpha}_{t_2} = \begin{cases} 0 & \text{for } t \leq \frac{l_r}{V} \\ \alpha_t \frac{V}{l_r} & \text{for } \frac{l_r}{V} < t < \frac{l_r+l}{V} \\ \alpha_t & \text{for } t \geq \frac{l_r+l}{V}. \end{cases} \quad (26.126)$$

Computation with anti-roll bar.

The computation is then repeated after adding the stiffness of the anti-roll bar to that of the suspensions. The roll natural frequency is now $\omega = 1.13 \text{ Hz}$.

The results are reported in non-dimensional form in Fig. 26.37. Results obtained with both the actual and the optimum damping are reported for the case without anti-roll bar. In this case, the actual damping is smaller than the optimum and the difference between the two results is small.

As expected, the steady state inclination of the body coincides with the transversal slope of the road, if the effect of the weight is neglected. If weight is accounted for, the final inclination of the body is greater. The nonlinear model has been integrated numerically to check whether the results obtained are realistic: owing to the low values of the angles, the difference between the linearized and the nonlinear results is negligible.

If an anti-roll bar is present the whole curve decreases, when the effect of weight is taken into account. If the latter is neglected, the effect of the anti-roll bar is minimal.

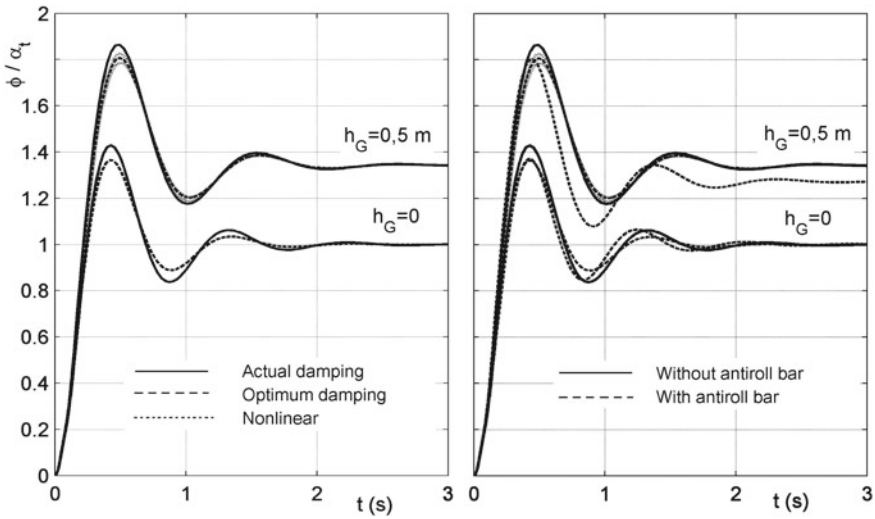


Fig. 26.37 Time history of the roll angle when the vehicle manages a ramp leading from level road to a transversal slope α_t . Model with 1 degree of freedom

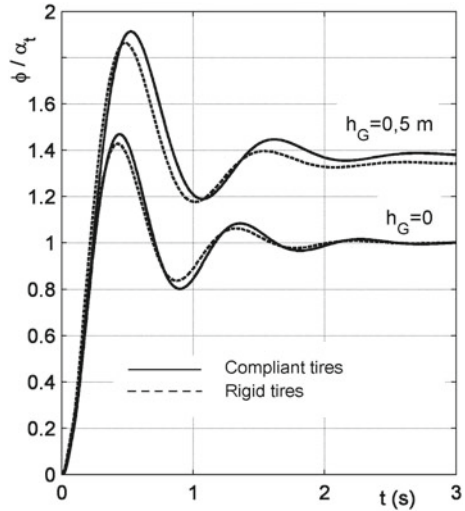
26.6.2 Model with Many Degrees of Freedom

A simple model with three degrees of freedom may be used to take rolling of unsprung masses and compliance of the tires into account. The unsprung masses are modelled as rigid bodies free to rotate about the roll axis of the vehicle. It is clear that this model is a rough approximation, particularly if independent suspensions are used. This further approximation, however, does not worsen matters, because the largest errors come from studying roll motion without taking into account that they are coupled with handling motions.

The linearized equation for the study of roll motion is

$$\begin{aligned}
 & \begin{bmatrix} J_x & 0 & 0 \\ 0 & J_{x_1} & 0 \\ 0 & 0 & J_{x_1} \end{bmatrix} \begin{Bmatrix} \ddot{\phi} \\ \ddot{\phi}_1 \\ \ddot{\phi}_2 \end{Bmatrix} + \begin{bmatrix} \Gamma_1 + \Gamma_2 & -\Gamma_1 & -\Gamma_2 \\ -\Gamma_1 & \Gamma_1 + \Gamma_{p_1} & 0 \\ -\Gamma_2 & 0 & \Gamma_2 + \Gamma_{p_2} \end{bmatrix} \times \\
 & \times \begin{Bmatrix} \dot{\phi} \\ \dot{\phi}_1 \\ \dot{\phi}_2 \end{Bmatrix} + \begin{bmatrix} \chi_1 + \chi_2 - m_s g h_G & -\chi_1 & -\chi_2 \\ -\chi_1 & \chi_1 + \chi_{p_1} & 0 \\ -\chi_2 & 0 & \chi_2 + \chi_{p_2} \end{bmatrix} \begin{Bmatrix} \phi \\ \phi_1 \\ \phi_2 \end{Bmatrix} = \quad (26.127) \\
 & = \begin{Bmatrix} 0 \\ \Gamma_{p_1} \dot{\alpha}_{t_1} + \chi_{p_1} \alpha_{t_1} \\ \Gamma_{p_2} \dot{\alpha}_{t_2} + \chi_{p_2} \alpha_{t_2} \end{Bmatrix},
 \end{aligned}$$

Fig. 26.38 Time history of the roll angle when the vehicle manages a ramp leading from level road to a transversal slope α_t . Model with three degrees of freedom



where $\chi_i, \chi_{p_i}, \Gamma_i, \Gamma_{p_i}$ are the stiffness and the damping of the suspensions and of the tires. The excitation is given by the transversal slope of the road α_{t_1} and α_{t_2} at the front and rear axles.

Equation (26.127) can be solved numerically and allows the natural frequencies of roll oscillations to be computed.

To drastically simplify the model, the moment of inertia of the unsprung masses and the damping of the tires can be neglected. The equations of motion are thus a set of one second-order equation plus two first-order ones. The state space equation so obtained is of the fourth order:

$$\begin{aligned} \begin{Bmatrix} \dot{v}_\phi \\ \dot{\phi} \\ \dot{\phi}_1 \\ \dot{\phi}_2 \end{Bmatrix} &= \begin{bmatrix} 0 & m_s g h_G / J_x & -\chi_{p_1} / J_x & -\chi_{p_2} / J_x \\ 1 & 0 & 0 & 0 \\ 1 & \chi_1 / \Gamma_1 & -(\chi_1 + \chi_{p_1}) / \Gamma_1 & 0 \\ 1 & \chi_2 / \Gamma_2 & 0 & -(\chi_2 + \chi_{p_2}) / \Gamma_2 \end{bmatrix} \times \\ &\times \begin{Bmatrix} v_\phi \\ \phi \\ \phi_1 \\ \phi_2 \end{Bmatrix} + \begin{bmatrix} \chi_{p_1} / J_x & \chi_{p_2} / J_x \\ 0 & 0 \\ \chi_{p_1} / \Gamma_1 & 0 \\ 0 & \chi_{p_2} / \Gamma_2 \end{bmatrix} \begin{Bmatrix} \alpha_{t_1} \\ \alpha_{t_2} \end{Bmatrix}. \end{aligned} \tag{26.128}$$

Example 26.12 Consider the vehicle of the previous example, assuming that the stiffness of the tires is 125 kN/m. Assuming a value of 1.48 m for the track, the torsional stiffness for the unsprung masses is $\chi_1 = \chi_2 = 136.9$ kNm/rad. The results are reported in Fig. 26.38 in nondimensional form.

As is clear from the figure, the effect of the compliance of the tire is not large.

26.7 Effect of Nonlinearities

26.7.1 Shock Absorbers

As previously stated, shock absorbers are far from being linear viscous dampers. In fact, most automotive shock absorbers are unsymmetrical, with a damping which is larger in the rebound stroke. Apart from the nonlinearities in the behavior of the shock absorbers and those due to the geometry of the suspension, along with asymmetries purposely built in, other unwanted nonlinear effects, such as dry friction, are often present. Particular care must be devoted to the effects of lateral loads in McPherson suspensions, due to a more or less pronounced dependence of the characteristics on temperature and cavitation. The latter phenomenon is primarily felt at high temperature, and consists in the vaporization of the fluid or the expansion of the gasses dissolved in it.

Moreover, even in cases where shock absorbers are assumed to act in the same direction as other forces, some deviations may occur in practice, introducing further nonlinearities that should be accounted for.

By neglecting the inertia of moving elements and temperature variations, the force exerted by a shock absorber may be considered as a function of both relative displacement and relative velocity of its endpoints:

$$F = F(z, \dot{z}) . \quad (26.129)$$

The experimental results are often reported in the form of a force-displacement plot (Fig. 26.39a). If the force were proportional to velocity (viscous damping) the plot obtained in harmonic motion conditions would be an ellipse, with a ratio between its axes proportional to the frequency. If the characteristics were linear but unsymmetrical (i.e., bilinear) the plot would be made by two semi-ellipses, one above (the smallest) and one below (the largest) the abscissa's axis.

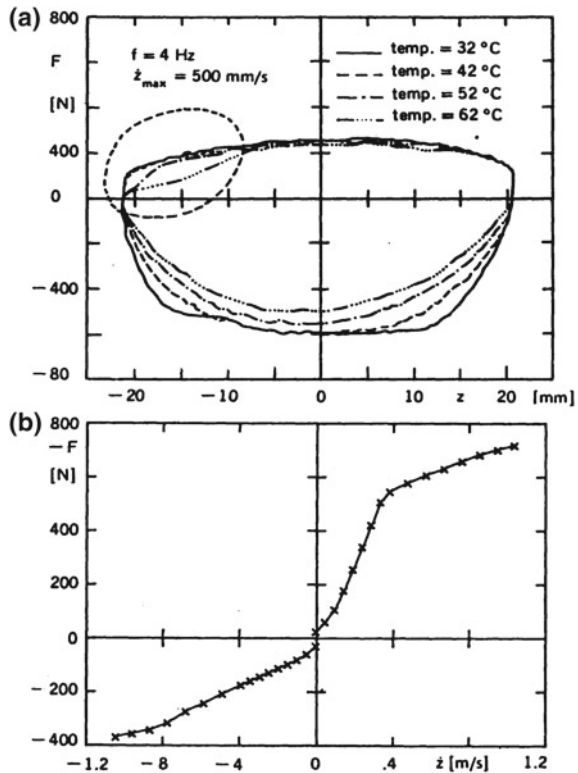
The force-speed plot (characteristic plot) of the same shock absorber is reported in Fig. 26.39b. If no cavitation occurs, the force depends only on the speed, i.e., the intersections of the surface (26.129) with planes with \dot{z} constant are horizontal straight lines, and the characteristic diagram is unique. In this case, force F depends only on \dot{z} and may be written as the sum of a linear characteristic (viscous damping), an odd function $f_o(\dot{z})$ and an even function $f_e(\dot{z})$ of the speed \dot{z} ¹³

$$F = -c \dot{z} - f_e(\dot{z}) - f_o(\dot{z}) . \quad (26.130)$$

The two functions are, respectively, the *deviation from symmetry* and the *deviation from linearity*.

¹³G. Genta, P. Campanile, *An Approximated Approach to the Study of Motor Vehicle Suspensions with Nonlinear Shock Absorbers*, *Meccanica*, Vol. 24, 1989, pp. 47- 57.

Fig. 26.39 **a** Force-displacement experimental plot for a shock absorber at various temperatures. Note the anomaly, likely due to cavitation, in the second quadrant. **b** Force-speed plot for the same shock absorber, obtained in slightly different conditions



In the simplest case of bilinear characteristic, only the former is present and the characteristic is

$$F = -c\dot{z} [1 + \mu \operatorname{sgn}(\dot{z})] . \tag{26.131}$$

The characteristic of a shock absorber described by Eq. (26.131) is plotted for various values of μ , in Fig. 26.40a.

The experimental characteristics of two automotive shock absorbers are plotted in Fig. 26.41. The characteristic of the first is bilinear, and may be approximated with good precision using Eq. (26.131) with:

$$c = 3.25 \text{ kNs/m} , \quad \mu = 0.3846 .$$

The characteristic of the second is more complicated and can be expressed by Eq. (26.130) with

$$c = 1000 \text{ kNs/m} , \quad f_o = 268.6\sqrt{|\dot{z}|} + 350 |\dot{z}| , \\ f_e = 268.6\sqrt{|\dot{z}|}\operatorname{sgn}(\dot{z}) - 350\dot{z} ,$$

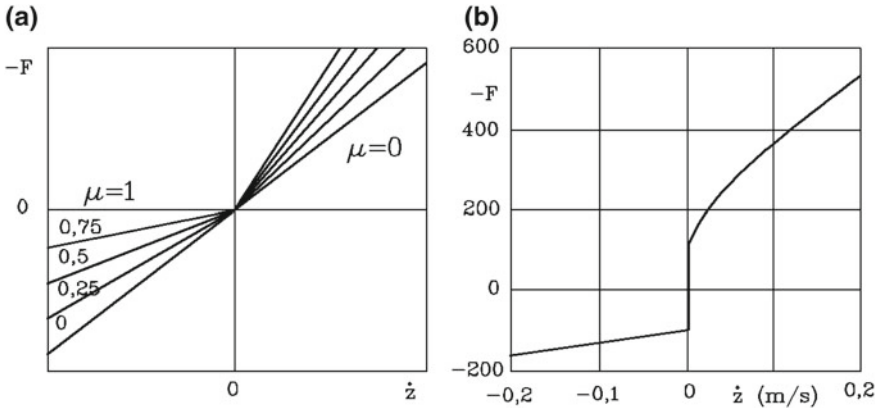


Fig. 26.40 a Characteristics of bi-linear shock absorbers (Eq. (26.131)), with various values of μ . b Effect of dry friction on the characteristics of a nonlinear nonsymmetric shock absorber

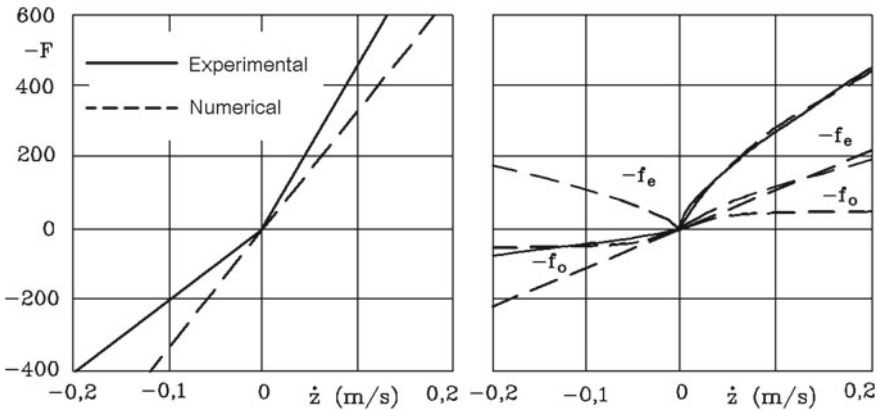


Fig. 26.41 Characteristics of two shock absorbers, one bi-linear and the other one nonlinear

where \dot{z} is in m/s.

A step function centered in the origin can be added to $f_o(\dot{z})$ to include dry friction in the model. The characteristics of Fig. 26.41b with dry friction added is shown in Fig. 26.40b.

Consider a quarter-car model with a single degree of freedom with a nonlinear shock absorber whose characteristic is expressed by Eq. (26.130). The equation of motion is

$$m\ddot{z} + c\dot{z} + Kz + f_e(\dot{z} - \dot{h}) + f_o(\dot{z} - \dot{h}) = c\dot{h} + Kh . \tag{26.132}$$

In this case, it is easier to write the equation in terms of relative displacement

$$z_r = z - h,$$

instead of the displacement z , obtaining

$$m\ddot{z}_r + c\dot{z}_r + Kz_r + f_e\dot{z}_r + f_o\dot{z}_r = -m\ddot{h}. \tag{26.133}$$

Because the system is nonlinear, the response will be a generic periodic but non-harmonic law even if the forcing function is harmonic. It may, at any rate, be expressed by a Fourier series

$$z_r = z_0 + \sum_{i=0}^{\infty} z_i \sin(i\omega t + \phi_i), \tag{26.134}$$

where all harmonics, including that of order 0, may be present, because the nonlinear function contains both even and odd terms. If the nonlinearities are not too strong, a first approximation solution may be obtained by truncating the series after the term with $i = 1$. Working in phase with the response and not with the excitation, it is possible to write

$$\begin{cases} h = h_0 \sin(\omega t - \phi) \\ z_r = z_0 + z_1 \sin(\omega t) \end{cases} \tag{26.135}$$

By introducing solution (26.135) into Eq. (26.133), the latter transforms into the algebraic equation

$$\mathcal{F}(t) = 0, \tag{26.136}$$

where

$$\begin{aligned} \mathcal{F}(t) = z_1 [& (K - m\omega^2) \sin(\omega t) + c\omega \cos(\omega t)] + \\ & + z_0 K + f_e(\omega z_1 \cos(\omega t)) + f_o(\omega z_1 \cos(\omega t)) + \\ & - \omega^2 m h_0 [\cos(\phi) \sin(\omega t) - \sin(\phi) \cos(\omega t)]. \end{aligned} \tag{26.137}$$

An approximated solution for z_0 and z_1 may be obtained by stating that Eq. (26.136) holds as an average for a whole period, instead of holding in each instant. This may be formalized by stating that the integral of the virtual work

$$\mathcal{F}(t)\delta z_r = \mathcal{F}(t) [\delta z_0 + \delta z_1 \sin(\omega t)] \tag{26.138}$$

for a period vanishes.

Because the virtual displacements δz_0 and δz_1 are arbitrary, this amounts to stating

$$\begin{cases} \int_0^T \mathcal{F}(t) dt = 0 \\ \int_0^T \mathcal{F}(t) \sin(\omega t) dt = 0 \end{cases} \tag{26.139}$$

Since the integrals over a period of sine and cosine functions and of all odd functions of any trigonometric function vanish, the first equation yields

$$z_0 K T + \int_0^T f_e (\omega z_1 \cos (\omega t)) dt = 0 . \tag{26.140}$$

It follows then that

$$z_0 = -\frac{1}{2\pi K} \int_0^{2\pi} f_e (\omega z_1 \cos (\omega t)) d (\omega t) . \tag{26.141}$$

In the case of the bi-linear shock absorber, from Eq. (26.131) follows

$$f_e = c \dot{z} \mu \operatorname{sgn} (\dot{z}) = c \omega z_1 \mu |\cos (\omega t)| \tag{26.142}$$

and then

$$z_0 = -\frac{c \omega z_1 \mu}{2\pi K} \int_0^{2\pi} |\cos (\omega t)| d (\omega t) = -\frac{2c \omega z_1 \mu}{\pi K} . \tag{26.143}$$

From simple symmetry considerations, it follows that

$$\begin{aligned} \int_0^T f_e (\omega z_1 \cos (\omega t)) \sin (\omega t) dt &= 0 \\ \int_0^T f_o (\omega z_1 \cos (\omega t)) \sin (\omega t) dt &= 0 \end{aligned}$$

and then the second Eq. (26.131) yields

$$z_1 (K - m \omega^2) = \omega^2 m h_0 \cos (\phi) . \tag{26.144}$$

The phasing between the forcing function and the harmonic component of the response can be computed by stating that the energy dissipated in a cycle by the damper is equal to the energy supplied by the forcing function

$$\int_0^T [c \dot{z} + f_e (\dot{z}) + f_o (\dot{z})] \dot{z} dt = \int_0^T -m \ddot{h} \dot{z} dt , \tag{26.145}$$

that is

$$\begin{aligned} \int_0^T [c z_1 \omega \cos^2 (\omega t) + f_e (\omega z_1 \cos (\omega t)) \cos (\omega t) + \\ + f_o (\omega z_1 \cos (\omega t)) \cos (\omega t)] dt = -m h_0 \omega^2 \int_0^T \cos^2 (\omega t) \sin (\phi) dt . \end{aligned} \tag{26.146}$$

Because

$$\int_0^T f_e(\omega z_1 \cos(\omega t)) \cos(\omega t) dt = 0, \tag{26.147}$$

it follows that

$$c z_1 \omega + \frac{1}{\pi} \int_0^{2\pi} f_o(\omega z_1 \cos(\omega t)) \cos(\omega t) d(\omega t) = -m h_0 \omega^2 \sin(\phi). \tag{26.148}$$

Equations (26.144) and (26.148) allow the two remaining unknowns, z_1 and ϕ to be computed. By adding the squares of the two equations, it follows that

$$z_1^2 (K - m\omega^2)^2 + \left[c\omega z_1 + \frac{1}{\pi^2} \int_0^{2\pi} f_o(\omega z_1 \cos(\omega t)) \cos(\omega t) d(\omega t) \right]^2 = \omega^4 m^2 h_0^2. \tag{26.149}$$

Once function $f_o(\dot{z})$ has been stated, this equation allows the amplitude of the motion z_1 to be computed.

By dividing Eq. (26.148) by Eq. (26.144) it follows that

$$\phi = \text{artg} \left[-\frac{\pi c z_1 \omega + \int_0^{2\pi} f_o(\omega z_1 \cos(\omega t)) \cos(\omega t) d(\omega t)}{\pi z_1 (K - m\omega^2)} \right]. \tag{26.150}$$

It is then possible to demonstrate that the even function (deviation from symmetry) causes a displacement of the center of oscillation from the static equilibrium position, but has little effect on the dynamic response of the system. If the deviation from symmetry is neglected, the characteristics of the shock absorber can be linearized in the origin, and it is possible to use the equivalent linear viscous damping to study the small oscillations of the system. This explains why linearized models may be used even when the effect of nonlinearities seems to be important. This holds true even for small oscillations.

Example 26.13 Consider a quarter-car with two degrees of freedom with the parameters typical of the suspension of a small car: $m_s = 240$ kg, $m_u = 25$ kg, $K = 20, 8$ kN/m, $P = 125$ kN/m. Assume that the shock absorber is nonlinear and asymmetrical, and that its characteristics may be modeled using Eq. (26.131) with

$$c = 1.8 \text{ kNs/m}, \quad \mu = 0.65.$$

Moreover, dry friction is also present. It may be modeled using the odd function

$$f_o = 60 \text{ sign}(\dot{z}) \text{ N}.$$

Compute the response to harmonic excitation with amplitude $h_0 = 100$ mm by numerically integrating the equation of motion, and compare this result with the linearized solution and with the approximated solution of the nonlinear equation. Repeat the computation for an amplitude of the forcing function of 10 mm.

The equation of motion is Eq. (26.22), to which the nonlinear terms are added. However, to simplify the equation, it is possible to substitute coordinates

$$\begin{cases} z_1 = z_u - h \\ z_2 = z_s - z_u \end{cases} \tag{26.151}$$

for variables z_s and z_u .

Neglecting the damping of the tire, the equation of motion becomes

$$\begin{aligned} & \begin{bmatrix} m_T & m_s \\ m_s & m_s \end{bmatrix} \begin{Bmatrix} \ddot{z}_1 \\ \ddot{z}_2 \end{Bmatrix} + \begin{bmatrix} 0 & 0 \\ 0 & c \end{bmatrix} \begin{Bmatrix} \dot{z}_1 \\ \dot{z}_2 \end{Bmatrix} + \\ & + \begin{bmatrix} P & 0 \\ 0 & K \end{bmatrix} \begin{Bmatrix} z_1 \\ z_2 \end{Bmatrix} + \begin{Bmatrix} 0 \\ f_e(\dot{z}_2) + f_o(\dot{z}_2) \end{Bmatrix} = \begin{Bmatrix} m_T \ddot{h} \\ m_s \ddot{h} \end{Bmatrix}, \end{aligned} \tag{26.152}$$

where

$$m_T = m_s + m_u, \quad f_e = -c\mu\dot{z} \operatorname{sgn}(\dot{z}) \tag{26.153}$$

and f_o is given by the above mentioned expression.

A solution of the type of Eq. (26.135) is

$$\begin{cases} h = h_0 \sin(\omega t - \phi) = h_0 [\sin(\omega t) \cos(\phi) - \cos(\omega t) \sin(\phi)] \\ z_2 = z_{20} + z_{21} \sin(\omega t) \\ z_1 = z_{10} + z_{11s} \sin(\omega t) + z_{11c} \cos(\omega t) \end{cases} \tag{26.154}$$

By introducing this solution into the first equation of motion, which is linear, and remembering that the damping of the tire has been neglected, it follows that

$$\begin{cases} z_{10} = 0 \\ z_{11s} = \omega^2 \frac{-m_T h_0 \cos(\omega t) + m_s z_{21}}{P - \omega^2 m_T} \\ z_{11c} = \omega^2 \frac{m_T h_0 \sin(\omega t)}{P - \omega^2 m_T} \end{cases} \tag{26.155}$$

By introducing the values of the unknowns so obtained into the second equation of motion, an equation formally identical to that of a quarter-car with a single degree of freedom (Eqs. (26.136) and (26.137)) is obtained, once

$$z_{20}, \quad m_s \frac{P - \omega^2 m_u}{P - \omega^2 m_T}, \quad h_0 \frac{P}{P - \omega^2 m_T} \tag{26.156}$$

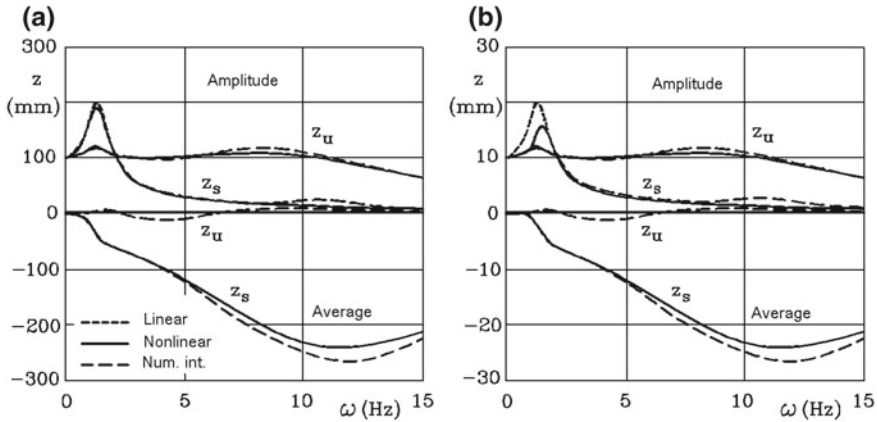


Fig. 26.42 Response to a harmonic forcing function with amplitudes of 100 mm (a) and 10 mm (b) as a function of frequency for a quarter-car model with two degrees of freedom provided with a nonlinear shock absorber

are substituted for z_1 , m_s and h_0 .

The results for a forcing function with an amplitude of 100 mm are reported in Fig. 26.42a. It is clear that the amplitude of the motion of both the sprung and unsprung masses (in terms of z_s and z_u and not of z_1 and z_2) obtained using numerical integration and the approximated nonlinear computations are close to each other. Moreover, the amplitude of the motion almost coincides with that obtained from the linearized model, with the difference that in this case there is a displacement of the central position of the oscillation.

The results obtained for an amplitude of the forcing function of 10 mm are shown in Fig. 26.42b. In this case, there is some difference between the linearized and the nonlinear solution at low frequency, due to dry friction that locks the suspension in this condition. In general, however, the accuracy of the linearized model is confirmed.

26.7.2 Springs

Dry friction in leaf springs introduces hysteresis and an apparent increase of stiffness in low amplitude motion. A qualitative force-deflection characteristic of a leaf spring is shown in Fig. 26.43. The hysteresis cycle is readily visible. The overall elastic behavior is practically linear, with a hysteresis cycle occurring about the straight line representing the average stiffness. If small amplitude oscillations occur about the equilibrium position, the apparent stiffness is strongly dependent on the amplitude, with a value tending to infinity when the amplitude tends to zero. This behavior is typical of dry friction that causes the spring to lock when very small movements are

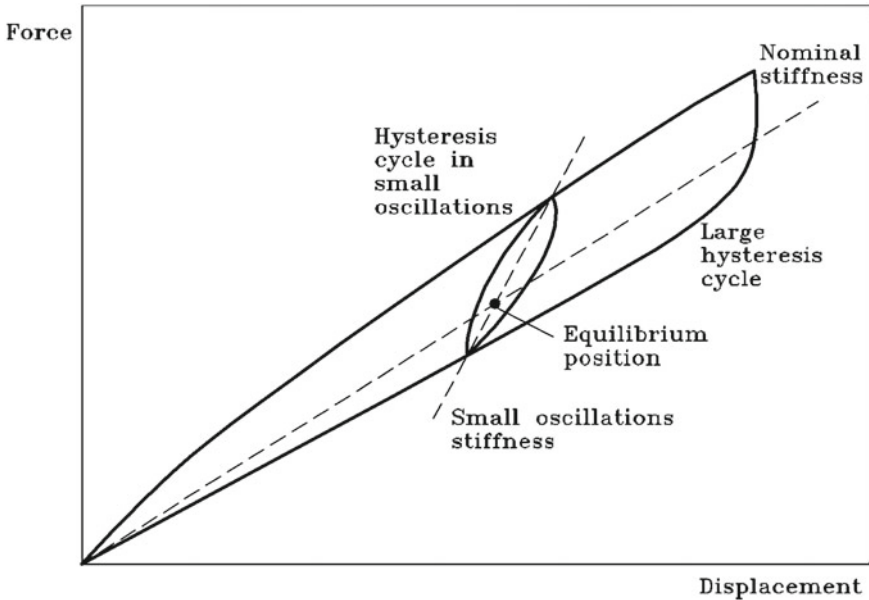


Fig. 26.43 Load-deflection characteristics of a leaf spring exhibiting hysteretic behavior. The hysteresis cycle for small displacements about the equilibrium position is shown

required. The stiffness for the small oscillations typical of ride behavior can then be much larger than the overall stiffness of the spring.

The presence of dry friction makes linear models inapplicable, or at least makes their results inaccurate, and causes a deterioration of the ride qualities of the suspension.

Other nonlinearities may be introduced by nonlinear springs, which are sometimes used for industrial vehicles in order to avoid large variations of the natural frequencies with the load. Air springs are also widely used on industrial vehicles, and their characteristics are strongly nonlinear. However, nonlinearities of the behavior of the springs can be dealt with in the same way as those due to the kinematics of the suspensions and, in the motion about any equilibrium condition, a linearized study holds with good approximation.

26.8 Concluding Remarks on RIDE Comfort

The linearized study of suspension motions, based primarily on quarter-car models, shows that the value of shock absorber damping for optimizing comfort is the same as that for reducing the dynamic component of the force on the ground to a minimum, and hence optimizing handling. However, some results obtained considering the root

mean square value of the acceleration and the dynamic component of the force show that, even when using a simplified linearized model, the value optimizing comfort is lower than that optimizing handling.

The last statement is also confirmed by other considerations. Firstly, the reduction of the force is not the only goal in handling optimization. The displacement of the sprung with respect to the unsprung masses is also important. Every type of suspension has some deviations from a perfect kinematic guide, thus causing the wheels to be set in a position different from the nominal (e.g., changes of the camber angles, roll steer etc.); this negatively affects the handling characteristics of the vehicle. The larger the displacement of the sprung mass, the worse the problem.

Operating in the same way as for minimizing the acceleration, it can be shown that the value of the damping minimizing displacement is

$$c = \sqrt{\frac{m(P + K)(P + 2K)}{2P}}, \quad (26.157)$$

which is higher than the optimum value computed above.

This also suggests an increase in the stiffness of the suspensions and goes against the criterion of “the softer the better” deriving from consideration of the vertical acceleration alone.

Another point is linked to roll oscillations. The damping of the shock absorbers is usually chosen with bounce in mind; this causes rolling motions in most cases to be excessively underdamped. When anti-roll bars are used, the situation becomes worse: By increasing roll stiffness without increasing the corresponding damping, they cause a more marked underdamped behavior and a decrease of the dynamic stability of roll motions. This not only increases the amplitude of rolling motions and the dynamic load transfer, while lowering the roll angle in steady state conditions, but also makes rollover in dynamic conditions easier.

The increase of shock absorber damping beyond the value defined above as optimum is effective in reducing these effects, which affect handling more than comfort.

On the other hand, the need for reducing jerk to increase comfort goes in the opposite direction. The value of damping minimizing jerk is lower than that minimizing acceleration, which leads to better comfort when damping is decreased.

The effect of the stiffness of springs on comfort is in a way contradictory: On one hand, as already stated, the need of reducing vertical accelerations suggests that stiffness be reduced as much as possible, but this would lead to very low natural frequencies which may, in turn, cause motion sickness and similar effects.

The compliance of the frame or of other parts of the vehicle may also affect riding comfort. The effect of the compliance of those elements that, in simplified models, are assumed to be stiff, is at any rate smaller than the effect the flexibility of the same elements has on handling. While, as already stated, the compliance of the body in bending in the xy plane and above all the torsional compliance about the z axis may have a strong effect (usually reducing performance) on handling, bending compliance in the xz plane may affect comfort, though not always in a negative way.

The local compliance of the body and the frame may strongly affect acoustic and vibrational comfort when it leads to natural frequencies that can be excited by the forcing functions that are always present on a vehicle. A typical example is the compliance of the supporting structure of the engine ancillaries (alternator, air conditioning compressor, etc.) that may cause resonances of the system made by the same elements, the supporting brackets, the belts and other elements connected to them. Because such a system is located close to, or even directly on, the engine, which is a strong source of excitations at various frequencies, many resonant vibrations are possible.

As usual, when local resonances are possible, there are many different cures:

- Increasing the damping of the system, usually by adding damping material, to reduce the amplitude of vibration below acceptable limits. This is the simplest cure, one that may induce a non-negligible increase of weight and often gives only marginal improvements. A typical example is the application of damping paints or sheet metal covered by damping material on the floor or the firewall.
- Increasing the stiffness of the structure, so as to increase the natural frequencies and thus move the resonance to frequencies at which there is little excitation. The opposite method, reducing the stiffness to decrease the natural frequencies, is usually not applicable in the automotive field, because it would cause excessive deformations and would, at any rate, induce several low frequency resonances. This cure usually causes a weight penalty as well and to increase the stiffness of a vibrating system without also increasing the damping makes the system more underdamped, with the consequence of increasing the amplitude of vibration in case a resonance occurs.
- Reducing the amplitude of the excitation at the source. Although this is the most effective cure, it is seldom applicable. To reduce the vibration caused by imbalance of rotating elements the best procedure is to improve balancing, but the prescribed balancing grade is usually chosen compatibly with constraints such as construction techniques and costs. Moreover, wear can reduce balance over time and the compliance of rotating elements may make it difficult to obtain good balancing in all operating conditions.
- Preventing vibration transmitted from the source to the resonant element. This often requires design changes or innovative concepts. For instance, the transmission of vibration from the engine to the passenger compartment is drastically reduced, with improvements in acoustic and vibrational comfort, by substituting the standard rigid linkage for gearbox control with a device based on flexible cables.
- Adding dampers close to the zones affected by vibration. The use of dynamic vibration absorbers is widespread in automotive technology, both on the chassis and in the engine (crankshaft dampers, etc.). Because the components of the vehicle are excited by a number of frequencies in a wide range, damped vibration absorbers (i.e., containing dissipative elements) are usually used instead of purely dynamic absorbers. The example given for the quarter-car with dynamic vibration absorber can be extended to other cases.